This is it.

Bistability, High Speed Modulation, Noise and Pulsations in GaAlAs Semiconductor Lasers

Thesis by

Christoph S. Harder

In Partial Fulfillment of the Requirements

for the Degree of

Doctor of Philosophy

California Institute of Technology

Pasadena, California

1983

(Submitted May 25, 1983)

To my Parents

Acknowlegments

I would like to express my sincere gratitude to my advisor, Professor Amnon Yariv, for his encouragement and support throughout my graduate studies at Caltech. His keen scientific intuition and extraordinary physical insights have been a constant inspiration. It has been a privilege to be a member of his highly motivated and talented quantum electronic research group.

I would like to thank Dr. Kam-Yin Lau and Mr. Kerry Vahala, who collaborated in much of the work presented here. A special thanks also goes to Dr. Schlomo Margalit for many fruitful and enlightening discussions and to Dr. Nadav Bar-Chaim who taught me how to grow crystals by liquid phase epitaxy. In addition, I would like to thank also Mr. Desmond Armstrong and Mr. Lawrence Begay for their expert technical assistance in construction and maintenance of experimental apparatus.

I would also like to express my appreciation to my fellow students, in particular I would like to thank Dr. Liew-Chuang Chiu and Mr. John S. Smith for their help and collaboration and Dr. Pei-Chuang Chen, Dr. Joseph Katz, Dr. Uziel Koren, Dr. Israel Ury, Dr. Daniel P. Wilt and Mr. Kit-Lai Yu for their participation in this work.

I also gratefully acknowledge the financial support of a Fulbright Scholarship and the support received from the California Institute of Technology, the National Science Foundation and the Office of Naval Research.

Finally, my deepest gratitude goes to my parents for their constant support and encouragement.

Abstract

This thesis describes seven different subjects relevant to semiconductor laser diodes which fall in the following three categories: Bistability and pulsations, high speed modulation and noise.

Bistable semiconductor lasers based on inhomogeneous current injection, achieved with a split contact scheme, were proposed around 20 years ago. However, actual devices showed no or only a small hysteresis and they were in addition beset by pulsations for reasons not well understood at the time. In this thesis we show that lasers with an optimized design can display bistability with a giant hysteresis. Crucial to the understanding of the bistable laser is a negative differential resistance across the absorber section, reminiscent of a tunnel diode characteristic. Depending on the electrical biasing circuit this negative differential resistance leads to bistability or light-jumps and self-pulsations. A simple model based on the conventional rate equations explains the observed behavior. Investigation of the switching dynamics of this optoelectronic device reveals a delay time which is critically dependent on the trigger pulse amplitude and which is typically in the order of a few nanoseconds at a power-delay product of 100pJ. We also investigate the characteristic of this laser coupled to an external optical cavity and we demonstrate that this bistable laser can be used as a self-coupled stylus for optical disk readout. Under a different biasing condition this laser coupled to an external optical cavity can be used to generate ultrashort optical pulses through passive mode locking. Unlike previous mode locking techniques, the method presented here does not rely on absorption introduced by damaging the crystal and is consequently much more reliable.

The high speed modulation behavior of semiconductor lasers is investigated

theoretically and experimentally. In this thesis we derive the fundamental limits of injection lasers for pulse modulation and small signal modulation. We place emphasis on developing laser structures optimized for high frequency modulation and experiments on such structures show that they can be modulated at frequencies up to 8GHz. At these frequencies the parasitic elements can no longer be neglected and they are included in the analysis.

The noise equivalent circuit of a semiconductor laser diode is derived from the rate equations including Langevin noise sources. This equivalent circuit allows a straightforward calculation of the noise and frequency modulation characteristics of a laser diode combined with electronic components. The field spectrum of injection lasers is observed also experimentally. It is a unique feature of injection lasers that their linewidth is increased through a strong amplitude phase coupling by the factor $(1+\alpha^2)$ where α is the linewidth enhancement factor. A model is developed which shows that the same factor α enters in the small signal modulation characteristics and a careful measurement of the small signal amplitude and phase modulation at high frequencies enables us to obtain this important factor α for the first time by a direct measurement.

Table of contents

Chapter 1 Introduction

1.1	Semiconductor laser diodes	1
1.2	Outline of the thesis	5
1.3	References	9

Chapter 2 Electrical equivalent circuit of an injection laser diode

2.1	Introduction	12
2.2	Rate equations	12
2.3.	Equivalent circuit	16
2.4	References	24

Chapter 3 High speed modulation

3.1	Introduction	26
3.2	Pulse modulation	27
3.3	Photodiode calibration	31
3.4	Optimizing of the small signal modulation bandwidth	38
3.5	Parasitic elements and driving circuit considerations for high frequency modulation	46
3.6	Outlook	58
3.7	References	61

Chapter 4 A bistable semiconductor laser

4.1	Optical bistability	63
4.2	Bistability and pulsations in semiconductor lasers with inhomogeneous current injection	64
4.3	Outlook	100
4.4	References	102

Chapter 5 Mode locking

5.1	Introduction	105
5.2	Passive mode locking of buried heterostructure lasers with a nonuniform current injection	107
5.3	Large signal analysis of pulsations	114
5.4	References	121

Chapter 6 Amplitude noise in semiconductor laser diodes

6.1	Introduction	123
6.2	Noise equivalent circuit of a semiconductor laser diode	125
6.3	Shot noise and thermal noise	138
6.4	References	144

Chapter 7 Phase noise in semiconductor laser diodes

7.1	Introduction	146
7.2	Measurement of the linewidth enhancement factor α	149
7.3	Observation of the relaxation resonance effects in the field spectrum of semiconductor lasers	157
7.4	References	162

Chapter 8 Monolithic integration

8.1	Introduction	164
8.2	Monolithic integration of a GaAlAs buried heterostructure laser and a bipolar phototransistor	167
8.3	References	172

Chapter 1

Introduction

1.1 Semiconductor laser diodes

Stimulated coherent emission from semiconductor GaAsP and GaAs p-n junctions was observed in 1962 by four groups [1],[2],[3],[4]. Six years later, lasing action had been obtained in a wide variety of semiconductor materials covering the wavelength range between 0.5μm to 20μm. With the introduction of the heterojunction concept to confine injected carriers and stimulated emission to a thin layer, pumping current densities necessary to initiate lasing could be reduced drastically. Continous wave (cw) lasing of GaAlAs diodes was obtained at room temperatures in 1970. Since then activities focused on how to make use of the tremendous commercial potential of semiconductor lasers as highly efficient, compact and cheap light sources which can be modulated directly at very high frequencies. The basic concept of the double heterostructure laser diode has not changed much in recent years. Research and development has been directed towards improving reliability, power capability, optical beam quality and the spectral characteristic. Two material systems dominate nowadays the injection laser diode activities; the GaAs/GaAlAs system because of its mature technology and short lasing wavelength (0.7μm to 0.9μm) and the InP/InGaAsP system because of its lasing wavelength range (1.1μm to 1.7μm) which coincides with the low loss window and dispersion minimum in optical fibers.

The state of the art is quite impressive. Degradation rates of 10^{-5} h^{-1} at 100°C temperature and extrapolated lifetimes in excess of 10^7 h at room temperature for GaAlAs lasers have been obtained [5]. Lasers which operate cw emitting the optical power stably into one single longitudinal and transverse mode at output powers up to 40mW are commercially available [6] and arrays of phase locked lasers with output powers up to 2.6W have been reported [7]. Differential power efficiencies (the conversion efficiency from electrical input power to optical output power) of 80% have been measured and threshold currents as low as 2.5 mA (corresponding to a power dissipation of 5 mW) have been demonstrated [8]. Amplitude and phase fluctuations of the best laser structures have been shown to be at the quantum mechanical limit. Nevertheless, there is still room to improve some of the characteristics of the lasers and research and development efforts are now directed towards tailoring semiconductor lasers for specific applications such as lightwave communication (long wavelength, stable spectrum), laser printers (high power, good beam quality), audio disks (insensitivity to reflections, cheap mass production) and microwave links (high speed modulation, low power dissipation), to name a few.

Throughout this thesis a familiarity with semiconductor lasers is assumed. Comprehensive treatments of semiconductor laser diodes can be found in the books by Casey and Panish [9], Kressel and Butler [10], and Thompson [11].

Traditionally, data transmission over long distances has been done either through coaxial cables or microwave links. With the development of low loss optical fibers lightwave transmission has become a very attractive alternative [12]. Single mode optical silica fibers have attenuation as low as 3dB/km at $\lambda = 0.8\mu m$ and 0.2dB/km at $\lambda = 1.55\mu m$ [13] and the optical dispersion can be made to vanish at any wavelength between 1.3 μm and 1.6 μm [14] by balancing waveguide and material dispersion, thus allowing for high data rates over long

distances. Optical power levels in fiber systems are rather low, typically 1mW or even less, which limits analog transmission to special applications. Systems requiring a large signal to noise ratio such as lightwave data transmission use nearly exclusively a digital format. InGaAs laser diodes between 1.3 μm and 1.55 μm are used as light emitters, at a wavelength of minimum fiber loss and dispersion, and transmission of 2Gbit/s without repeater over a 51km long fiber have already been demonstrated [15]. These long wavelength lasers still have two problems: a strong dependence of the threshold current on temperature and a spectral broadening under high speed modulation. The threshold current is kept constant by temperature stabilizing the laser and the spectral width is maintained narrow by either using distributed Bragg reflector (DBR) structures, a three mirror cavity or injection locking the laser [16] to a single mode laser.

Optical disks are already being used as high density storage media [17]. The information is encoded in the reflectivity of the optical disk and is read out by a laser as shown in Fig. 1.1. At the time there are three different systems: audio disks with the at 44 kHz sampled signal stored digitally, video disks with the signal encoded in an fm format, and disks for binary mass storage with a capacity in excess of 10 Gbit/disk. In the first two applications the signal is only read (which can be done with a laser power of 1mW) but the mass storage system operates in a write/read mode which requires a high power (around 40mW) laser with a very good beam quality. Since the pixel size on the optical disk is given by the diffraction limited spot it is desirable to use a laser with a short wavelength. The current standard is 780nm.

Semiconductor lasers are also being used in laser printers with an IR sensitized CdS photoconductor drum [18].

An exciting future application is the transmission of microwave signals over

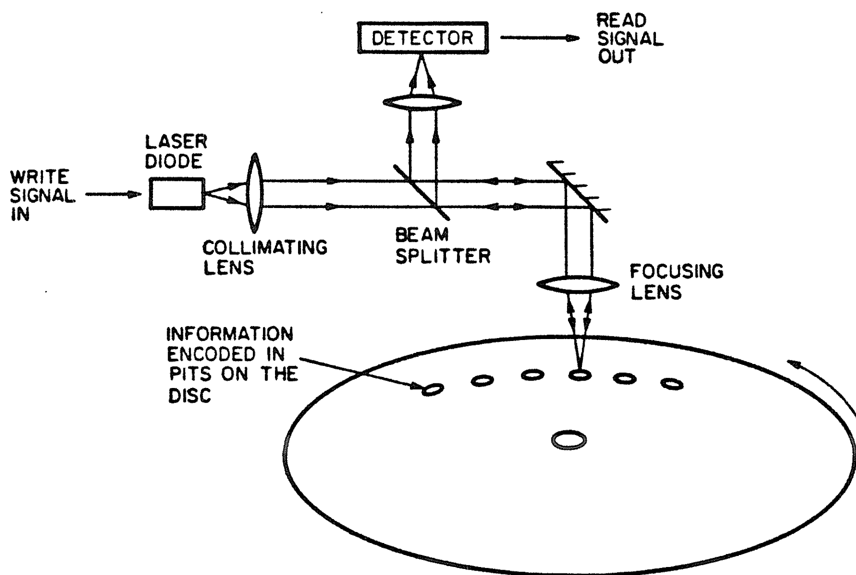

Figure 1.1.1. View of an optical disk system for data storage. The data can be written on the disk and read out by a semiconductor laser.

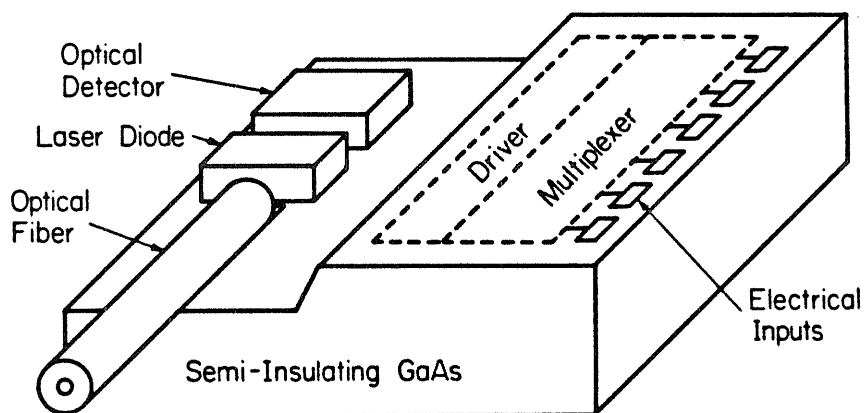

Figure 1.1.2. View of an integrated optoelectronic transmitter (IOEC). This monolithic circuit multiplexes several electrical data-streams on a laser diode and the intensity modulated light is injected into an optical fiber.

short distances through optical fibers. Microwave links consist normally of bulky waveguides or lossy coaxial cables. Optical fibers could be used if the microwave signal is modulated on an optical carrier, i.e. by directly intensity modulating a semiconductor laser diode with the microwave signal. Since microwave integrated circuits are fabricated on GaAs substrate (because of the high speed electronic components obtainable on GaAs such as MESFET, HEMT and hetero-junction bipolar transistor) it is tempting to integrate high speed electrical circuitry and semiconductor lasers monolithically. Such an integrated optoelectronic circuit IOEC, proposed some ten years ago by Yariv [19], shows a superior performance compared to its hybrid counterpart in high speed behavior, reliability and complexity. Although the two technologies for electronic and optical devices have developed independently it has been shown that they are compatible. Similarly, high speed digital data buses (at several Gbit/s) connecting logic circuits have problems of power dissipation, crosstalk, electromagnetic interference and speed. Replacing the electrical bus by an optical bus would improve the performance appreciably. In Fig. 1.1.2 a view of a possible digital IOEC is shown.

1.2 Outline of the thesis

In this thesis seven topics relevant to injection lasers will be presented. Most of the experimental and modeling work has been done with GaAlAs lasers, but the results are in general also applicable to other diode lasers i.e. InGaAsP lasers.

In chapter two the electrical equivalent circuit of a semiconductor laser diode is derived. Semiconductor laser diodes are opto-electronic devices with optical as well as electrical characteristics. Many applications of injection lasers, in particular those which involve high frequency modulation, require an accurate

representation of the electrical impedance characteristic of the laser diode. This electrical representation is derived from the rate equations [20]. This electrical equivalent circuit is used extensively in chapter three to evaluate different electrical driving circuits.

In chapter three the high frequency modulation behavior is investigated, theoretically and experimentally. There exists a great deal of interest in directly modulating injection lasers at very high frequencies, 10 GHz to 20 GHz. In this chapter we derive the fundamental modulation limits of injection lasers for pulse modulation [21] and small signal modulation [22], [23], [24]. Emphasis of previous experimental and theoretical work was placed merely on investigating modulation characteristics of existing laser structures and not on developing laser structures optimized for high frequency modulation. This chapter places emphasis on the latter and a systematic analysis on how various device parameters affect high frequency response yields general guide lines for constructing a laser geared towards high speed modulation. At very high frequencies parasitic elements can no longer be neglected and they are included in the analysis. Experiments with optimized lasers showed that they can be modulated up to 8 GHz [23] at room temperatures and it is expected that this can still be further improved by cooling the laser. The longitudinal mode behavior under modulation is also investigated experimentally.

In chapter four fabrication, measurement and analysis of bistable lasers are presented [25], [26], [27], [28], [29]. Bistable semiconductor lasers based on inhomogeneous current injection (with a split contact scheme) were proposed around 20 years ago. However actual devices showed no or only a small hysteresis and they were in addition beset by pulsations for reasons not well understood. We demonstrated that with an optimized design bistable lasers with a large hysteresis and no pulsation can be obtained. Crucial to the understanding

of the bistable laser was the discovery of a negative differential resistance across the absorber section, reminiscent of a tunnel diode. This chapter has two interesting aspects: first the static and dynamic properties of a bistable laser such as critical slowing down and instabilities are studied extensively and second, self pulsations which are still encountered in aged injection lasers can be understood as a direct consequence of inhomogeneous pumping conditions and remedies are recommended to eliminate them.

In chapter five we present a novel method to passively mode lock a semiconductor laser. We present experimental results of GaAlAs buried heterostructure semiconductor lasers with a split contact coupled to an external cavity [30]. The split contact structure is used to introduce a controllable amount of saturable absorption, which is necessary to initiate passive mode locking. Unlike previous mode locking techniques, the method presented does not rely on absorption introduced by damaging the crystal and is consequently much more reliable. We have obtained pulses with a full width at half-maximum of 35ps and shorter pulses should result by improving the coupling between laser diode and external optical cavity and by using a modified laser structure.

In chapter six a theoretical analysis of amplitude noise in injection lasers is presented. The noise equivalent circuit of a semiconductor laser diode is derived from the rate equations including Langevin noise sources [31]. This equivalent circuit allows a straightforward calculation of the noise and modulation characteristics of a laser diode combined with electronic components, and the interactions between electrical circuit and laser diode can be analyzed easily.

In chapter seven the field spectrum of semiconductor lasers is investigated. The fine structure of the fieldspectrum as predicted by Vahala and Yariv [32], [33] is experimentally observed. It is a unique feature of injection lasers that

their linewidth is increased through a strong amplitude phase coupling by the factor $(1+\alpha^2)$ where α is the linewidth enhancement factor. A model is developed which shows that the same factor α enters in the small signal modulation characteristics [34]. A careful measurement of the small signal amplitude and phase modulation at high frequencies enables us to obtain this important factor α for the first time by a direct measurement.

In chapter eight advantages of IOEC's are discussed and fabrication and measurements of a simple integrated repeater are presented [35]. The repeater consists of a heterojunction bipolar phototransistor and a high quality buried heterostucture laser.

The work described in the thesis was the subject, in part, of the follo lished articles, [20 - 31], [33 - 36]. In addition the following invited presented which were based on this work [37], [38].

1.3 References

1. R. N. Hall, G. E. Fenner, J. D. Kingsley, T. J. Soltys, and R. O. Carlson, Phys. Rev. Lett., vol. 9, p. 366, 1962.

2. M. I. Nathan, W. P. Dumke, G. Burns, F. N. Dill, and G. J. Lasher, Appl. Phys. Lett., vol. 1, p. 62, 1962.

3. M. Holonyak and S. F. Bevacqua, Appl. Phys. Lett., vol. 1, p. 82, 1962.

4. T. M. Quist, R. H. Rediker, R. J. Keyes, W. E. Krag, B. Lax, A. L. McWhorter, and H. J. Zeigler, Appl. Phys. Lett., vol. 1, p. 91, 1962.

5. D. Botez, Appl. Phys. Lett., vol. 36, p. 190, 1980.

6. H. D. Wolf, K. Mettler, K. H. Zschauer, Jap. J. of Appl. Phys., vo

1981.

7. D. R. Scifres, C. Lindstroem, R. D. Burnham, W. Streifer, T. L. Paoli, Electron. Lett., vol. 19, p. 170 (1983).

8. W. T. Tsang, R. A. Logan, Electron. Lett., vol. 18, p. 845, 1982.

9. H. C. Casey, and M. B. Panish, "Heterostructure lasers", Academic Press, New York, 1978.

10. H. Kressel, and J. K. Butler, "Semiconductor lasers and heterojunction LEDs", Academic Press, New York, 1977.

11. G. H. B. Thompson, "Physics of semiconductor laser devices", John Wiley and Sons, Chichester, England, 1980.

12. J. R. Jones, IEEE J. Quantum Electron., vol. 18, p.1524, 1982.

13. K. Inada, IEEE Trans. Microwave Theory Tech., vol. 30., p. 1412, 1982.

14. A. Sarkar, presented at the Optical Fiber Communication Conference, New

Orleans, paper MF1, Feb. 1983.

15. J. I. Yamada, A. Kawana, H. Nagai and T. Kimura, IEEE Trans. Microwave Theory Tech., vol. 30, p. 1525, 1982.

16. K. Iwashita, K. Nakagawa, IEEE J. Quantum Electron., vol. 18, p.1669, 1982.

17. R. A. Bartolini, Proc. IEEE, vol. 70, p. 589, 1982.

18. J. C. Urbach, T. S. Fisli, G. K. Starkweather, Proc. IEEE, vol. 70, p. 597, 1982.

19. A. Yariv, Proc. Esfahan, Symposium on fundamental and applied laser physics, M. S. Feld, A. Javan, and N. A. Kurnit Eds., Wiley Interscience, New York, p. 897, 1973.

20. J. Katz, S. Margalit, Ch. Harder, D. Wilt, A. Yariv, IEEE J. Quantum Electron., vol. 17, p. 4 (1981).

21. T. L. Koch, L. C. Chiu, Ch. Harder, A. Yariv, Appl. Phys. Lett., vol. 41, p. 6 (1982).

22. K. Y. Lau, Ch. Harder, A. Yariv, Opt. Commun., vol. 36, p. 472 (1981).

23. K. Y. Lau, N. Bar-Chaim, I. Ury, Ch. Harder, A. Yariv, to be published in Appl. Phys. Lett. (1983).

24. K. Y. Lau, N. Bar-Chaim, I. Ury, Ch. Harder, A. Yariv, to be published in Appl. Phys. Lett. (1983).

25. Ch. Harder, K. Y. Lau, A. Yariv, Appl. Phys. Lett., vol. 39, p. 382 (1981).

26. Ch. Harder, K. Y. Lau, A. Yariv, Appl. Phys. Lett., vol. 40, p. 139 (1982).

27. K. Y. Lau, Ch. Harder, A. Yariv, Appl. Phys. Lett., vol. 40, p. 198 (1982).

28. K. Y. Lau, Ch. Harder, A. Yariv, Appl. Phys. Lett., vol. 40, p. 369 (1982).

29. Ch. Harder, K. Y. Lau, A. Yariv, IEEE J. Quantum Electron., vol. 18, p. 1351

(1982).

30. Ch. Harder, J. S. Smith, K. Y. Lau, A. Yariv, to be published in Appl. Phys. Lett. (1983).

31. Ch. Harder, J. Katz, S. Margalit, A. Yariv, IEEE J. Quantum Electron., vol. 18, p. 333 (1982).

32. K. Vahala, A. Yariv, to be published in IEEE J. Quantum Electron. (1983).

33. K. Vahala, Ch. Harder, A. Yariv, Appl. Phys. Lett., vol. 42, p. 211 (1983).

34. Ch. Harder, K. Vahala, A. Yariv, Appl. Phys. Lett., vol. 42, p. 328 (1983).

35. N. Bar-Chaim, Ch. Harder, J. Katz, S. Margalit, A. Yariv, Appl. Phys. Lett., vol. 40, p. 556 (1982).

36. U. Koren, T. R. Chen, Ch. Harder, A. Hasson, K. L. Yu, L. C. Chiu, S. Margalit, A. Yariv, Appl. Phys. Lett., vol. 42, p.403 (1983).

37. Ch. Harder, K. Y. Lau, A. Yariv, invited paper presented at the integrated and guided wave optics conference, FC1, Pacific Grove, California, January 1982.

38. Ch. Harder, K. Y. Lau, A. Yariv, invited paper presented at the 12th international quantum electronics conference, TU6, Munich, Germany, June 1982.

Chapter 2

Electrical equivalent circuit of an injection laser diode

2.1 Introduction

The many applications of laser diodes, in particular those which involve high frequency modulation or combined operation with electronic components and circuits, require an accurate representation of the electrical characteristic of a laser diode. An injection laser is an opto-electronic element whose electrical characteristics are as important as its optical ones. These electrical characteristics are derived in this chapter from the standard rate equations [1] which describe the interaction between photons and electrons. They are augmented by an equation for the carrier density as a function of the applied junction voltage. A small signal analysis of these equations produces the electrical equivalent circuit [2], [3], [4].

2.2 Rate equations

The rate equations of an injection laser for the electron density n and photon density p are [1], [5], [6], [7], [8].

$$\frac{dn}{dt} = \frac{i}{e\,Vol} - r(n) - v_{gr}g(n)p \tag{2.2.1}$$

$$\frac{dp}{dt} = v_{gr}g(n)p\Gamma - \frac{p}{\tau_p} + \beta\Gamma r(n) \tag{2.2.2}$$

Under normal operating conditions the input variable is the pump current i. In

the equation above, Vol is the volume of the active region (the region which has an inverted population) and e the electronic charge. The carriers recombine at a rate r(n), v_{gr} is the group velocity of the light in the mode, g(n) is the power gain in cm^{-1} and Γ is the optical confinement factor given by $\Gamma \equiv \frac{Vol}{Vol_{op}}$, where Vol_{op} is the volume of the optical field. The photon lifetime τ_p includes all the losses, $\tau_p \equiv \frac{1}{v_{gr}(\alpha + \frac{1}{L}\ln(\frac{1}{R}))}$ where α is the distributed loss, L is the length of the optical cavity and R is the mirror reflectivity. The last term in equation (2.2.2) is equal to the amount of spontaneous emission which is added to the radiation field and β is the spontaneous emission factor.

In writing the rate equations in this particular form several assumptions have been made implicitly. First we have assumed that the active volume is pumped homogeneously. Deliberate inhomogeneous pumping can lead to very interesting effects such as bistability and self-pulsations and we investigate this situation extensively in chapter four. In the rate equations above the carrier density and photon density have been averaged spatially and we will discuss briefly how reasonable this is along the three coordinates separately. Since the active region is very thin, typically 0.1μm, the optical field and the carrier density are essentially constant in this dimension [7] and averaging is a good approximation. To analyze the effects of averaging along the cavity length, Moreno [8] compared the results of traveling wave equations and the spatially averaged equations, and he found reasonable agreement as long as the mirror reflectivity is larger than R=0.2. For usual lasers, which have a reflectivity of R=0.3, the spatially averaged rate equations are therefore a good approximation. Reducing the mirror reflectivity by an anti-reflection coating below R=0.2 leads to superluminescent damping of the relaxation resonance which has been analyzed and

verified experimentally [9]. The density variations in the transverse direction can be taken into account by introducing local rate equations which incorporate diffusion terms of the carriers [11]. The main effect of this diffusion term is to damp the relaxation resonance, by an amount which depends heavily on the laser structure [11]. We have also assumed that electrons and photons are contInous variables. This is not true since, roughly speaking, photons can only be added or extracted from the mode in integer units and the same holds for the electrons in the total system. This constraint on stimulated and spontaneous emission rates causes shot noise, that is amplitude fluctuations. This quantum mechanical noise can be included by adding Langevin noise sources to the rate equations. McCumber [12] has shown that an expression for these Langevin noise sources can be obtained from a simple shot noise model. We use his analysis in chapter six to derive these noise sources and obtain a noise equivalent circuit.

The spontaneous emission factor β is equal to the relative amount of spontaneous power which is fed into the lasing mode. The spontaneous emission factor varies among different structures and directly influences the strength of the relaxation resonance. The numerical value of β has been calculated classically (an approach which still must be justified since the calculation of β is a quantum mechanical problem [13]) by Suematsu [14] and Petermann [15] as the amount of power which a dipole radiator couples into the lasing mode. We will develop here a simple derivation of β.

We start with a basic result of quantum mechanics which states that the power fed into one mode from an inverted population is proportional to the number of photons in this mode P_1 plus 1.

$$\text{power gain} \propto (P_1+1) \tag{2.2.3}$$

In semiconductor lasers an inversion factor n_{sp} must be included, n_{sp} is equal to the ratio of total stimulated emission to net stimulated emission [16]. In injection lasers this factor n_{sp}, which is often also called spontaneous emission factor, depends weakly on the carrier density n and has been measured to be $n_{sp} \approx 2.7$ [16] in a buried heterostructure laser. Equation (2.2.3) is only valid if P_1 is equal to the number of photons in one quantum mechanical mode [13]. Very often the rate equation (2.2.2) describes actually the photon density in K quantum mechanical modes, i.e. in multimode lasers or in gain guided structures $K=\sqrt{1+\chi^2}$ [13], where χ is the astigmatism factor [15]. Including n_{sp} and K, equation (2.2.3) reads now:

$$\text{power gain} \propto \left(\frac{P}{Kn_{sp}}+1\right) \tag{2.2.4}$$

where P is the total number of photons in the modes which are included in the rate equation (2.2.2). By equating the ratio of spontaneous to stimulated emission as obtained from the equations (2.2.2) and (2.2.4) we find:

$$\beta \equiv \frac{v_{gr}\, g(n)}{Vol_{op}\, r(n)} Kn_{sp} \tag{2.2.5}$$

If the laser is operated well above threshold, gain and spontaneous emission are clamped to values given by the rate equations, and we can rewrite equation (2.2.5).

$$\beta \approx \frac{1}{\tau_p\, i_{th}/e} Kn_{sp} \tag{2.2.6}$$

For τ_p=1.5ps, i_{th}=10mA and K=1 we obtain $\beta \approx 3\times10^{-5}$, note that β is just inversely proportional to the photon lifetime and the threshold current, two easily measurable parameters. We can simplify equation (2.2.5) also by using the relation between stimulated and spontaneous emission [16].

$$\beta \approx \frac{1}{N} K \tag{2.2.7}$$

$$N \equiv \frac{8\pi n_{gr}^3 \nu^2}{c^3} \mathrm{Vol}_{op} \, \Delta\nu$$

N is the number of quantum mechanical modes which fit into the volume Vol_{op} and under the spontaneous linewidth $\Delta\nu$. This equation (2.2.7) simply states that the spontaneous emission is equally distributed into all different modes. Please note that in the analysis above we moved the lineshape function pretty freely in and out of the integral which has to be taken over the energy. The numerical value of β obtained from a lengthy classical calculation [15] differs from the quantum mechanical value by a numerical factor which is close to one.

$$\beta = \frac{c^3}{4\pi^2 n_a n n_{gr} \nu^2} \frac{1}{\mathrm{Vol}_{op} \Delta\nu} K \tag{2.2.8}$$

where n_a is the index of refraction of the material in the active region and n is the effective index of refraction of the mode.

2.3 Equivalent circuit

The rate equations (2.2.1) and (2.2.2) appear highly nonlinear, but a numerical solution shows that at pump levels which are larger than a threshold current i_{th} the carrier density n is clamped to n_{th} [17]. Each additional injected carrier recombines immediately through stimulated emission and contributes with a constant efficiency to the radiation field. Because of this mechanism, the emitted light depends linearily on the current above threshold [17], and it is actually a very good approximation to linearize the rate equations under all operating conditions as long as the carrier density is clamped and we will do this now to derive the equivalent circuit. We restate the rate equations:

$$\frac{dn}{dt} = \frac{i}{e\,Vol} - r(n) - v_{gr}g(n)p \tag{2.3.1}$$

$$\frac{dp}{dt} = v_{gr}g(n)p\Gamma - \frac{p}{\tau_p} + \beta\Gamma r(n) \tag{2.3.2}$$

A small signal analysis around the bias point i_0 is performed and we let:

$$i = i_0 + i_1 \tag{2.3.3}$$

$$n = n_0 + n_1 \tag{2.3.4}$$

$$p = p_0 + p_1 \tag{2.3.5}$$

The spontaneous recombination rate $r(n)$ and the gain $g(n)$ are expanded around the bias point.

$$r(n_0 + n_1) = r(n_0) + \frac{n_1}{\tau} \tag{2.3.6}$$

$$v_{gr}g(n_0 + n_1) = G(n_0) + An_1 \tag{2.3.7}$$

Depending on linear or bimolecular recombination rate $r(n)$, τ is given by

$$\text{linear: } r(n) = \frac{n}{\tau_s} \rightarrow \tau \equiv \tau_s \tag{2.3.8}$$

$$\text{bimolecular: } r(n) = Bn^2 \rightarrow \tau \equiv \frac{1}{2Bn_0} \tag{2.3.9}$$

A is the differential gain coefficient , τ_s is the spontaneous carrier life time and B is the recombination coefficient. Proceeding with the small signal analysis we obtain the static equations for the biasing points:

$$0 = \frac{i_0}{eVol} - r(n_0) - G(n_0)p_0 \tag{2.3.10}$$

$$0 = G(n_0)p_0\Gamma - \frac{p_0}{\tau_p} + \beta\Gamma r(n_0) \tag{2.3.11}$$

These equations can be solved to find the carrier density n_0 and the photon density p_0 at the bias point given by the pump current i_0. The small signal equa-

tions are:

$$\frac{dn_1}{dt} = \frac{i_1}{eVol} - (Ap_0 + \frac{1}{\tau})n_1 - G(n_0)p_1 \qquad (2.3.12)$$

$$\frac{dp_1}{dt} = (Ap_0 + \frac{\beta}{\tau})\Gamma n_1 - \Gamma\,\beta\frac{r(n_0)}{p_0}p_1 \qquad (2.3.13)$$

The carrier density of the electrons is given as a function of the quasi-Fermi level of the electrons E_{Fn}.

$$n = N_C\frac{2}{\sqrt{\pi}}F_{1/2}(\frac{E_{Fn} - E_C}{kT}) \qquad (2.3.14)$$

where N_C is the effective density of states of the conduction band, $F_{1/2}$ is the Fermi integral, $E_{Fn} - E_C$ is the difference between the quasi-Fermi level of the electrons and the conduction band edge and kT is the thermal energy. A similar equation holds for the holes. It is a unique feature of semiconductor lasers that the quasi-Fermi levels can be accessed directly since the externally applied voltage v is equal to the difference of the quasi-Fermi levels, $v = (E_{Fn} - E_{Fh})/e$. It is this feature that puts injection lasers in a different class than other laser systems, and we will show in the following chapters that many interesting effects encountered in injection lasers are a direct consequence of this fact. For the small signal analysis we let:

$$v = v_0 + v_1 \qquad (2.3.15)$$

An approximation of the Fermi-integral [18] gives the following relation between small signal voltage v_1 and carrier fluctuations n_1.

$$v_1 = mV_T\,\frac{n_1}{n_0} \qquad (2.3.16)$$

$$m = 2 + \frac{n_0}{2\sqrt{2}}(\frac{1}{N_V} + \frac{1}{N_C})$$

where $V_T = \frac{kT}{e}$ is the thermal voltage.

Now consider the separate problem of the electrical circuit shown in Fig. 2.3.1. The equation for the voltage v_1 and the current i_L can be obtained by inspection:

$$\frac{dv_1}{dt} = -\frac{v_1}{RC} + \frac{i_1}{C} - \frac{i_L}{C} \tag{2.3.17}$$

$$\frac{di_L}{dt} = \frac{v_1}{L} - \frac{R_{se}}{L} i_L \tag{2.3.18}$$

By comparing the small signal rate equations (2.3.12) and (2.3.13) with the circuit equation (2.3.17) and (2.3.18) and using (2.3.16) we find the values of the different elements of the equivalent circuit:

$$C \equiv \frac{en_0 Vol}{mV_T} \tag{2.3.19}$$

$$R \equiv \frac{mV_T}{en_0 Vol} \frac{1}{Ap_0 + \frac{1}{\tau}} \tag{2.3.20}$$

$$L \equiv \frac{mV_T}{en_o Vol} \frac{1}{\Gamma G(n_0)} \frac{1}{Ap_0 + \frac{\beta}{\tau}} \tag{2.3.21}$$

$$R_{se} \equiv \beta \frac{mV_T}{en_0 Vol} \frac{r(n_0)}{p_0 G(n_0)} \frac{1}{Ap_o + \frac{\beta}{\tau}} \tag{2.3.22}$$

The bias points n_0 and p_0 are the solution of the static equation, they are an explicit function of the drive current i_0. We find also that the current through the inductor i_L is directly proportional to the optical signal p_1.

$$i_L = eG(n_0)Vol\, p_1 \tag{2.3.23}$$

Typical values of the elements are shown in Fig. 2.3.3 for a laser with the following parameters: $Vol=300\times5\times0.2\mu m^3$, $r(n)=\frac{n}{\tau_s}$ with τ_s=3ns, τ_p=2ps, $v_{gr}g(n)=A(n-n_{tr})$ with $A=0.5\times10^{-6}cm^3s^{-1}$ and $n_{tr}=5\times10^{17}cm^{-3}$. The threshold current is defined as $i_{th}=\frac{eVol}{\tau_s}(\frac{1}{A\tau_p} + n_{tr})$ =24mA. As an application the input

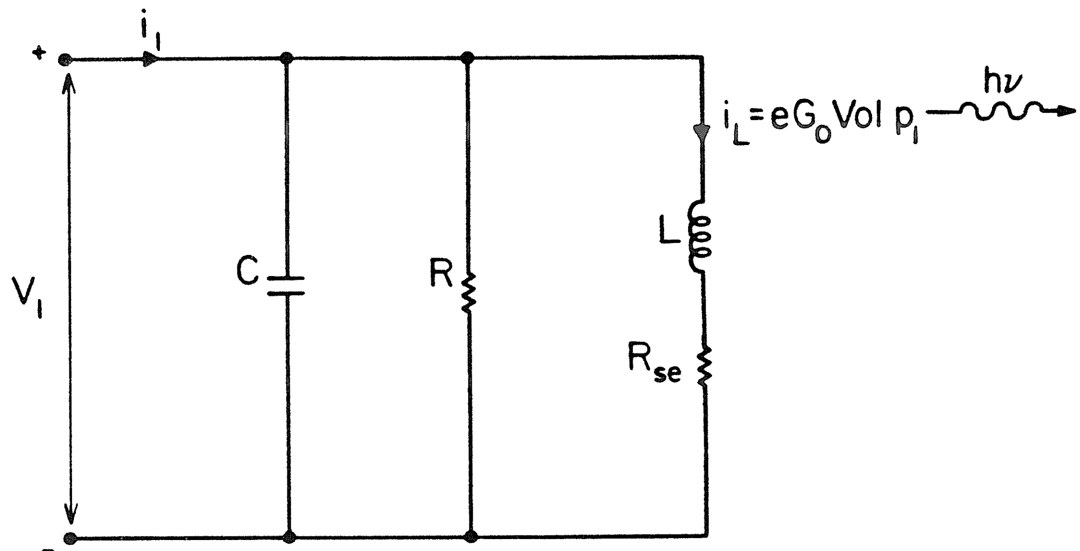

Figure 2.3.1. Equivalent circuit of an injection laser diode. The electrical input variables are i_1 and v_1 and the output variable is the optical signal p_1 which is directly proportional to the current i_L through the inductor. The modulated optical output power is $P_{out,1} = \frac{1}{2} p_1 \hbar\omega v_{gr} \ln(\frac{1}{R})$ (see equation 2.3.26).

impedance Z(s) is calculated and shown in Fig. 2.3.3 for different bias points.

$$Z(s) = \frac{s\frac{1}{C} + \frac{R_{se}}{LC}}{s^2 + s(\frac{1}{RC} + \frac{R_{se}}{L}) + \frac{1}{LC}(1 + \frac{R_{se}}{R})} \tag{2.3.24}$$

$$Z(s) = \frac{N(s)}{s^2 + s\frac{\omega_r}{q_r} + \omega_r^2}$$

$$\omega_r = \sqrt{\frac{1}{LC}(1 + \frac{R_{se}}{R})}$$

As can be seen from Fig. 2.3.3, for most low frequency applications, the laser diode has an extremely low impedance, but at high frequencies (around the relaxation resonance ω_r) the impedance becomes appreciably large and can no longer be neglected. The injection laser is a second order system with a relaxation resonance ω_r and a quality factor q_r which is typically fairly large. We will encounter this relaxation resonance many more times and its value is obtained from equation (2.3.24) to be approximately (for a small R_{se}, that is, for a small β).

$$\omega_r \approx \frac{1}{\sqrt{LC}} = \sqrt{\frac{Ap_0}{\tau_p}} \tag{2.3.25}$$

A typical value for $\frac{\omega_r}{2\pi}$ is 1GHz to 3GHz. The optical power emitted from one mirror facet as a function of the photon density p inside the cavity is given by

$$P_{out} = \frac{1}{2} p\, \hbar\omega v_{gr} \ln(\frac{1}{R})\, A_{mode} \tag{2.3.26}$$

where $\hbar\omega$ is the energy of one photon, A_{mode} is the cross section of the mode and $P_{out} = P_{out,0} + P_{out,1}$. We define the transfer characteristic of the laser diode T(s) as the small signal response of the light output $P_{out,1}$ generated by the injected current i_1 and we find by inspection of the equivalent circuit.

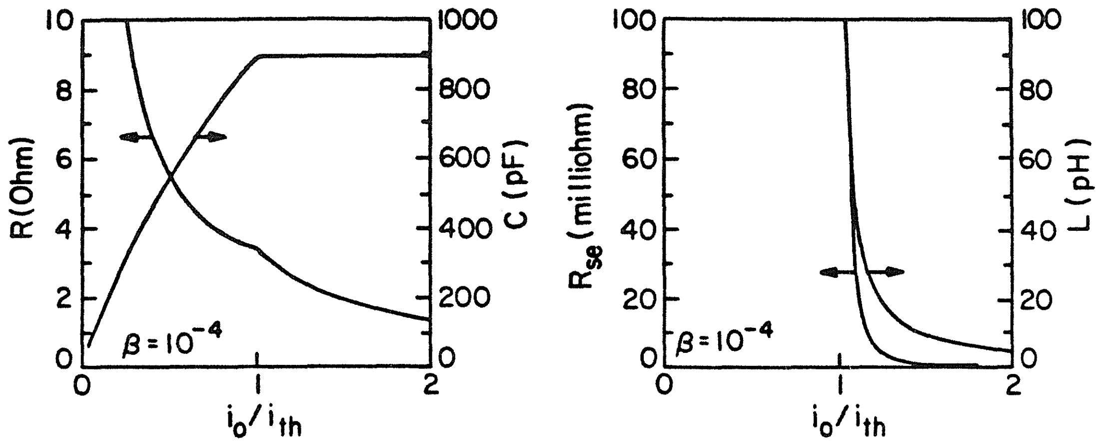

Figure 2.3.2. Numerical values of the elements of the equivalent circuit as function of the bias point i_0.

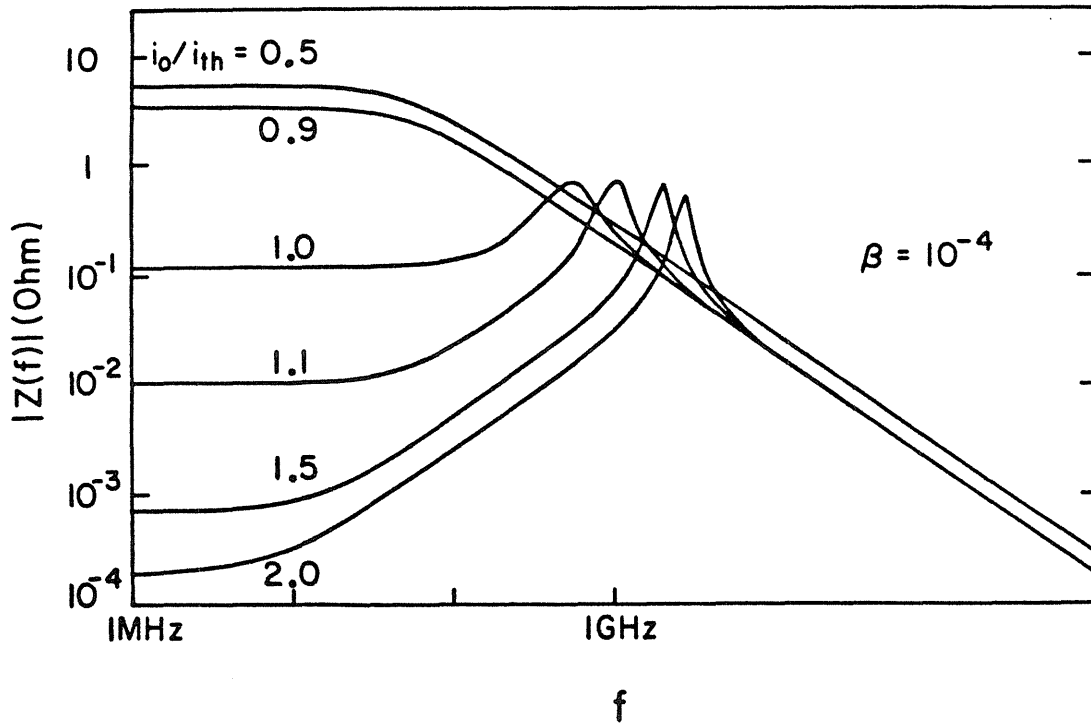

Figure 2.3.3. Input impedance of the intrinsic laser diode as function of the frequency for different bias currents i_0.

$$T(s) \equiv \frac{P_{out,1}(s)}{i_1(s)} = \frac{K}{s^2 + s\frac{\omega_r}{q_r} + \omega_r^2} \tag{2.3.27}$$

$$K \approx \frac{1}{2}\frac{\hbar\omega}{e}\frac{Ap_0}{\tau_p}\frac{\frac{1}{L}\ln(\frac{1}{R})}{\alpha + \frac{1}{L}\ln(\frac{1}{R})}$$

This transfer characteristic has the form of a second order lowpass and the modulation efficiency drops drastically above ω_r. For most applications the useful small signal modulation bandwidth is therefore limited to frequencies below ω_r, the relaxation frequency. In the next chapter we will discuss methods to push ω_r through clever device design towards higher frequencies and we will try to outline fundamental limits. It will turn out that parasitic elements such as the contact resistance, bondwire inductance and capacitance play an important role in the overall modulation response and we will make extensive use of the equivalent circuit augmented with the parasitic elements to evaluate different driving circuits.

2.4 References

1. H. Statz, G. deMars, " Quantum Electronics", edited by C. H. Townes, Columbia University (1960).

2. M. Morishita, T. Ohmi, J. Nishizawa, Solid-State Electron., vol. 22, p. 951 (1979).

3. J. Katz, S. Margalit, Ch. Harder, D. Wilt, A. Yariv, IEEE J. Quantum Electron., vol. 17, p. 4 (1981).

4. Ch. Harder, J. Katz, S. Margalit, J. Shacham, A. Yariv, IEEE J. Quantum Electron., vol. 18, p. 333 (1982).

5. K. Y. Lau, A. Yariv, " Semiconductors and Semimetals", edited by W. T. Tsang, Academic Press, New York (1983).

6. K. Y. Lau, thesis, California Institute of Technology, Pasadena (1981).

7. D. P. Wilt, thesis, California Institute of Technology, Pasadena (1981).

8. J. B. Moreno, J. Appl. Phys., vol. 48, p. 4152 (1977).

9. K. Y. Lau, A. Yariv, Appl. Phys. Lett., vol. 40, p. 452 (1982).

10. K. Y. Lau, I. Ury, N. Bar-Chaim, Ch. Harder, A. Yariv, to be published in Appl. Phys. Lett.

11. D. P. Wilt, K. Y. Lau, A. Yariv, J. Appl. Phys., vol. 52, p. 4790 (1981).

12. D. E. McCumber, Phys. Rev., vol. 141, p. 306 (1966).

13. A. Yariv, S. Margalit, IEEE J. Quantum Electron., vol. 18, p. 1831 (1982).

14. Y. Suematsu, K. Furuya, Trans. IECE Japan, vol. E60, p. 467 (1977).

15. K. Peterman, IEEE J. Quantum Electron., vol. 15, p. 566 (1979).

16. C. H. Henry, R. A. Logan, F. R. Merritt, J. Appl. Phys, vol. 51, p. 3042 (1980).

17. H. Kressel, J. K. Butler, " Semiconductor Lasers and Heterojunction LEDs", Academic Press, New York (1977).

18. W. B. Joyce, R. W. Dixon, Appl. Phys. Lett., vol. 31, p. 354 (1977).

Chapter 3

High speed modulation

3.1. Introduction

The ability to modulate GaAlAs laser diodes directly by modulating the pump current at frequencies up to a few GHz opens up important applications such as transmission of microwave signals through optical fibers [1]. From the analysis of the previous chapter it is clear that the useful *small signal modulation frequency range* is limited to that below the relaxation resonance, which is typically around two to three GHz. In this chapter we will investigate at first how one can try to get around this limitation by using *nonlinear transient effects* , i.e. by injecting huge current pulses into the laser diode. The simple rate equations suggest that arbitrarily short light pulses can be generated by injecting extremely short and intense current pulses into the laser diode. We will show experimentally that this is not true and that the shortest pulses which can be generated have a width on the order of 10ps. Clearly the simple rate equations are no longer valid on such a time scale.. Such pulse modulation schemes are also not very suitable for high bit rate communication systems since they have serious pattern effect (intersymbol interference) problems, which can only be overcome through a complex driving circuitry. However, the pulse modulation scheme is extremely useful to generate a train of short pulses (as short as 20 picoseconds), which can be used as a clocking signal to synchronize large systems.

The small signal modulation scheme does not suffer from these pattern effects and we will therefore concentrate in the second part of this chapter on this small signal modulation. The following questions will be addressed: How can one push the relaxation resonance towards higher frequencies, what are the practical limits, how should one design an optimized laser and what is the effect of parasitic elements such as the bondwire inductance, mount capacitance and contact resistance on the high speed performance.

3.2 Pulse modulation

In an attempt to overcome the basic limitations of the maximum bit rate of semiconductor lasers as predicted by the small signal analysis, nonlinear transient effects are considered as potentionally useful. In the small signal modulation scheme great care is taken to choose a modulation depth which is small enough to avoid nonlinear transients. The opposite is true for pulse modulation, i.e. the laser is initially biased well below threshold and a current pulse is injected to switch the laser on. Pulses in the picosecond range (15ps to 30ps) have been obtained by microwave current injection [2] and by pumping the laser with short, intense electrical pulses [3]. We do not attempt to present here an analysis of this pulse generation scheme since this has already been done [4], [5] but we will try to give an intuitive explanation to how these pulses are generated. We will show how short optical pulses generated by injecting current pulses to a laser diode can be used to calibrate our photodiodes for the following measurements.

A common feature in all these pulse generation schemes is that the laser is initially biased below the threshold current. The optical pulse is generated by abruptly injecting a huge current pulse into the diode. The carrier density rises and the round trip gain for the light in the laser cavity increases rapidly to a

value well above one. The lasing field builds up exponentially starting out from spontaneous emission and it takes a delay time (corresponding to a few round trips) for the stimulated emission to reach a rate large enough to deplete the gain. The condition for short optical pulses is essentially that the electrical pulse is shorter than the delay time of the laser, i.e. when the stimulated transitions deplete the gain, the pumping process has already been terminated. The stimulated emission depletes the inversion in a few round trip times and the light pulse can therefore be very short. Since these optical pulses are too short to be measured with a photodiode the pulsewidth must be obtained by other techniques. The width can be estimated from an autocorrelation measurement which is done in a standard way employing phase matched second harmonic generation in a $LiIO_3$ crystal [6]. This measurement system, built in our laboratory is shown in chapter five, Fig. 5.2.1. Short optical pulses are generated in this experiment with a Mitsubishi TJS laser which is biased below threshold. A train of current pulses at a repetition rate of 100MHz generated with a step recovery diode (comb-generator HP 33002A) is superimposed through a microwave bias network (HP 33150A). The current pulses have a FWHM of around 120ps; bias current and pulse amplitude are adjusted to obtain light pulses as short as possible. Fig. 3.2.1 shows a typical SHG trace which consists of a broad peak with a FWHM of around 50ps with a periodic substucture with a period of 5.5ps, corresponding to a multiple echo spaced by the round trip time in the laser cavity of 190 μm length, or, in the frequency space, due to beating of the different longitudinal modes which are spaced by 182 GHz. Assuming exponential shape this second harmonic trace corresponds to a pulse width of $\tau = \frac{50ps}{\sqrt{2}} = 35ps$ [6].

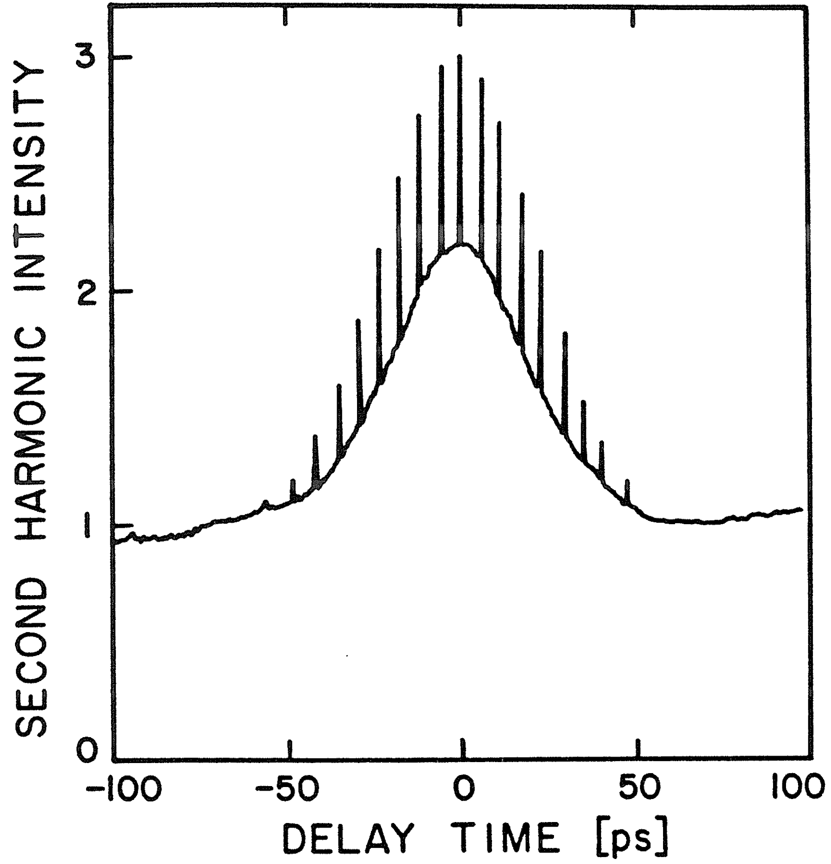

Figure 3.2.1. Autocorrelation trace of a TJS laser driven by current pulses. The FWHM of this pulse is τ = 35ps.

It is relatively easy to generate short pulses by this method and one is tempted to extrapolate communication systems based on this principle with a bit rate of $\frac{1}{\tau} \approx$ 30Gbit/s. This is impossible for three reasons. First, there is a finite time delay between the onset of the current pulse and the turn on of the laser. This time delay could be made shorter by increasing the current pulse amplitude which is a problem since such sources are not readily available. Second, the laser returns slowly back to its initial condition after each pulse, typically within the spontaneous lifetime of the carriers, which is in the order of one nanosecond. Placing the pulses closer together than the spontaneous lifetime causes the amplitude of one pulse to depend on the amplitude of the previous pulse. Since the information is encoded in the amplitude of the pulses this pattern effect causes intersymbol interference. Several methods have been devised to overcome this limitation; Danielson [4] suggested that it is possible by carefully adjusting the modulating current pulse to make the conditions at the end of the pulse equal to the prepulse level; a method which requires extremely fine control of the current pulse. This requirement can be eased in the bipolar pulsing scheme [5] where each current pulse is followed by a negative going swing which forces the laser back to its initial condition. Third, pulsed lasers operate in a transient regime and their optical spectrum is very wide; the light is emitted into several longitudinal modes and due to chromatic dispersion in fibers this modulation scheme cannot be used for long distance communication. However, a train of optical pulses can be extremely useful as an optical clock to synchronize a system.

One would like to know if the light pulses generated by this scheme can be made much shorter by pumping the laser with shorter and more intense current pulses. This has not been investigated since such current sources are

not readily available and the problem cannot be easily analyzed since it is not clear if the rate equations still hold on a time scale of a few round trips. To investigate this problem we fabricated a buried heterostructure laser with a transparent contact as shown in Fig. 3.2.2 and pumped the active region optically with sub picosecond pulses. The experiments and an analysis have been published by Koch, Chiu, Harder and Yariv [7], and we state here only the results and the conclusions. The laser used in this experiment is $80\mu m$ long and pumped optically within a picosecond from no bias to an estimated carrier density of $\approx 10^{19} cm^{-3}$. The laser emitts a light pulse with a wide spectrum. The output at short wavelengths ($\lambda \approx 700nm$) is shown in Fig. 3.2.3, the pulse has a FWHM of 1.2ps. The output at long wavelengths is shown in Fig. 3.2.4, it consists of a primary peak with a FWHM of around 20ps followed by a secondary peak. This secondary peak is probably due to intervalley scattering of the carriers [7]. We conclude from these experiments that optical pulses generated by an ultrashort pumping pulse injection scheme cannot be made arbitrarily short. The ultimate pulse performance is limited by intervalley scattering and electron heating effects to around 10ps to 20ps and other methods, such as passive or active mode locking have to be used to generate shorter pulses.

3.3 Photodiode calibration

A photodiode is an efficient and simple quadratic detector of the optical field [8], its output is a photocurrent which is proportional to the flux of photons which fall on the detector area. In avalanche photodiodes the carriers generated by the internal photoeffect are multiplied in a high field region in the diode through impact ionization and these avalanche photodiodes have therefore a much higher sensitivity. The gain-bandwidth product of this avalanche amplification process can be very large, the silicon avalanche photodiode we use

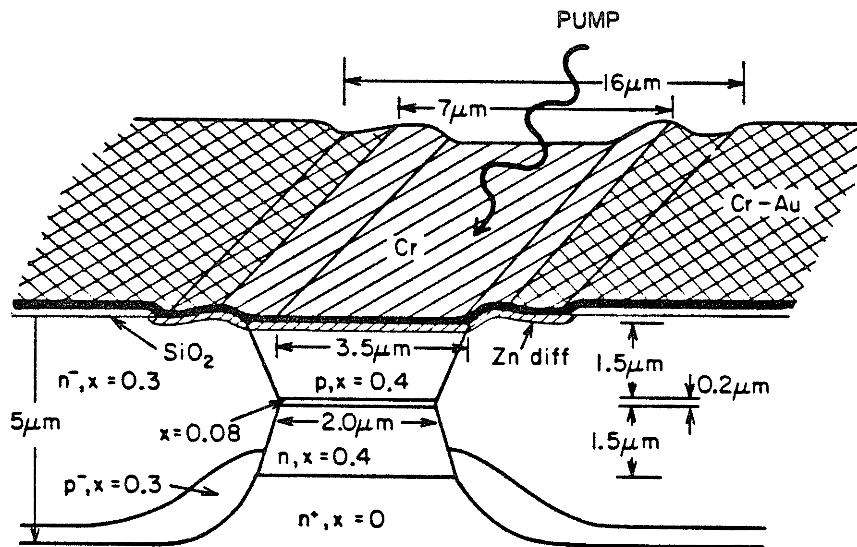

Figure 3.2.2. Geometry of a buried heterostructure laser with a transparent contact. This laser can be pumped electrically or optically.

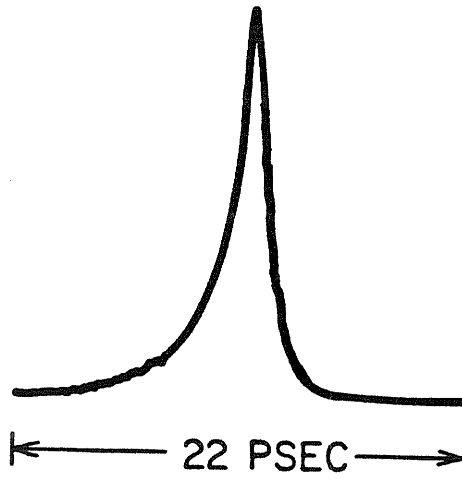

Figure 3.2.3. Short wavelength BH laser output under high pumping conditions. The pulse FWHM is 1.2ps.

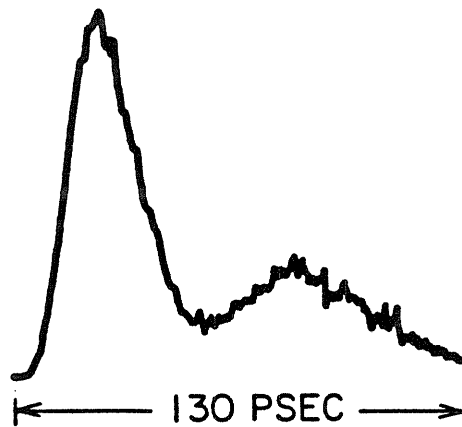

Figure 3.2.4. Long wavelength BH laser output under high pumping conditions. Primary peak of the pulse has a FWHM of 21.6ps.

has a quantum efficiency of 20% at $\lambda = 910nm$ and a gain-bandwidth product of 200GHz (AEG Telefunken S171P). The photodiode is operated in a mount of our own design and is, depending on the specific experiment, ac-coupled or dc-coupled to the microwave measurement equipment. Laser diodes as well as the photodiode are connected through 50Ω coaxial cables and striplines to the microwave test station.

The equivalent circuit which we developed in chapter two consists of lumped circuit elements and we will augment it in this chapter with lumped parasitic impedances. This modeling is correct since the geometric size of the whole circuit is much smaller than a wavelength of the electrical signal, i.e. 3cm at 10GHz. However it is impossible to measure these impedances at these high frequencies directly as the dimensions of the measurement system are too large. The only parameters which can be measured are the scattering parameters, i.e. s-parameters. Actually, we can only measure the s-parameters of the complete electro-optical system between the reference planes 1 and 3, as shown in Fig. 3.3.1. We would like to measure the modulation response of the laser diode A_{mod} which is equal to the modulated optical power $P_{out,1}$ (at plane 2 in Fig. 3.3.1) divided by the injected drive current i_{in+}; $A_{mod} \equiv \frac{P_{out,1}}{i_{in+}}$. A microwave measurement yields the coefficients of the scattering matrix and together with a knowledge of the frequency response of the photodiode $T_{Ph} \equiv \frac{i_{Ph}}{P_{op}}$ we find the modulation response of the laser, $A_{mod} = -\frac{s_{21}}{\kappa\, T_{Ph}}$. Usually we are only interested in the absolute value of the modulation response and only rarely in the deviation from a linear phase response. In order to get rid of the coupling factor κ we very often normalize the frequency response to its value at low frequencies.

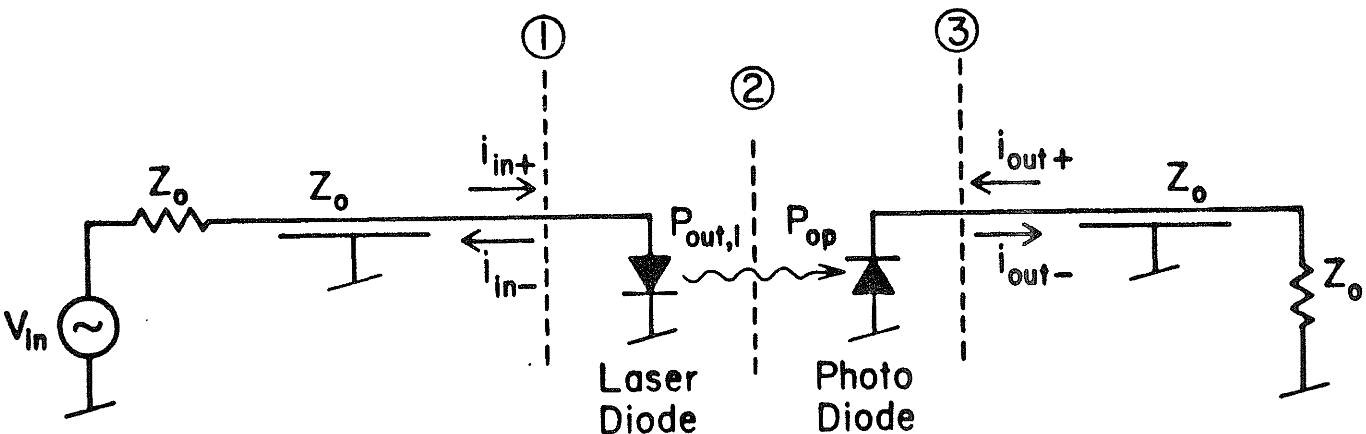

$$\kappa P_{out,l} = P_{op} \qquad i_{Ph} = i_{out-}$$

$$\begin{bmatrix} i_{in-} \\ i_{out-} \end{bmatrix} = -\begin{bmatrix} s_{11} & s_{12} \\ s_{21} & s_{22} \end{bmatrix} \begin{bmatrix} i_{in+} \\ i_{out+} \end{bmatrix}$$

$$s_{21} = -\left.\frac{i_{out-}}{i_{in+}}\right|_{i_{out+}=0}$$

$$s_{21} = -\kappa \frac{P_{out,l}}{i_{in+}} \frac{i_{out-}}{P_{op}} = -\kappa A_{mod} \cdot T_{Ph}$$

$$A_{mod} = \frac{P_{out,l}}{i_{in+}} \; ; \; T_{Ph} = \frac{i_{Ph}}{P_{op}}$$

Figure 3.3.1. Arrangement of the high frequency modulation measurement.

For a measurement of the laser response, the photodiode has to be calibrated exactly, which is a nontrivial task. The photodiode is calibrated with a train of light pulses generated through the pulse modulation scheme, as described above in section 3.2. The pulse length is around 35ps (as we measured with the autocorrelator described in section 3.2) and the pulses have therefore a flat spectrum up to frequencies in excess of 10GHz. In Fig. 3.3.2 the pulse response of the photodiode is shown on a sampling scope (Tektronix S-1, 25ps risetime). The photodiode risetime is around 180ps, FWHM of the pulse is around 250ps and this diode response has a diffusion tail which extends up to 1ns. The relative frequency response is obtained directly from the microwave analyzer. One additional measurement is made to obtain the frequency response down to dc (zero frequency). This dc calibration is of utmost importance for measurements where one has to know the exact relative modulation depth of the light emitted by the laser. The carefully obtained response of the photodiode together with the biasing cicuitry is plotted in Fig. 3.3.3, this calibration curve has an error of $\pm$1dB between dc and 3 GHz. The response does not depend on the avalanche multiplication factor as long as the avalanche gain is smaller than 40. The initial drop in the response during the first few hundred megahertz is due to the diffusion tail and the resonance around 400 MHz is due to the biasing circuitry.

For clarity, the six most important modulation responses, which we will use very often, are summarized: The intrinsic laser response $T \equiv \frac{P_{out,1}}{i_1}$, the current injection ratio $R_i \equiv \frac{i_1}{i_{in+}}$, the overall laser response $A_{mod} \equiv |\frac{P_{out,1}}{\text{input signal}}|$ (this response is very often normalized with respect to its value at low frequencies), the scattering parameter $s_{21} \equiv -\frac{i_{out-}}{i_{in+}}$, $s_{11} \equiv -\frac{i_{in-}}{i_{in+}}$, and the photodiode

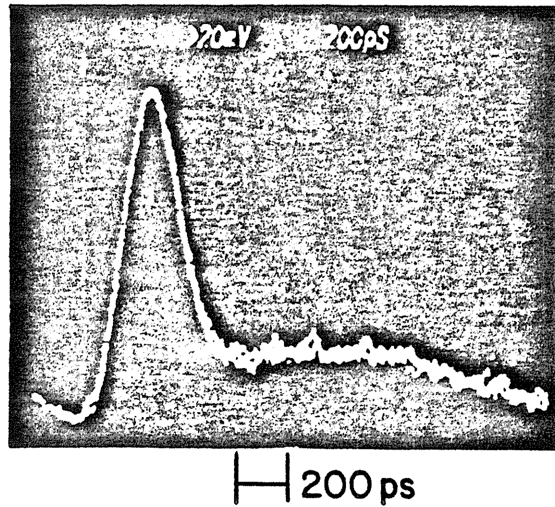

Figure 3.3.2. Pulse response of a silicon avalanche photodiode (AEG-Telefunken S171P). The risetime is 180ps, FWHM is 250ps and the diffusion tail extends up to 1ns.

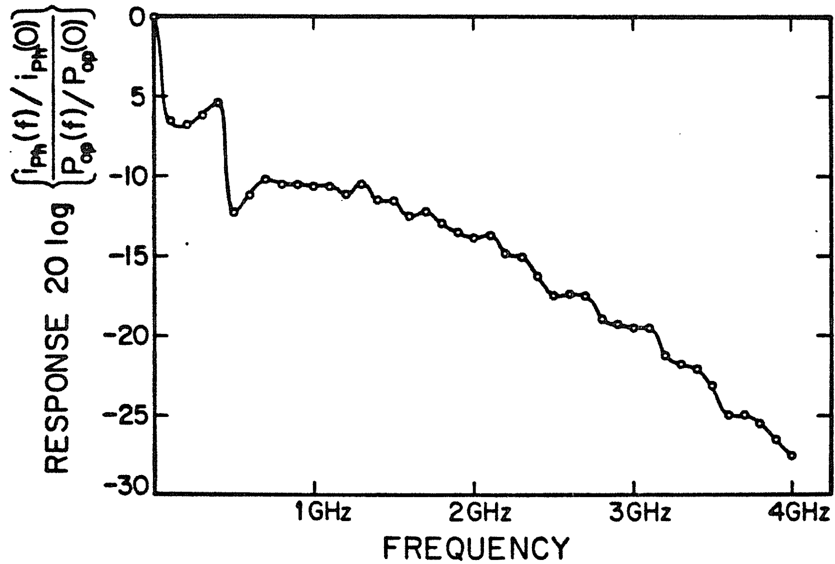

Figure 3.3.3. Frequency response of a photodiode (AEG-Telefunken S171P) from dc to 4GHz.

response $T_{Ph} \equiv \frac{i_{Ph}}{P_{op}} = \frac{i_{out-}}{P_{out,1}\,\kappa}$, κ is equal to the relative amount of laser light which is captured by the photodiode.

3.4 Optimizing of the small signal modulation bandwidth

The practical direct modulation bandwidth of semiconductor lasers is commonly accepted to be in the lower GHz range ($\lesssim$ 2GHz). Recent experimental work [9] has shown that a modulation bandwidth of 4-5 GHz is possible in a number of common laser structures. However, achieving that kind of modulation bandwidth requires that the lasers be biased at a level well above their nominal ratings, dangerously close to the point of castatrophic damage. Previous work emphasized more the investigation of the modulation characteristics of existing lasers than developing lasers with parameters optimized for high speed modulation. This section will place its emphasis on the latter. Experimental and theoretical results presented below show that modulation bandwidths in the X-band ($\gtrsim$ 10GHz) can be achieved with lasers operating reliably within the limits of their ratings, provided that a number of features are incorporated in the lasers. Among those features is the use of a short laser cavity, which is explicitly investigated in our experiments. The reason underlying the use of these features in high frequency lasers will be discussed.

The modulation bandwidth of semiconductor lasers is widely accepted to be equal to ν_r, the relaxation oscillation frequency, although it is well recognized that the relaxation resonance, whose magnitude varies considerably among lasers [9], [10], can limit the useful bandwidth to somewhat below ν_r. Nevertheless, as a standard for comparison, the modulation bandwidth is simply taken as ν_r. A small signal analysis of the common rate equations gives:

$$\omega_r = 2\pi\times\nu_r = \sqrt{\frac{\Gamma n_{tr}A\tau_p+1}{\tau_s\tau_p}(\frac{i_0}{i_{th}}-1)} \tag{3.4.1}$$

where i_0 and i_{th} are the pump current and the threshold current, τ_s and τ_p are the spontaneous carrier and photon lifetime, respectively, Γ is the optical confinement factor, A is the optical gain coefficient, and n_{tr} is the carrier density at which the material becomes transparent. Earlier work has often assumed that $\Gamma n_{tr}A\tau_p \ll 1$ [11], which is normally violated since $\Gamma n_{tr}A\tau_p$ is typically between one and three [12], [13]. This approximation also leads to numerical differences between measured and calculated values of ν_r [14], [15]. Equation (3.4.1) is not a very convenient form of expressing how ν_r depends on the intrinsic parameters A, τ_s and τ_p, since the quantity i_{th} in equation (3.4.1) also depends on these parameters. For instance, the suggestion that the modulation bandwidth can be increased by decreasing τ_s [16] is fallacious because this also increases i_{th}. A more desirable expression for the laser modulation bandwidth can be obtained by reconsidering the following rate equations:

$$\frac{dn}{dt} = \frac{i}{eVol} - Bn^2 - A(n-n_{tr})p \tag{3.4.2}$$

$$\frac{dp}{dt} = A(n-n_{tr})p\Gamma - \frac{p}{\tau_p} + \beta Bn^2\Gamma \tag{3.4.3}$$

where n and p are respectively the electron and photon densities, Vol is the active volume, B is the radiative recombination coefficient, and a stimulated transition rate linear in the carrier density is assumed [17], [18]; β is the fraction of the spontaneous emission entering the lasing mode, $\tau_p=1/v_{gr}(\alpha+\frac{1}{L}\ln\frac{1}{R})$ where v_{gr} is the group velocity of the light, α is the distributed loss, L is the length of the cavity and R is the mirror reflectivity. A standard small signal analysis of equation (3.4.2) and (3.4.3) (with the only approximation being $\beta \ll 1$) gives

$$\nu_r = \frac{1}{2\pi}\sqrt{\frac{Ap_0}{\tau_p}} \tag{3.4.4}$$

where p_0 is the steady state photon density in the active region. It is reassuring to see that we obtained exactly the same result in chapter two from the equivalent circuit. It is worthwhile to have a closer look at equation (3.4.4). Identical to the small signal analysis done in chapter two we make a small signal analysis of the rate equations (3.4.2) and (3.4.3) and assume that $\beta << 1$:

$$\frac{dn_1}{dt} = \frac{i_1}{eVol} - (2Bn_0+Ap_0)n_1 - A(n_0-n_{tr})p_1 \tag{3.4.5}$$

$$\frac{dp_1}{dt} = Ap_0\Gamma n_1 \tag{3.4.6}$$

We force $n_1(t)$ now to be a step function and we find from equation (3.4.6) that the photon density reacts with a time constant $\tau_1 = \frac{1}{Ap_0\Gamma}$ and from equation (3.4.5) we find that the carrier density n_1 reacts to a step function $p_1(t)$ with a time constant of $\tau_2 = \frac{1}{A(n_0-n_{tr})}$. The gain is clamped to $A(n_0-n_{tr}) = \frac{1}{\tau_p\Gamma}$ as can be seen from equation (3.4.3). The relaxation resonance is due to the interplay of these two time constants, $\nu_r = \frac{1}{2\pi}\sqrt{\frac{1}{\tau_1\tau_2}} = \frac{1}{2\pi}\sqrt{\frac{Ap_0}{\tau_p}}$.

Equation (3.4.4) suggests three obvious ways to increase the relaxation frequency, by increasing the optical gain coefficient or the photon density, or by decreasing the photon lifetime. The gain coefficient A can be increased roughly by a factor of five by cooling the laser from room temperature to 77K [13]. Biasing the laser at higher currents would increase the photon density in the active region, which simultaneously increases the optical output power density I_{out} according to :

$$I_{out} = \frac{1}{2} p_0 \hbar \omega v_{gr} \ln(\frac{1}{R}) \qquad (3.4.7)$$

Catastrophic mirror damage occurs at a power density of $I_{out,cat}$ = 1MW/cm^2 for a laser with a mirror reflectivity of R = 0.3 [17]. This sets an upper limit on the maximum permissible photon density, and hence the maximum modulation bandwidth. This limit can be increased considerably by using a window structure, such as the crank TJS [18], the window stripe [19], the window buried laser [20] or the window v-channeled substrate inner stripe laser [21].

The third way to increase the modulation bandwidth is to reduce the photon lifetime by decreasing the length of the laser cavity. Such a laser must be driven at higher current densities and thermal effects due to excessive heating will limit the maximum attainable modulation bandwidth. To illustrate these points the relaxation frequency as a function of the cavity length and the pump current density is plotted in Fig. 3.4.1a using equation (3.4.4) and the static solutions of equation (3.4.2) and (3.4.3). Also plotted in Fig. 3.4.1 is the power density at the mirror using equation (3.4.7). As an example, a common laser with a cavity length of 300 μm operating at an output optical power density of 0.8MW cm^{-2} possesses a bandwidth of 5.5GHz, and the corresponding pump current density is 3kA/cm^2. Operating at an identical power density, the bandwidth is 8GHz for a shorter laser with a cavity length of 100 μm, but the corresponding current density is 6kA/cm^2. Almost all lasers have such a geometry that the temperature rise in the active region is proportional to the current density and we will therefore use the current density as the second limiting factor in addition to the optical power output density. Some lasers (such as the TJS structures) have a different geometry and it has to be kept in mind that the limiting factor is actually just thermal heating. Figure 3.4.1.b shows plots of the same functions as in Fig 3.4.1.a but for a laser operating at liquid nitrogen

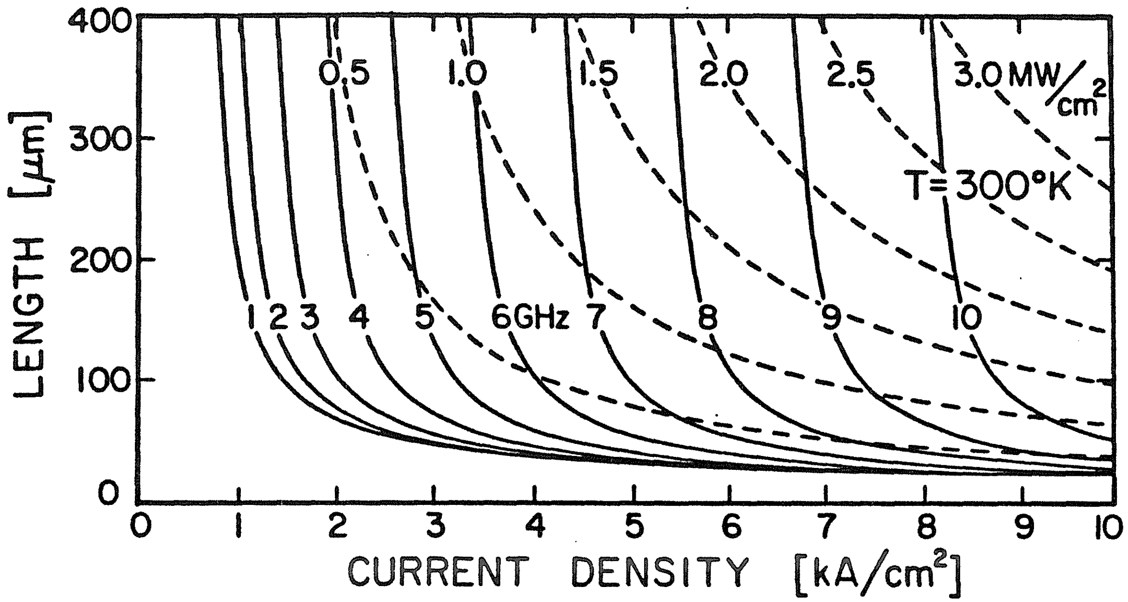

Figure 3.4.1a. Relaxation frequency ν_{rel} (solid lines) and optical power density outside the mirrors (dashed lines) as a function of the cavity length and pump current density at T=300 K. The following parameters are used: Active layer thickness = 0.15μm, $\alpha = 40\text{cm}^{-1}$, R = 0.34, $v_{gr} = 8\times10^{9}$ cm s^{-1}, $A = 2.56\times10^{-6}$ cm^{3}s^{-1}, $\Gamma = 0.5$, $n_{tr} = 1\times10^{18}$ cm^{-3}, $B = 1.5\times10^{-10}$ cm^{3}s^{-1}, $\hbar\omega = 1.5$eV, [13].

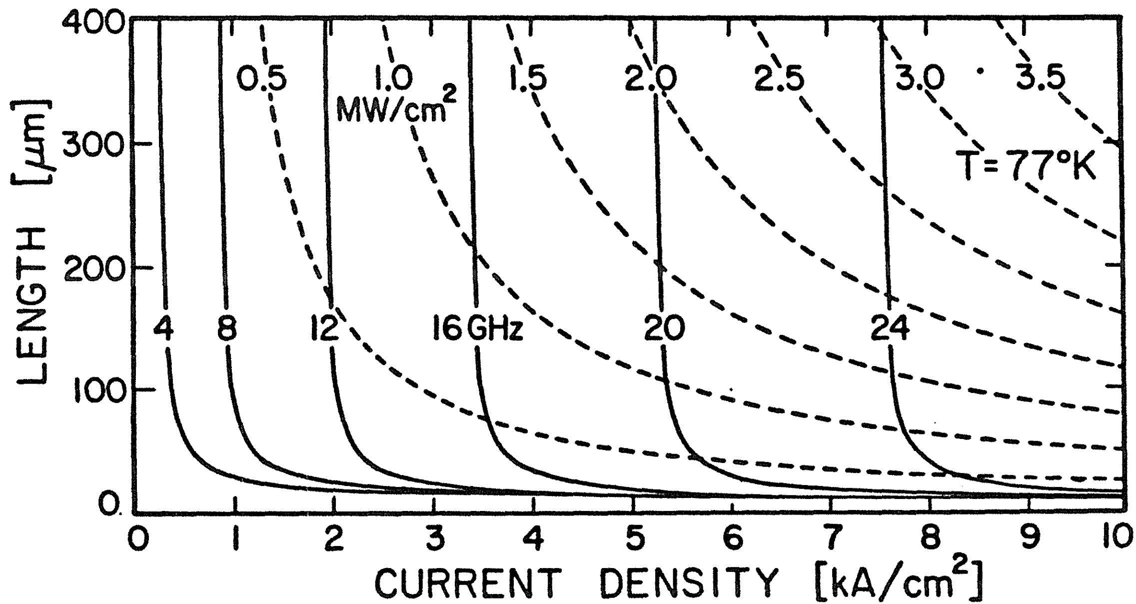

Figure 3.4.1b. Same as Fig. 3.4.1a but at T = 77K. The same parameters as in 3.4.1a are used except: $A = 1.45\times10^{-5}$ cm^{3}s^{-1}, $n_{tr} = 0.6\times10^{17}$ cm^{-3}, $B = 11\times10^{-10}$ cm^{3}s^{-1}, [13].

temperature. The increase in bandwidth is a direct result of the increase in A. It can be seen that a modulation bandwidth beyond 20 GHz can be achieved, however, incorporation of a short optical cavity and/or a window structure is imperative under these operating conditions.

Experiments have been performed to determine the modulation bandwidth achievable in a short-cavity laser. The lasers used were buried heterostructure lasers fabricated on a semi-insulating substrate (BH on SI) [22]. In addition to a low lasing threshold (typically $\leq$ 15mA) which is necessary to avoid excessive heating when operated high above threshold, these lasers possess very low parasitic capacitance [23] which otherwise would obscure modulation effects at high frequencies ($\gtrsim$ 5GHz). The lasers were mounted on a 50 Ω stripeline. A sweep oscillator (Hp8350) was used in conjunction with a network analyser (Hp8410 series) and a microwave s-parameter test-set (Hp8746B) to obtain the modulation data. The frequency response was obtained by normalizing the measured scattering parameter s_{21} with the photodiode response. We define the relative photodiode response in dB's as $20 \log \left| \frac{i_{Ph}(f)/i_{Ph}(0)}{P_{op}(f)/P_{op}(0)} \right|$ and the normalized laser response as $A_{mod} = \left| \frac{P_{out,1}(f)/P_{out,1}(0)}{i_{in+}(f)/i_{in+}(0)} \right|$. Figure 3.4.2a and 3.4.2b shows the cw light vs current characteristic of a short-cavity (120 μm) BH on SI laser, and the modulation responses at various bias points as indicated in Fig. 3.4.2a is shown in Fig. 3.4.2b. The modulation bandwidth can be pushed to beyond 8GHz as the catastrophic damage point is approached. Figure 3.4.3. shows the relaxation oscillation frequency of this laser as a function of $\sqrt{P_{out,0}}$ where $P_{out,0}$ is the output optical power, together with that of similar lasers with longer cavity lengths. All the lasers tested suffered catastrophic damage between 6-8 mW/facet. The advantage of a short-cavity laser in high frequency modulation is evident.

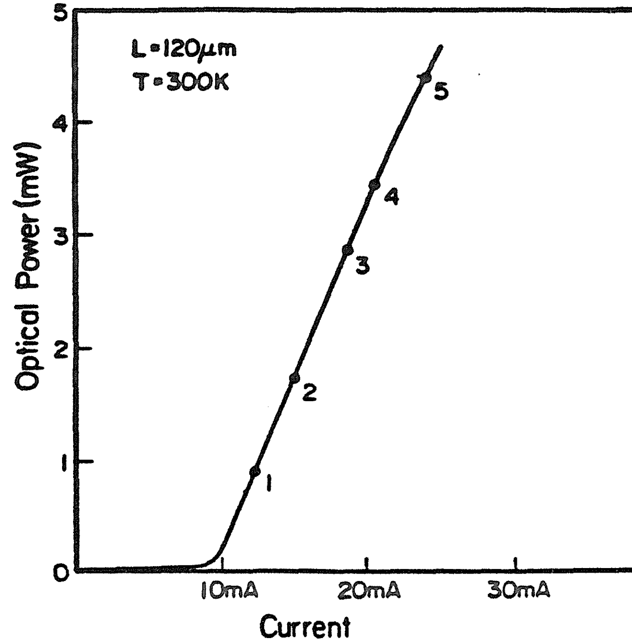

Figure 3.4.2a. Light current characteristic of a buried heterostructure (BH) laser on semiinsulating (SI) substrate. The length of the laser is L = 120μm. Modulation characteristics of this laser at various bias points indicated in the plot are shown in Fig. 3.4.2b.

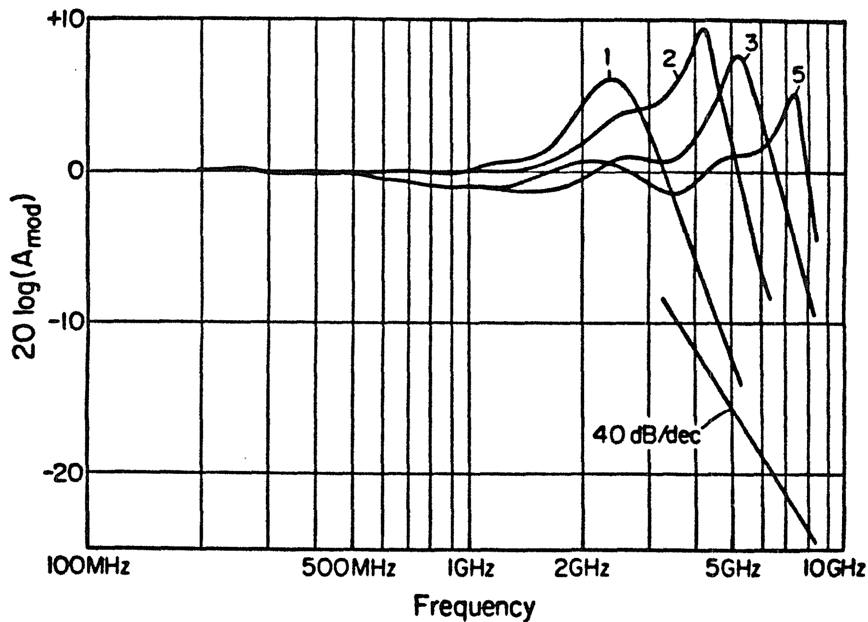

Figure 3.4.2b. The measured frequency response of a BH laser on SI substrate, $A_{mod} = \left| \frac{P_{out,1}(f)/P_{out,1}(0)}{i_{in+}(f)/i_{in+}(0)} \right|$.

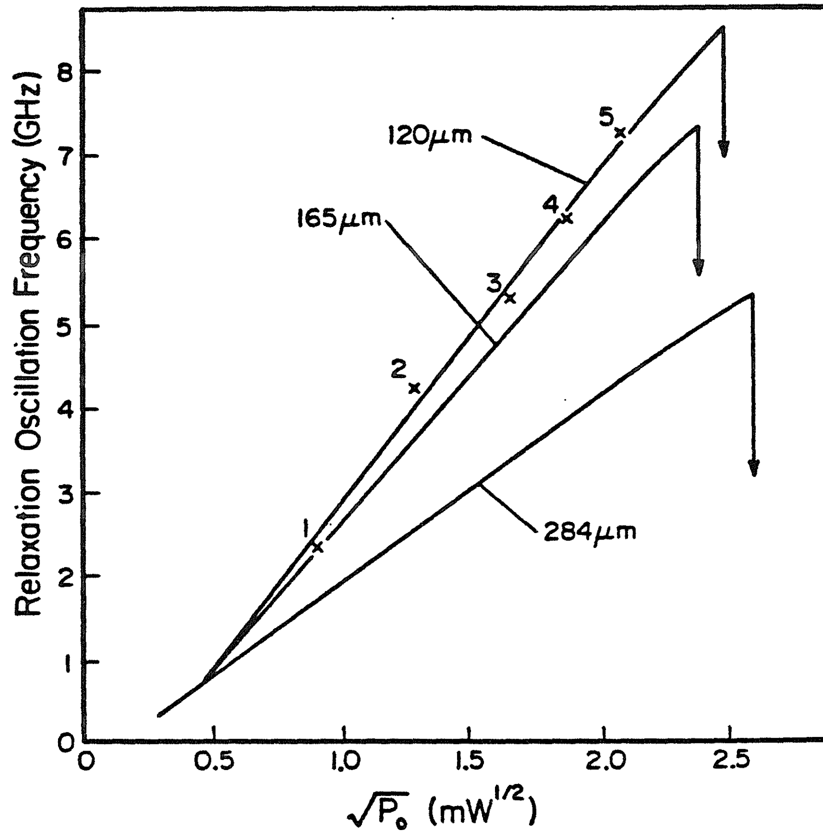

Figure 3.4.3. Measured relaxation oscillation resonance frequency of BH lasers on SI substrate of lasers of various cavity lengths, as a function of $\sqrt{P_0}$, where $P_0 \equiv P_{out,0}$ is the cw output optical power. The points of catastrophic damage are indicated by downward pointing arrows.

It is clear, from the above theoretical and experimental results, that an ideal high frequency laser should be one having a short cavity with a window structure, and preferably operating at low temperatures. This would shorten the photon lifetime, increase the intrinsic optical gain and the internal photon density without inflicting mirror damage. An absolute modulation bandwidth (at the point of catastrophic failure) of > 8GHz has already been observed in a 120 μm laser without any special window structure at room temperature. For reliable operation, however, the laser should be operated at only a fraction of its catastrophic failure power. That fraction depends on laser structure and amounts to 1/2 to 1/3 for commercial devices of comparable construction [24]. This would place the useful modulation bandwidth of these short-cavity BH lasers on semi-insulating substrate between 4.6 and 5.7 GHz [25]. The same laser at 77K without a window should have a modulation bandwidth of = 12GHz.

3.5 Parasitic elements and driving circuit considerations for high frequency modulation

A common source of concern when dealing with high frequency electronics is the adverse effects that parasitic elements might have on the device performance. Modulation of semiconductor laser diodes at high frequencies is no exception and some common problems that are not well understood are: Are the observed modulation characteristics due to the laser alone or are they due to parasitic elements? Will bond-wires limit the frequency response of laser diodes? Does one laser structure possess a larger parasitic capacitance than others? To answer these questions one must identify all the parasitic elements and, using the above developed equivalent circuit of the laser diode, calculate the degree to which these parasitic elements influence the modulation behavior. The substrate on which the laser diode is faricated is usually bonded to the

ground plane thus forming one electrical contact. The other electrical connection is made through a bondwire. This electrical interface can be modeled as a combination of inductors, capacitors and resistors. For a well constructed mount the capacitances and resistances can be neglected and the mount can be modeled as an inductor in series to the diode. The value of the bondwire inductance L depends not only on the length of the wire but also on its diameter and its proximity to the ground plane. A good wire bond is around 1mm long and has an inductance $L \approx 1nH$ and this value could be made smaller by using a bond ribbon instead of a bond wire. The parasitic elements are shown in Fig. 3.5.1 for three different typical classes of diode laser structures. The circuits of the first two classes, stripe (S) lasers and buried hetero (BH) structure lasers on conductive substrate have the same topology, but the values of the elements differ somewhat. The third type of laser, BH on semi-insulating (SI) substrate has a parasitic distributed capacitance in parallel which alters the modulation characteristics drastically. At first we will analyze the modulation characteristics of lasers on conductive substrate and later address the lasers on SI substrate.

Two different electrical driving circuits are used. Most often the diode lasers are driven directly from a 50Ω system as shown in Fig. 3.5.2a. The complete equivalent circuit of the laser diode as shown in Fig. 2.3.1 is substituted for the laser diode and the normalized transfer characteristic $A_{mod} = \left| \frac{P_{out,1}(f)/P_{out,1}(0)}{v(f)/v(0)} \right|$ is calculated using the network analysis program SPICE. The calculated response is plotted in Fig. 3.5.3 for four different combinations of the parasitic elements. It can be seen from Fig.3.5.3 that a contact resistance as large as $R_C = 20\Omega$ and a bondwire inductance as large as L=3nH do not have a significant influence on the modulation behavior. However a combi-

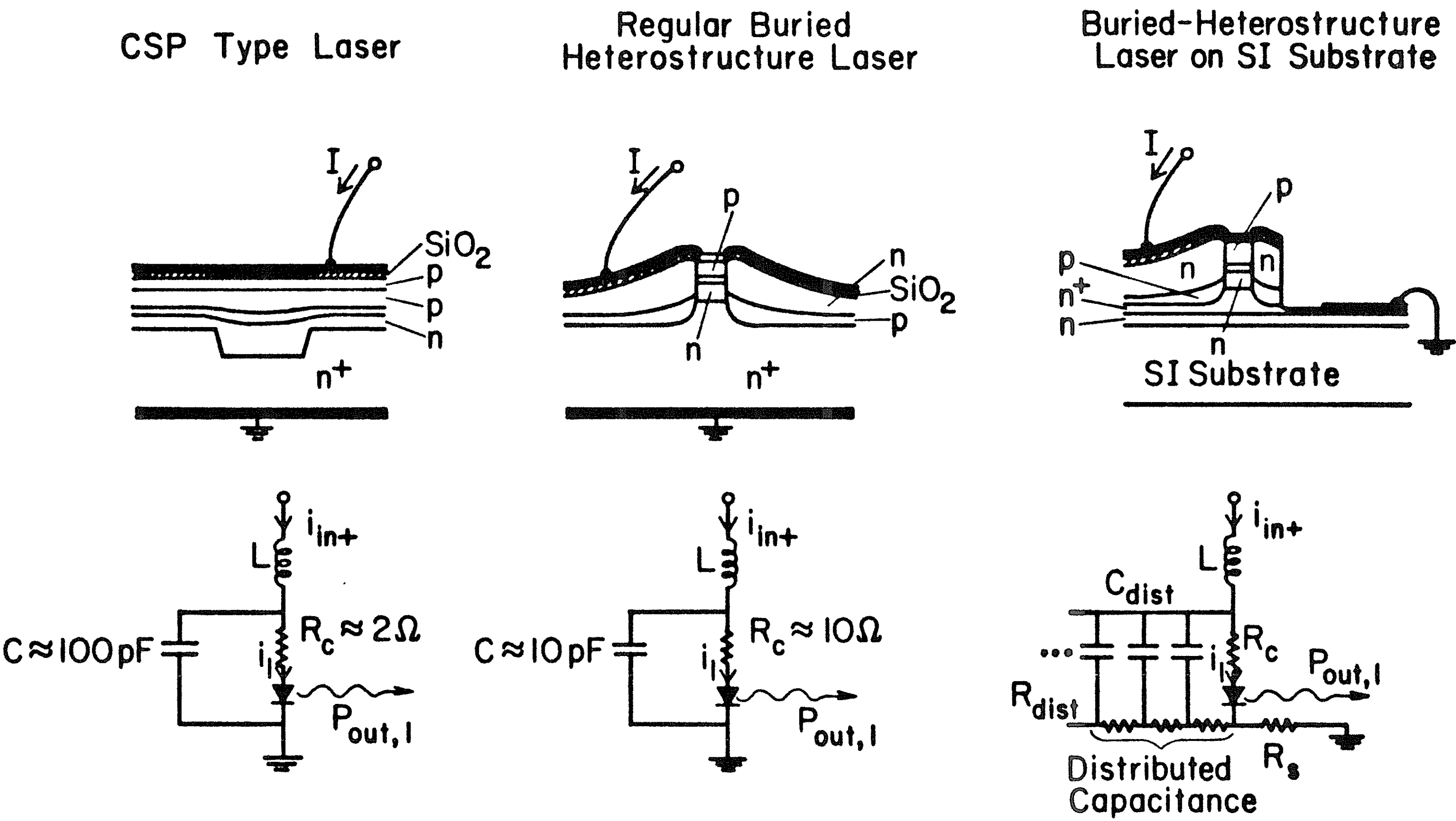

Figure 3.5.1. Comparison of parasitic elements in several laser structures: (a) CSP and other stripe-type geometry lasers on conductive substrate, (b) BH laser on conductive substrate, (c) BH laser on SI substrate.

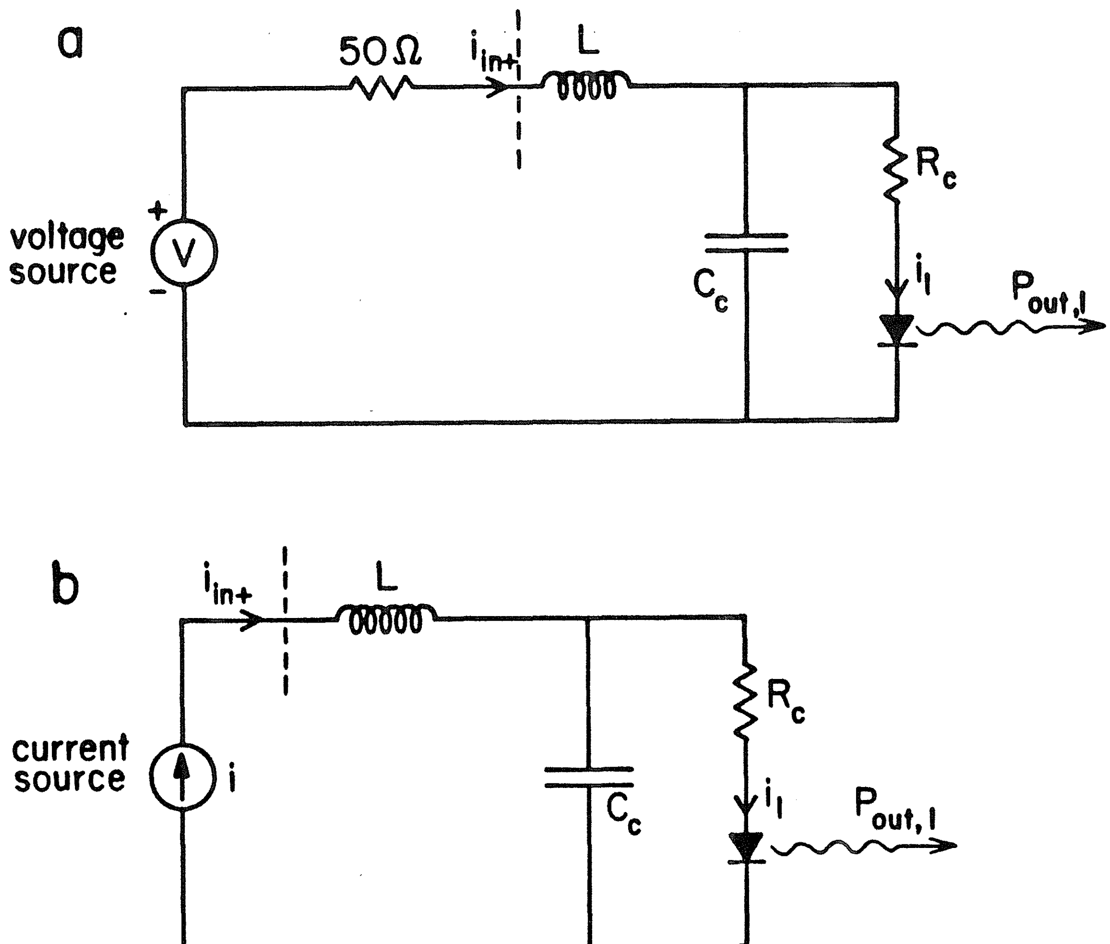

Figure 3.5.2. Equivalent circuit of a laser driven by: (a) 50Ω source, (b) current source.

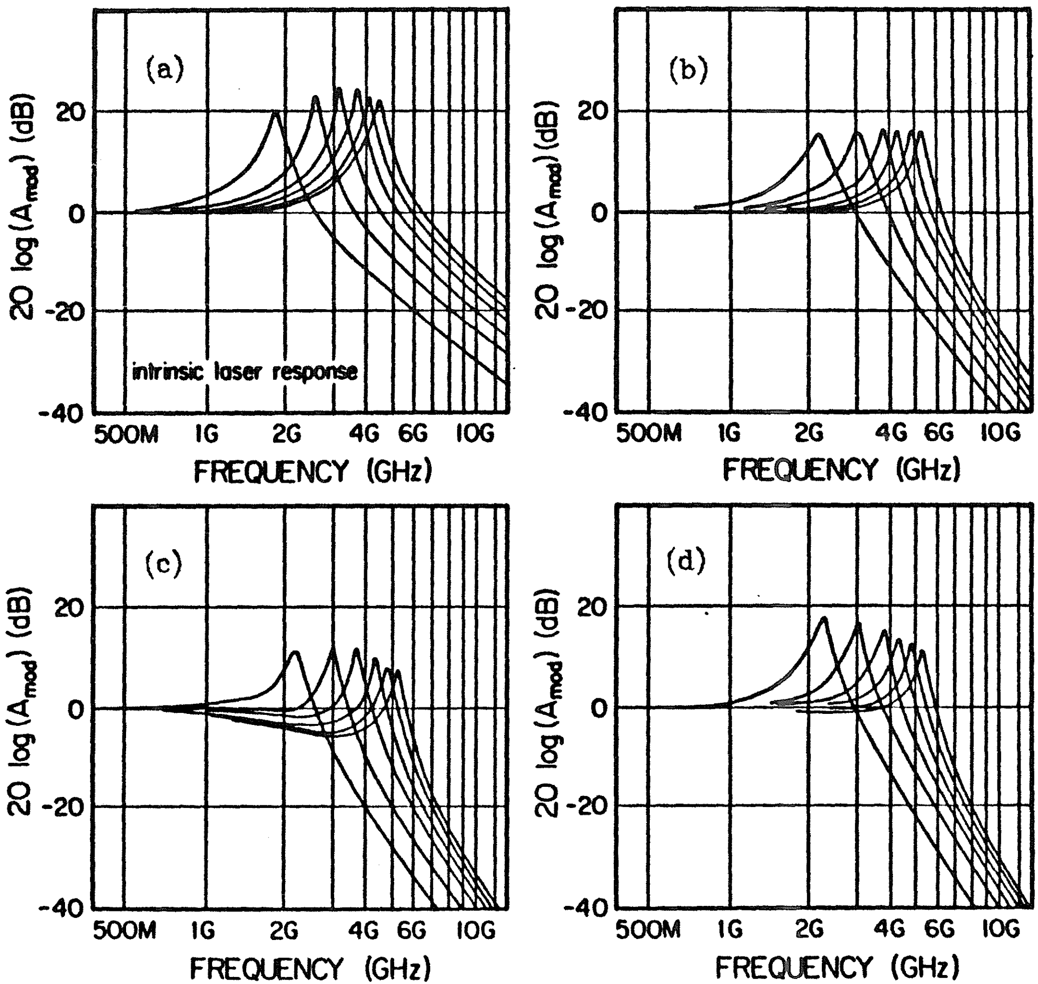

Figure 3.5.3. Simulated modulation response $A_{mod} = \left| \frac{P_{out,1}(f)/P_{out,1}(0)}{v(f)/v(0)} \right|$ of a laser driven by a 50Ω source at the biaspoints $i_0 = 1.2 \times i_{th}$, 1.4×, 1.6×, 1.8×, 2.0×, 2.2×. The effects of the parasitic elements are included: (a) intrinsic frequency response; (b) with parasitic elements (see Fig. 3.5.2), R_C =20Ω, L=1nH, C_C =3pF; (c) R_C =20Ω, L=1nH, C_C =10pF; (d) R_C =20Ω, L=3nH, C_C =3pF;

nation of a large contact resistance $R_C = 20\Omega$ and a large parasitic capacitance $C_C \geq 10pF$ causes a dip in the modulation response prior to the onset of the relaxation resonance (Fig. 3.5.3c). This effect has been observed experimentally [26].

In some experiments the lasers are driven by a MESFET, which is modeled (very simplified) as a current source (Fig. 3.5.2.b). If the MESFET is integrated with the laser diode monolithically, then, of course, there is no bondwire and L=0nH. The simulated response $A_{mod} = \left| \frac{P_{out,1}(f)/P_{out,1}(0)}{i(f)/i(0)} \right|$ is shown in Fig. 3.5.4. As expected the modulation response is much more sensitive to the shunt capacitance and a capacitance of $C_C = 10pF$ already severely influences the frequency response as can be seen in Fig. 3.5.4b. A small capacitance is thus seen to be imperative for high frequency modulation of a laser diode by a MESFET. This parasitic contact capacitance can be considerably decreased by constructing the laser on SI substrate, preferably monolithically with the MESFET and we will analyze the frequency response of the third class of lasers, buried heterostructure (BH) lasers on semi-insulating (SI) substrate. The major difference between the equivalent circuit of these lasers and other lasers is that the parasitic capacitance in the BH on SI laser is in the form of a distributed network, due to the particular geometry of this device. The resistance of the bottom n^+ contact layer provides an effective shielding of the capacitances far away from the junction, especially at high frequencies. Assume that the resistance per unit length of the bottom n^+ layer is R_{dist} and the parasitic capacitance per unit length between the top contact and the bottom n^+ layer is C_{dist}. Then, the effective impedance of the entire distributed RC ladder network is given by analogy to transmission line theory:

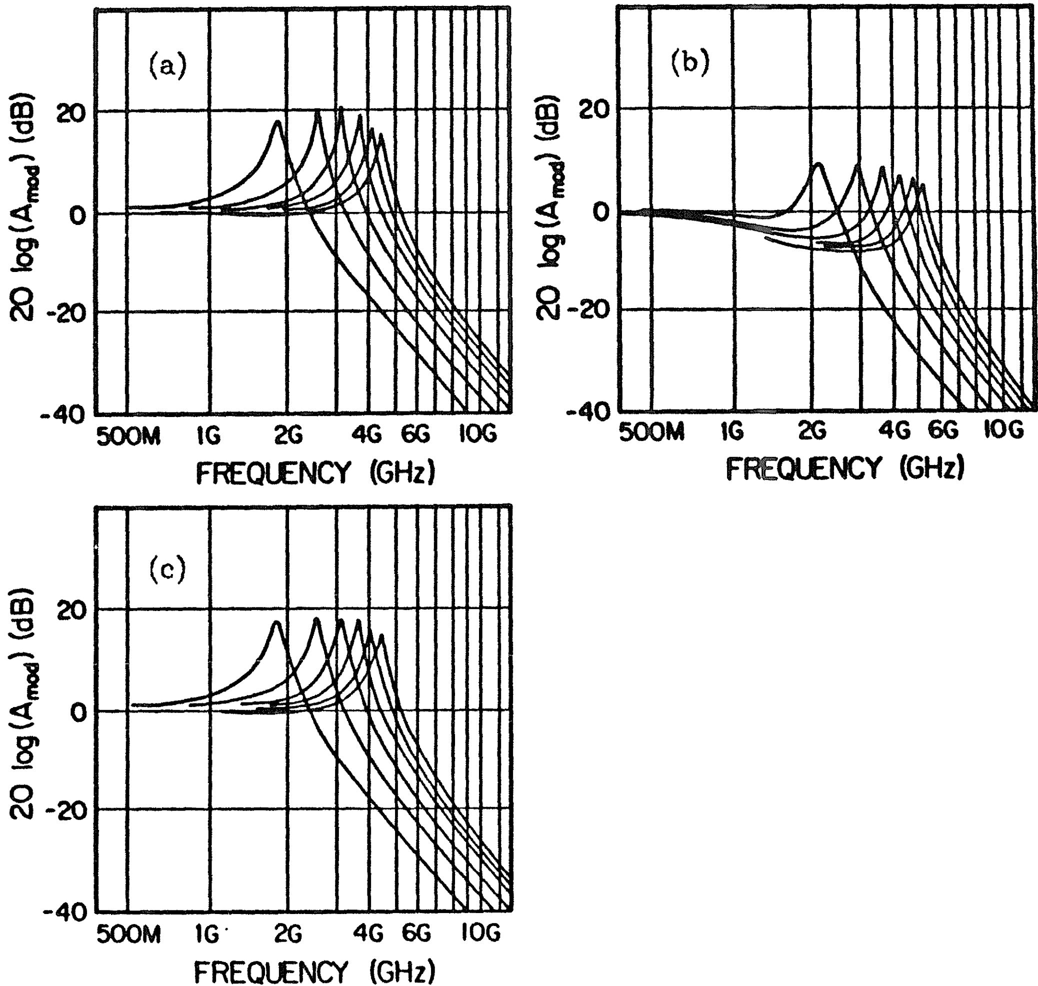

Figure 3.5.4. Simulated modulation response $A_{mod} = \left| \frac{P_{out,1}(f)/P_{out,1}(0)}{i(f)/i(0)} \right|$ of a laser driven by a current source at the biaspoints $i_0 = 1.2 \times i_{th}, 1.4\times, 1.6\times, 1.8\times, 2.0\times, 2.2\times$. The effects of the parasitic elements are included: (a) with parasitic elements (see Fig. 3.5.2), $R_C = 20\Omega$, L=1nH, C_C =3pF; (b) $R_C = 20\Omega$, L=1nH, C_C =10pF; (c) $R_C = 20\Omega$, L=3nH, C_C =3pF;

$$Z = Z_d \frac{1+e^{-2kW}}{1-e^{-2kW}} \tag{3.5.1}$$

where W is the width of the top contact, Z_d is the characteristic impedance of the ladder network:

$$Z_d = \sqrt{\frac{R_{dist}}{j\omega C_{dist}}} \tag{3.5.2}$$

and k is the "propagation constant":

$$k = \sqrt{j\omega R_{dist} C_{dist}} \tag{3.5.3}$$

At very high frequencies the real part of k is large with the physical significance that the voltage does not penetrate too far beyond the lasing junction. Capacitive elements "far away" do not charge up and consequently make negligible contributions to the parasitics. The total impedance of the distributed network is Z_d in this limit. To demonstrate that this distributed shunting network really exists, we calculate the reflection coefficient s_{11} and we compare it with a measurement taken from a BH laser on a SI substrate. The calculation fits very well the measurement as can be seen in Fig. 3.5.5. It is impossible to match the experimental s_{11} parameters without incorporating the distributed capacitance and resistance.

To illustrate the consequences of this distributed shunting network on the modulation response we assume that the laser is driven by a MESFET (a current source). Part of the input current is branched off to the distributed network. If the contact resistance is R_s, then the ratio of the current actually flowing through the laser i_l to the total input current i_{in+} (see Fig. 3.5.1) is simply $Z/(Z+R_s)$ where Z is given in equation (3.5.1). This injection ratio is plotted in Fig. 3.5.6 for several values of $R_{dist} \times W$ (= the total resistance of the n^+ bottom contact layer). It is assumed that $C_{dist} \times W$ = 5 pF (half of that of regular BH due

to a corresponding decrease in the size of the top contact) and $R_C = 15\Omega$. The case of $R_{dist} \times W = 0$ corresponds to a regular BH laser. For values of $R_{dist} \times W \gtrsim 60\ \Omega$, the drop in the injection ratio is less than 3 dB for frequencies as high as 5 GHz. The improvement over regular BH lasers, evident from Fig. 3.5.6, is supported by observations that little or no dip could be observed in the modulation response of the BH on SI lasers [25]

Another laser that has been fabricated on semi-insulating substrate is the transverse junction stripe laser (TJS) [26]. There is very little parasitic capacitance and the contact resistance is extremely small $R_C \approx 1\Omega$ in this laser compared with other lasers due to its particular geometry. This laser is therefore expected to be least affected by parasitic effects at high frequencies. This is supported by the fact that, like the BH on SI laser, little or no dip can be observed in the modulation characteristic of the TJS laser [27]. Assuming that TJS lasers possess zero parasitic capacitance, one can observe from Fig. 3.5.6 that the gain in modulation efficiency of the TJS laser over the BH on SI laser is no more than a few dB even at modulation frequencies as high as 10 GHz. Both lasers are thus suitable candidates for high frequency modulation.

Up to now we were only discussing the small signal problem and neglected completely the biasing questions. It is undesirable to supply the bias current through the high frequency circuit and the bias current through the diode is usually established with a biasing network (bias T) as shown in Fig. 3.5.7a. Such a bias T is awkward, expensive and it must be placed next to the laser (closer than the electrical wavelength λ) to prevent modulation response problems due to standing waves between the bias T and the laser. In Fig. 3.5.7b a much more elegant solution is presented, signal and bias current are supplied separately through a paralleled pair of MESFET's. The modulation of a MESFET at high frequencies is trivial since it is relatively easy to match the MESFET to the 50Ω line

IMPEDANCE OR ADMITTANCE COORDINATES

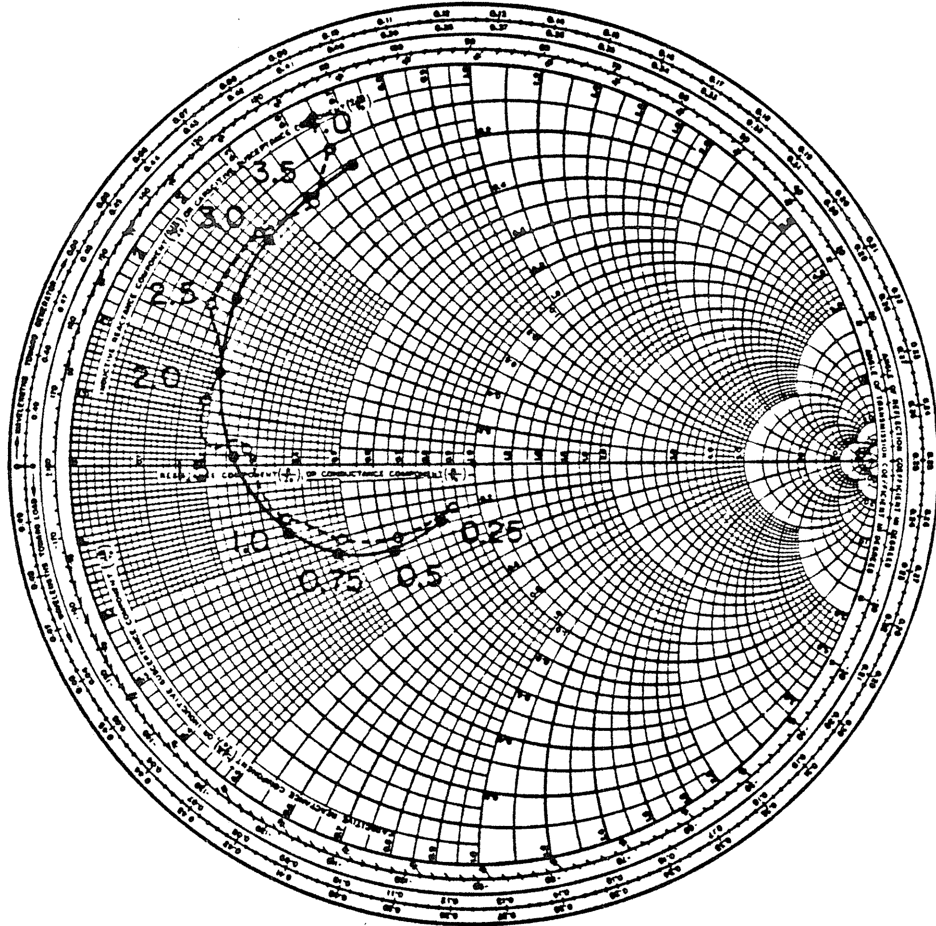

Figure 3.5.5. Electrical reflection coefficient s_{11} of a BH laser on SI substrate plotted on a Smith-Chart. The solid dots are calculated ones with $C_{dist} \times W = 5pF$, $R_{dist} \times W = 20\Omega$, $L = 1.2nH$, $R_s = 15\Omega$ at various frequencies as labelled on the chart (in GHz). The circles are measured ones.

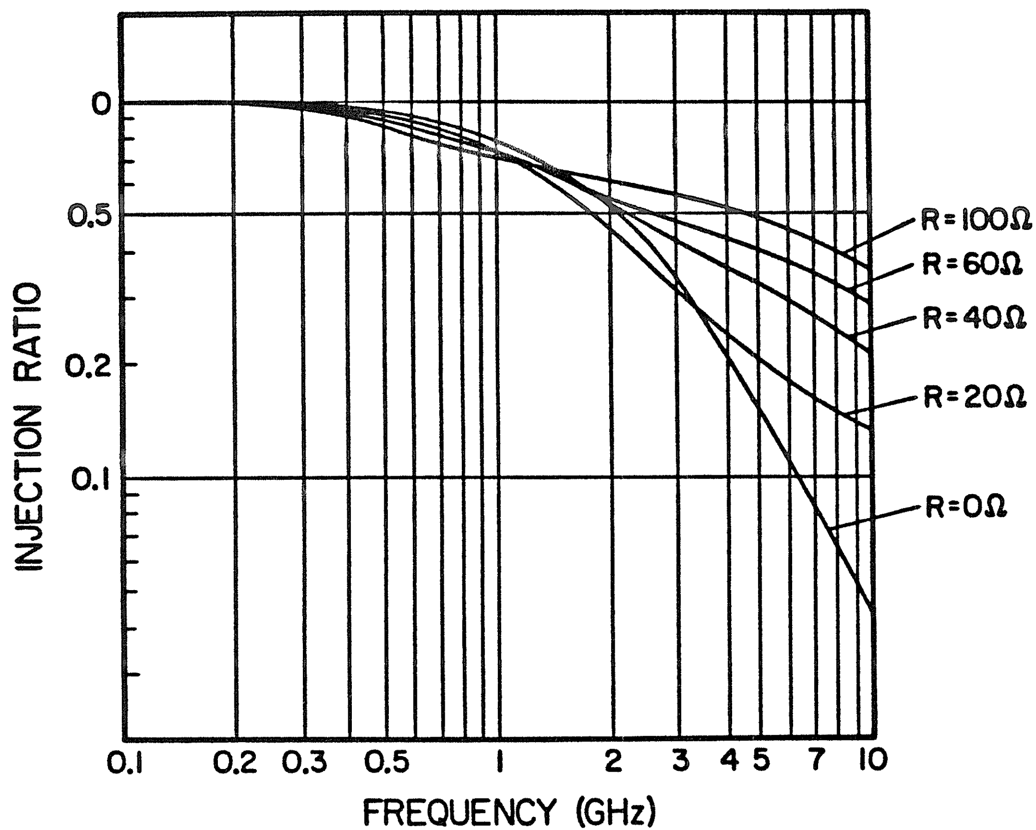

Figure 3.5.6. Current injection ratio $R_I = \left| \frac{i_1(f)}{i_{in+}(f)} \right|$ as a function of the frequency for different values of the distributed resistance, $R=R_{dist}\times W=100\Omega, 60\Omega, 40\Omega, 20\Omega$ and 0Ω, $R_C=15\Omega$. The case $R=0\Omega$ corresponds to a laser on conductive substrate.

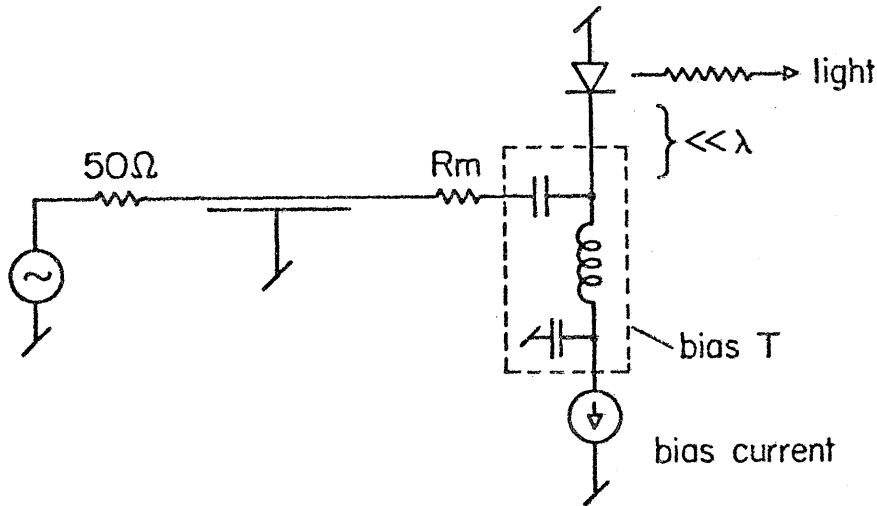

Figure 3.5.7a. Equivalent circuit of a laser which is biased through a bias T and driven from a 50Ω system. The resistor R_m is used to match the load to the 50Ω system.

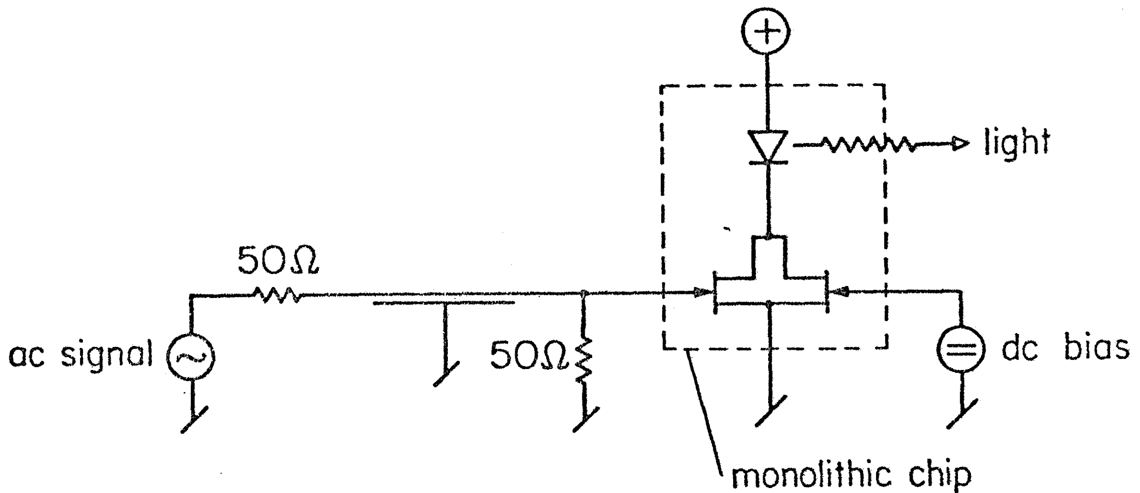

Figure 3.5.7b. Equivalent circuit of a laser with two MESFET's. One FET is suppling the bias current and the other FET adds the modulation current.

by shunting a 50Ω resistor from the gate to the ground. This driving circuit can be a hybrid one, or better, the MESFET's can be integrated monolithically with the laser on SI substrate.

To conclude this section, it appears that parasitic elements are not detrimental to high speed modulation of semiconductor lasers for frequencies up to ~ 3–4GHz. Lasers not specially designed for high frequency operation cannot operate above this frequency range anyway due to limitations such as heating and catastrophic mirror damage as described in section 3.4. We have shown that an optimized laser can be modulated at frequencies up to 10-20GHz (see Fig. 3.4.1). To be able to fully utilize this large bandwidth of the intrinsic laser it is important to design carefully the electrical driving circuit to keep the parasitics small. Two structures which have small parasitics are the BH laser on SI substrate and the TJS laser on SI substrate.

3.6 Outlook

We conclude this chapter by summarizing the results. The pulse modulation scheme of semiconductor lasers generates a train of ultrashort optical pulses. However, pattern effects are so severe that this pulse modulation scheme would seem useful only as a clock signal. The width of these pulses is ultimately limited by intervalley scattering and electron heating effects to around 20ps, and other methods such as passive or active mode locking must be used to generate a clock signal with shorter pulses. For optical communication purposes it is better to use the small signal modulation scheme. The diode lasers maintain useful modulation response as long as the modulation depth is not too large, i.e. as long as the carrier density in the active region is essentially clamped. Our experience is that even the spectrum remains essentially single mode up to several GHz modulation frequency as long as the modulation depth is smaller

than 90% as shown in Fig. 3.6.1. Such a large modulation depth is sufficient to transmitt digital data. Direct modulation rates in optimized laser diode structures of up to 8GHz have been observed, demonstrating the potential bit rate capacity of these solid state lasers [25].

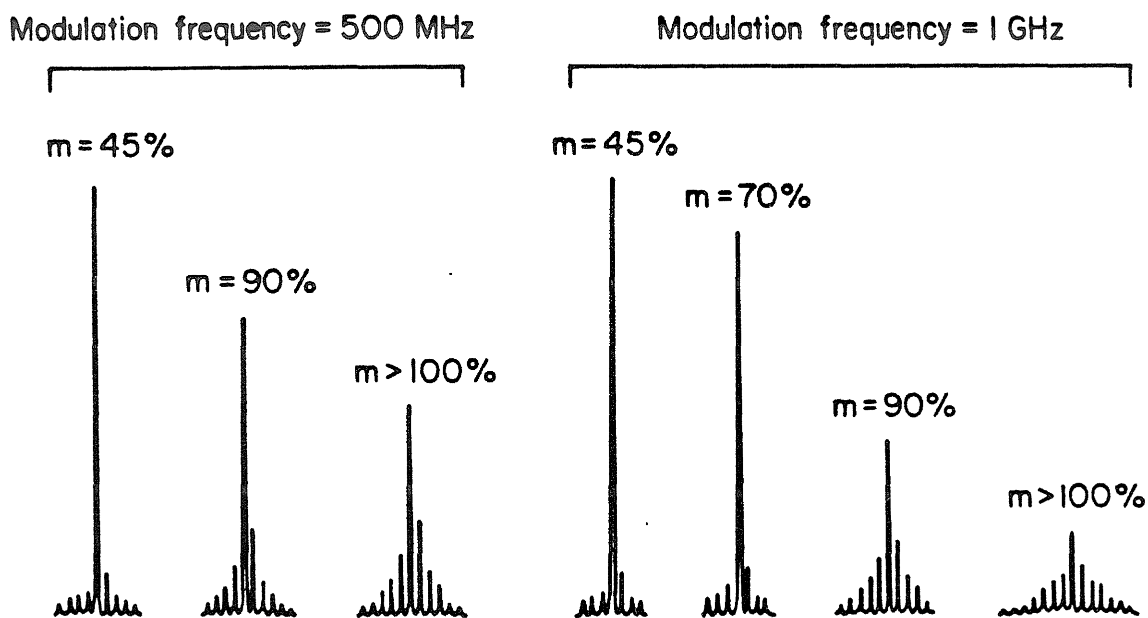

Figure 3.6.1. Time averaged longitudinal mode spectrum of a BH laser under modulation at various frequencies and modulation depths.

3.7 References

1. H. W. Yen, M. Barnoski, Appl. Phys. Lett., vol. 32, p. 182 (1978).
2. J. P. van der Ziel, R. A. Logan, IEEE J. Quantum Electron., vol. 18, p. 1340 (1982).
3. P. L. Liu, C. Lin, I. P. Kaminow, J. J. Hsieh, IEEE J. Quantum Electron., vol. 17, p. 671 (1981).
4. M. Danielsen, IEEE J. Quantum Electron., vol. 12, p. 657 (1976).
5. K. Y. Lau, thesis, California Institute of Technology, (Pasadena 1981).
6. E. P. Ippen, C. V. Shank, 'Picosecond Phenomena ", edited by S. L. Shapiro (Springer, New York 1978).
7. T. L. Koch, L. C. Chiu, Ch. Harder, A. Yariv, Appl. Phys. Lett., vol. 41, p. 6 (1982).
8. H. Melchior, 'Laser Handbook", edited by F. T. Arecchi, E. O. Schulz-DuBois (North-Holland Publ. Co., Amsterdam 1972).
9. L. Figueroa, C. Slayman and H.W. Yen, IEEE J. Quant. Electron., vol. 18, p. 1718 (1982).
10. K.Y. Lau and A. Yariv, Appl. Phys. Lett., vol. 40, p. 452 (1982).
11. H. Kressel and J. K. Butler, " Semiconductor Lasers and Heterojunction LED's", Academic, New York (1975).
12. C. H. Henry, R. A. Logan, F. R. Merritt, J. Appl. Phys., vol. 51, p. 3042 (1980).
13. F. Stern, J. Appl. Phys., vol. 47, p. 5382 (1976).
14. S.I. Gonda and S. Mukai, IEEE J. Quant. Electron., vol. 11, p. 545 (1975).
15. T. L. Paoli, Appl. Phys. Lett., vol. 39, p. 522 (1982).

16. K.J. Ebeling, L.A. Coldren, B.I. Miller and J.A. Rentschler, Appl. Phys. Lett., vol. 42, p. 6 (1983).

17. K. W. Wakao, N. Takagi, K. Shima, K. Hanamitsu, K. Hori, M. Takusagawa, Appl. Phys. Lett., vol. 41, p. 1113 (1982).

18. S. Takamiya, Y. Serwa, T. Tanaka, T. Sogo, H. Namizaki, W. Susaki, K. Shirahata, 7 th International Semiconductor Laser Conference, paper 8, London, 1980.

19. H. O. Yonezu, M. Ueno, T. Kamejima, I. Hayashi, IEEE J. Quant. Electron., vol. 15, p. 775 (1979).

20. H. Blauvelt, S. Margalit, A. Yariv, Appl. Phys. Lett., vol. 40, p. 1029 (1982).

21. Y. Yamamoto, H. Hayashi, T. Hayakawa, N. Miyauchi, S. Yano, T. Hijikata, Appl. Phys. Lett., vol. 42, p. 406 (1983).

22. N. Bar-Chaim, J. Katz, I. Ury and A. Yariv, Electron. Lett., vol. 17, p. 108 (1981).

23. I. Ury, K.Y. Lau, N. Bar-Chaim and A. Yariv, Appl. Phys. Lett., vol. 41, p. 126 (1982).

24. Hitachi laser diode application manual.

25. K. Y. Lau, N. Bar-Chaim, I. Ury, Ch. Harder, A. Yariv, to be published in Appl. Phys. Lett., (1983).

26. S. Nita, H. Namizaki, S. Takamiya, W. Susaki, IEEE J. Quantum Electron., vol. 15, p. 208 (1979).

27. L. Figueroa, K. Y. Lau, A. Yariv, Appl. Pys. Lett., vol. 36, p. 248 (1980).

Chapter 4

A bistable semiconductor laser

4.1 Optical bistability

An optical bistable device is exactly what its name implies, it can have two different stable output states for one given input condition. Such a device is interesting because it represents a new kind of optical nonlinearity and an element with such a nonlinearity is of practical importance because it offers the possibility of realizing optical memory, switching and signal processing devices. Diode lasers are opto-electronic components and we will discuss in this chapter the more general opto-electronic bistability, i.e. input and output of the device can be either optical or electrical variables. Such an opto-electronic bistable device might be even of greater practical importance because of its potential to perform opto-electronic signal processing. The bistable laser presented in the following section 4.2 consists of a Fabry-Perot cavity which contains two media, a gain medium and a medium with an absorption which can be easily saturated. This saturable absorber provides the intrinsic nonlinearity which is necessary for bistability. Experimental results of this bistable injection laser appear in references [1], [2], [3], [4], [5], [6], [7] and should be consulted for detailed information. In the next section 4.2 the most important experimental results and an analysis of this bistable laser are presented. This investigation is not only important for an understanding of the static and dynamic characteristics of bistable lasers but it also provides insight into the behavior of injection lasers

with an *inhomogeneous current* distribution. Many diode lasers which are initially well behaved develop pathological features, such as self pulsations and light jumps. It is known that during long term operation the contact and the material degrade and as a consequence aged lasers have current density and carrier density variations along the length of the cavity. A buried heterostructure laser with a split contact is an electrically and optically simple device to study the effects due to inhomogeneous current injection, to understand light jumps and pulsations and to recommend remedies to suppress them.

4.2 Bistability and pulsations in semiconductor lasers with inhomogeneous current injection

4.2.1 Introduction

Bistable semiconductor lasers based on inhomogeneous current injection resulting from a segmented contact structure were proposed over fifteen years ago [8]. However, actual devices fabricated to date showed no or only a small hysteresis [9], [10], [11], [12], [1]. In addition these devices were beset by pulsations of the optical output [1], [13], [14], [15], [16], [17] for reasons not well understood at the time. Recently, we demonstrated a bistable buried heterostructure laser with a large hysteresis and no pulsations [2], [3], [4]. Crucial to the understanding of the behavior of this bistable laser was the discovery of a negative differential resistance across the absorber section. Depending on the electrical bias condition, this negative resistance leads to (i) bistability with a very large hysteresis in the light-current characteristic with no self pulsations or (ii) a narrow hysteresis (or light jump) and self pulsations. This negative resistance suggests a new mechanism for the observed self pulsations which does not depend on the condition for the usually proposed repetively Q-

switching [13], [18], [19]. Experiments reveal that this bistable laser switches from one state to the other after a delay time which is critically dependent on the trigger pulse overdrive. This critical slowing down [20], [21] of the delay time will be discussed in some detail and a small signal interpretation of this phenomenon will be presented. In an analysis we will show that the observed complex behavior of a laser with inhomogeneous current injection can be explained with the conventional rate equations only when the electrical aspect of the laser diode is also taken into account. The electrical characteristic of the device also manifests a giant hysteresis which mimicks the optical hysteresis.

Even though this bistable laser switches within a few nanoseconds at power delay products of a few picojoules we do not believe that this device will be able to compete with conventional logic in the near future. Its main application will be in the field of opto-electronic signal processing, such as optical disk readout. We demonstrate successfully that this bistable laser can be used as an optical stylus for optical disk readout with an excellent signal to noise ratio (due to the bistable characteristic) and a large electrical output signal.

4.2.2 Static characteristic

CW-GaAs buried heterostructure (BH) lasers with a split contact on the top p-side as shown in Fig. 4.2.1 have been fabricated by a standard process in our laboratory [22] and typical dimensions and doping levels are given in the figure. The upper cladding layer of these BH lasers is only lightly p-doped in order to increase the lateral parasitic resistance R_p between the two contact pads which is measured to be around $60k\Omega$. It will be shown later that a high electrical isolation between the two segments is essential for the operation of this laser as a bistable element. Before the devices are cleaved, a $25\mu m$ wide gap is etched into the p-contact metallization. Near- and far field measurements show that the

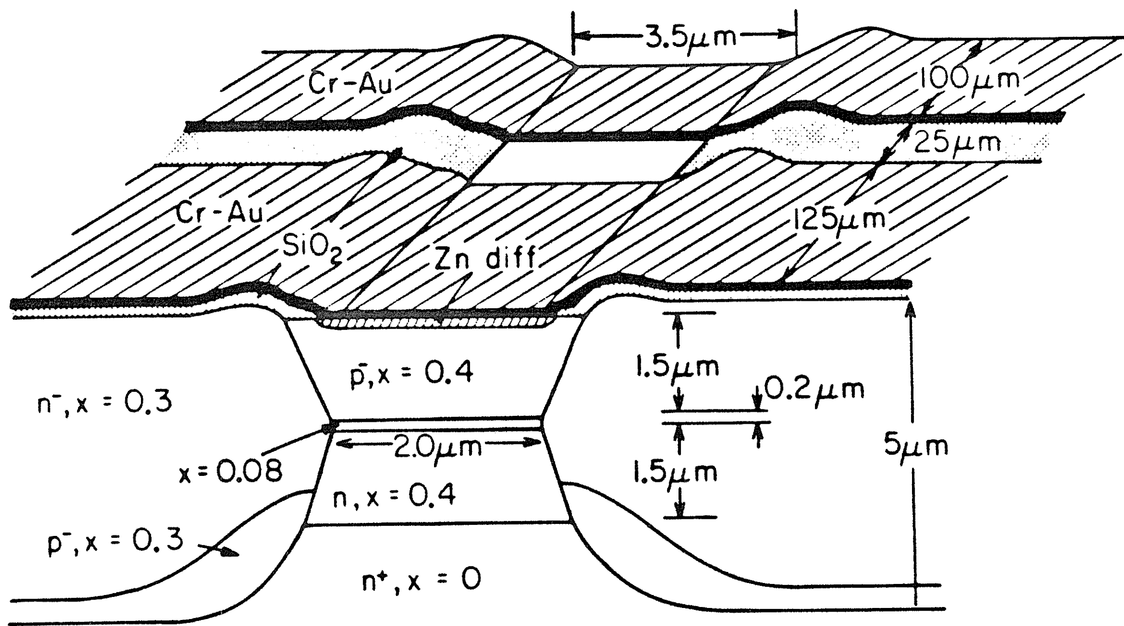

Figure 4.2.1. $Ga_{1-x}Al_xAs$ buried heterostructure laser with a segmented contact.

laser is always operating in the fundamental transverse mode, demonstrating the effectiveness of the dielectric waveguide. The BH structure thus makes it possible to isolate and study the effects of inhomogeneous excitation with a device whose electronic and optical properties are stable and simple.

If both sections are connected together, that is, under homogeneous excitation, the light-current characteristic displays the conventional linear behavior above threshold as shown in Fig. 4.2.2, curve (a). For bistable operation the absorber section (the section which is 100μm long) is pumped with a constant current I_2=−110μA. The light output is shown in Fig. 4.2.2 , curve (b) as function of I_1, the current through the gain section. This characteristic displays a large hysteresis extending from I_1=30mA (the switch-on current) to I_1=22mA (the switch-off current). The characteristic is also shown for I_2=−100μA, curve (c) and the sensitivity of the size of the hysteresis on the amount of saturable absorption (i.e., I_2) can be seen. Note, that I_2 is negative, that is, carriers are extracted from the absorber section.

In the lower half of Fig. 4.2.2 the voltage V_2 across the absorbing section is shown (curve (d) and curve (e)) as function of I_1. The main feature of this characteristic is that when the device is lasing (when the absorption is bleached) the voltage V_2 is clamped at 1.45 V, the bandgap voltage of GaAs. This demonstrates the one to one correspondence of the voltage across the contacts, the quasi-Fermi level separation and the carrier concentration in the active region.

In Fig. 4.2.3 the current-voltage characteristic (I_2–V_2) of the absorbing section is shown for different currents I_1 through the gain section. The negative differential resistance in this characteristic is of particular interest and deserves special attention. This negative differential resistance is, as will be shown, opto-electronic in origin and the mechanism causing it can be under-

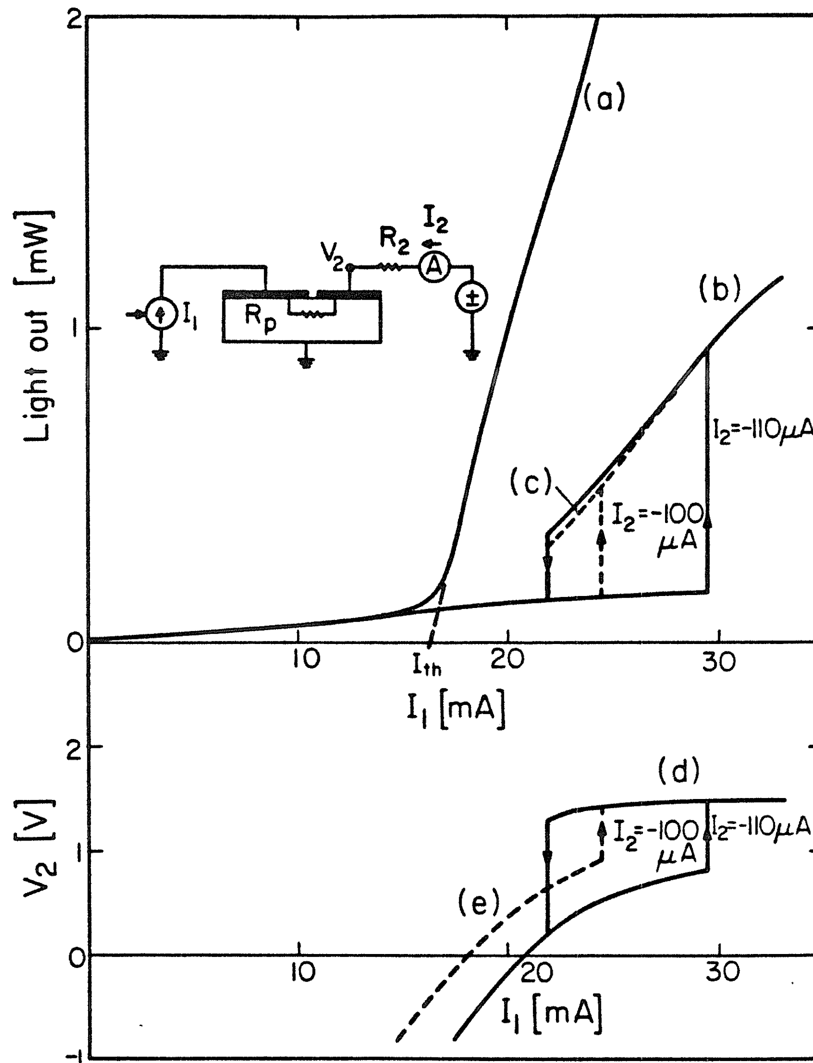

Figure 4.2.2. Measured static characteristic of the two segment contact laser. The top half shows the light-current characteristic. For homogeneous pumping: curve (a). I_{th} is the conventional threshold current. For inhomogeneous pumping: curve (b) for $I_2=-110\mu A$ and curve (c) for $I_2=-100\mu A$. The parasitic resistance is $R_p=60k\Omega$ and the current source impedance is $R_2=400k\Omega$. The lower half shows the voltage V_2 across the absorber section as function of I_1, the current through the gain section for $I_2=-110\mu A$ (curve (d)) and for $I_2=-100\mu A$ (curve (e)).

stood with the following simple model as illustrated in Fig. 4.2.4. Consider the bistable laser to consist of two parts, a gain section which is pumped with a constant current I_1 and an absorber section which acts like a photodiode within the optical cavity. The current I_2 through this photodiode consists of two terms: The first one is the normal diode current which depends exponentially on the applied voltage V_2 while the second term corresponds to a negative photo induced current I_{Ph} which is proportional to the photon density in the active region. (These photons are generated under the gain contact and guided to the absorbing region under the second contact). This photodiode characteristic is drawn on the right side of Fig. 4.2.4 for eight different photon densities, P=0 to P=7. We shall now show how the measured I_2–V_2 characteristic is produced. For zero voltage V_2 the absorption of the photodiode is strong thus suppressing stimulated emission and only a small photocurrent due to spontaneous emission in the gain section is generated. Increasing the voltage V_2 reduces the absorption thus favoring stimulated emission which increases the photon density thus generating a larger negative photo current in the absorbing diode. Increasing V_2 further increases the negative photo current I_{Ph} thus producing the negative slope. Finally, at large voltages V_2, the positive exponential term representing the normal diode behavior dominates and I_2 increases once more. This specific curve shown on the right side of Fig. 4.2.4 is obtained for a fixed gain current I_1. The whole set of curves as shown in Fig. 4.2.3 is obtained for different currents through the gain section.

4.2.3 Bistability and self-pulsations

We shall now show how the measured I_2–V_2 characteristic of the absorber section can lead under different bias condition to bistability or self-pulsation. The I_2–V_2 characteristic is shown again in Fig. 4.2.5 along with the characterization

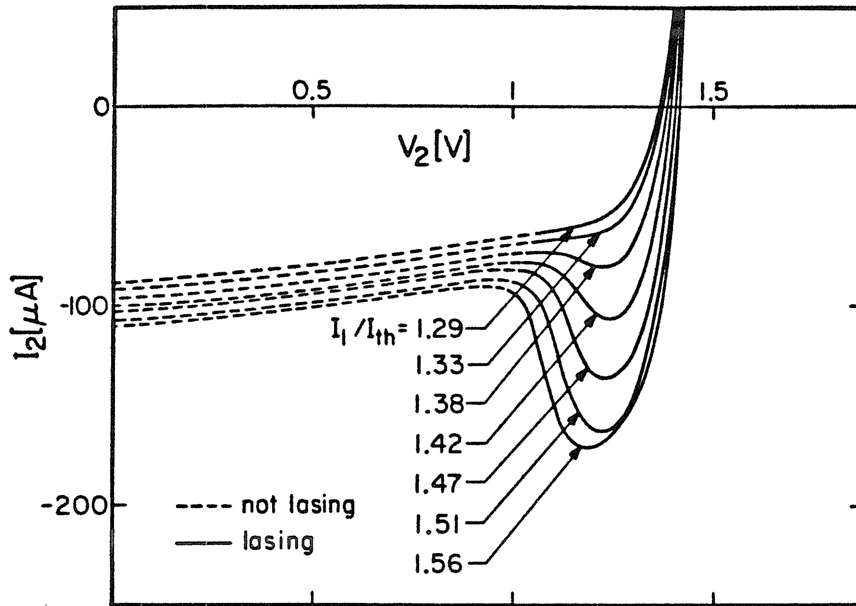

Figure 4.2.3. Current-voltage (I_2–V_2) characteristic of the absorber section for different currents I_1 through the gain section. I_{th} is defined in Fig. 4.2.2.

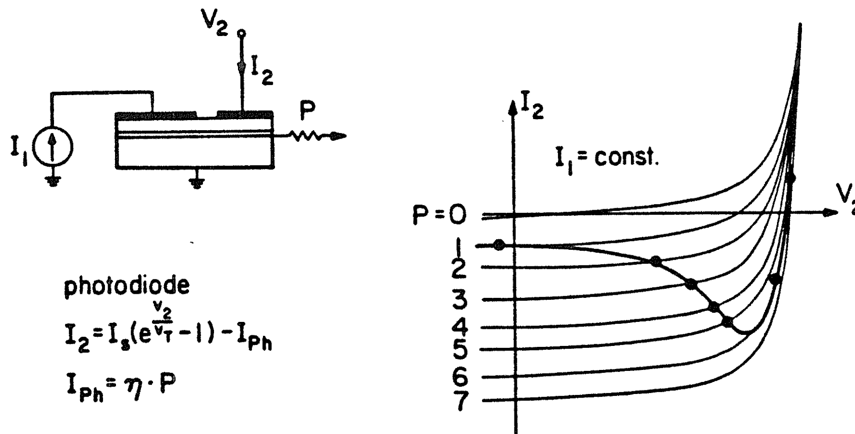

Figure 4.2.4. Model to explain the current- voltage (I_2–V_2) characteristic of the absorber section for a fixed current I_1 through the gain section. See text for explanation.

of the source driving this section, the load line. This line shows the voltage available to the absorber section as function of the current through it. The state of the system satisfying all static circuit equations is given by the intersection of the load line with the characteristic of the device. The state P_1 in Fig. 4.2.5 is the intersection of the absorber characteristic with the load line corresponding to a bias resistance of R_L=20kΩ and a current injection into the gain section of I_1/I_{th}=1.29. In this state the laser is switched off. Increasing I_1 causes the intersection point to move along the load line from P_1 to P_2 and at I_1/I_{th}=1.56 to jump to P_3 since this is the only intersection of the load line with the $I_2 - V_2$ characteristic. In this state the laser is switched on. A decrease of I_1 now causes the state to move back to P_4 and then tc jump back to P_5, at which point the laser is switched off. A laser with such a large load resistance will display a hysteresis in the light versus current I_1 characteristic. This can also be seen from the fact that the load line has two stable intersections with the I_2–V_2 characteristic, e. g. for I_1/I_{th}=1.47, the two stable states P_2 (switched off) and P_4 (switched on). The load line for a small resistance R_L=250Ω is also shown in Fig. 4.2.5, as the dotted line. This load line has always just one intersection with the characteristic of the device and the laser will consequently not display bistability. The laser with such a small load resistance can thus be biased to operate with its absorbing section in the regime of negative differential resistance. This leads to electrical microwave oscillation and concomittant light intensity pulsations.

The load resistance discussed above is essentially R_2 in parallel with R_p, $R_L=R_pR_2/(R_p+R_2)$ (see Fig. 4.2.2) and is thus always smaller than R_2 or R_p. Since bistable operation is only obtained with a large R_L, both, the source resistance R_2 and the parasitic resistance R_p have to be large. This is demonstrated in Fig. 4.2.6 where the light-current characteristic is shown for the two biasing

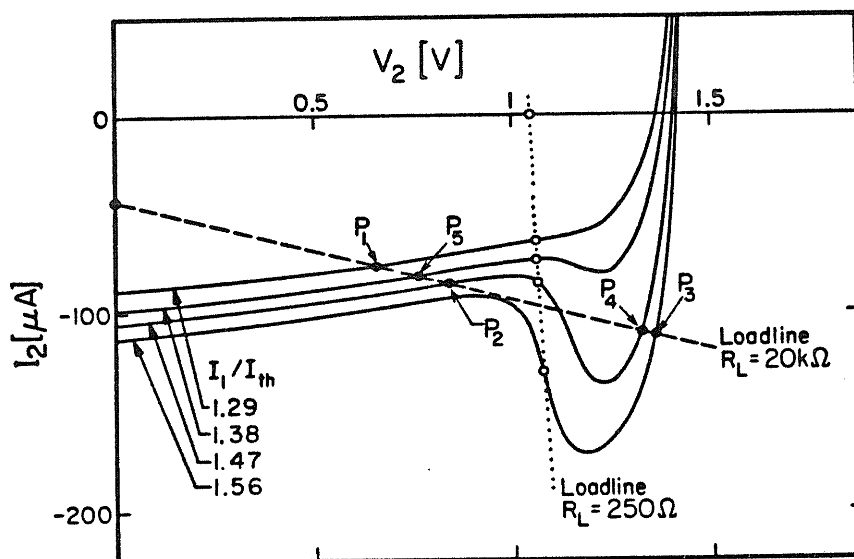

Figure 4.2.5. Current-voltage (I_2–V_2) characteristic of the absorber section for different currents I_1 through the gain section. Also shown are two load lines corresponding to a load resistance of R_L=20kΩ and R_L=250Ω.

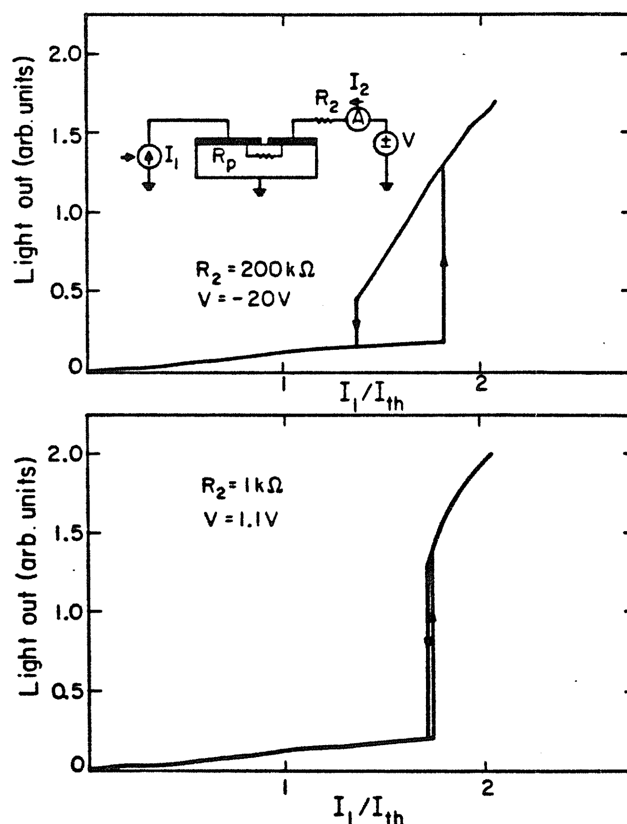

Figure 4.2.6. Light-current characteristic for two different bias conditions of the absorber section. The characteristic in the upper half corresponds to biasing the absorber section with a large resistance (current biasing), in the lower half to biasing the absorber section with a small resistance (voltage biasing).

situations discussed above, namely for a large R_L=46kΩ (top half) and a small R_L=1kΩ (bottom half). For a large R_L the characteristic displays indeed the predicted large hysteresis and the light output is always stable, no pulsations can be observed within the detector bandwidth of 5 GHz. For a small R_L the characteristic has only a very narrow hysteresis, a light jump and the light output oscillates at microwave frequencies. Since the negative differential resistance is not frequency selective (at frequencies below a few GHz) the device oscillates at the resonance of any frequency selective element coupled to the gain mechanism. Experiments show [1] that the device oscillates at the relaxation resonance frequency which is between 500 MHz and 2 GHz for this device depending on I_1. Our earlier lasers failed to produce a sizable hysteresis and were self pulsating [1] because their parasitic resistance (measured to be 1kΩ) was too small to allow bistable operation. The mechanism described above could possibly explain the development of self pulsations in aged lasers. Inhomogeneous excitation could be caused by degradation of the contacts or development of centers with enhanced nonradiative recombination. Note that these self pulsations are not due to a repetively Q-switched mechanism, but are the result of the opto-electronically generated negative resistance and do not result, as will be shown in section 4.2.5, from a sublinear gain dependence.

In Fig. 4.2.7 the laser emission spectra are shown for the cases of bistable (Fig. 4.2.7a) and pulsating (Fig. 4.2.7b) operation. In the bistable case the laser light is emitted into one longitudinal mode and the linewidth is limited by the resolution of the 3/ 4 m spectrometer to 0.2A. Under pulsating operating conditions, the spectrum breaks apart into some 10 longitudinal modes. Note, that the linewidth of each of the longitudinal modes is broadened. This cannot be due to unresolved transverse modes since far-field and near-field measurements show that the laser is always operating in the fundamental transverse mode. The

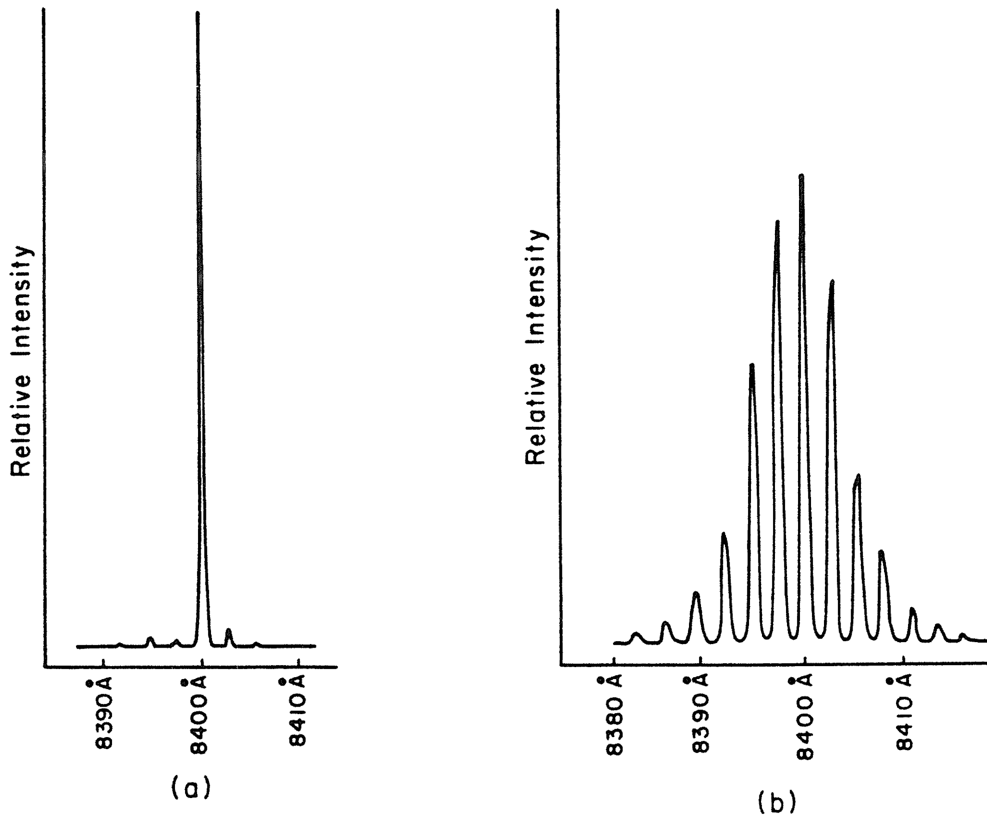

Figure 4.2.7. Optical spectrum of the laser: Under bistable operation (a), and under pulsating operation (b).

carrier concentration in the active region is oscillating with a large amplitude during pulsations thus causing the index of refraction in the active region to change [23] resulting in a periodical pulling of the Fabry-Perot modes. This effect could explain the broadening of the observed time averaged spectrum.

4.2.4 Switching

The laser has two stable states when biased within the hysteresis loop. The laser can be switched off by increasing the absorption for a short time by some means. This can be achieved by either increasing the current I_1 through the gain section for a short time (gain-switching), by injecting a positive current pulse into the absorber section (absorber-switching) or by bleaching the absorber with an externally injected optical pulse (optical switching). In this section we discuss the dynamics of the gain switching, in particular the technologically important problem of delays between trigger pulse and switching. Such delays are observed in almost every bistable system including electronic Schmidt-triggers and pure optical systems [20], [21] and it is well known that they can be reduced by increasing the trigger pulse amplitude. From a thermodynamic point of view the laser system undergoes a first order phase transition during the switching [24], [25]. As far as device applications are concerned one of the most important predictions gained from this thermodynamic point of view is that of the critical slowing down, i. e. an extremely slow return of the system to the equilibrium or a very slow response time to a perturbation in the victinity of the phase transition point [20], [21].

The delay between trigger pulse and switching of the laser can be very long compared to any physical lifetime associated with the system, such as electron-hole recombination or RC-time constant while the switching itself is relatively fast. For bistable operation the laser is biased at a constant current I_2 and at a

current I_1 corresponding to the middle of the hysteresis loop, e. g. for the device shown in Fig. 4.2.2 $I_2=-110\mu A$ and $I_1=26mA$. A small positive current pulse superimposed on I_1 switches the laser to the high (lasing) state while a subsequent negative pulse switches the laser back to the low state as shown in Fig. 4.2.8. A closer examination of the switch-on, as shown in Fig. 4.2.9, reveals a delay time that is dependent on the amount of trigger pulse overdrive. This delay time dependence on the switch pulse amplitude is shown in Fig. 4.2.10 and it can be divided into two regimes, a critical slowing down regime for small overdrive amplitudes and a noncritical regime for large overdrives.

The critical regime is only observed for very small overdrives and is characterized by a dramatic increase of the switching delay up to several hundred nanoseconds. The behavior is that of the conventional critical slowing down. At higher drive currents, the switching delay is relatively noncritical and is the time required for the carrier density in the gain and absorber section to rise to the level where lasing can occur. This time lapse is in the order of a fraction of the carrier lifetimes. A similar delay occurs during switch on of common injection lasers [26].

The carrier lifetime in the gain section where the carrier density is high is in the order of a few nanoseconds, while that one in the low carrier density absorber section is in the tens of nanoseconds. The dominating time constant is, unfortunately, the long one. Fig. 4.2.9a shows multiple traces of the switching behavior for four different drive currents (labelled I_1). The lowest trace of I_1 is very close to the threshold for switching and the critical slowing down in the corresponding light output is evident. The delay can be reduced drastically to below 20ns when the trigger current is increased to about 9 mA. In fact a switching delay of 5 ns can be achieved with a pulse of 10 mA which corresponds to an intrinsic power delay product of $5ns \times 10mA \times 2V = 100pJ$ for gain switching. While

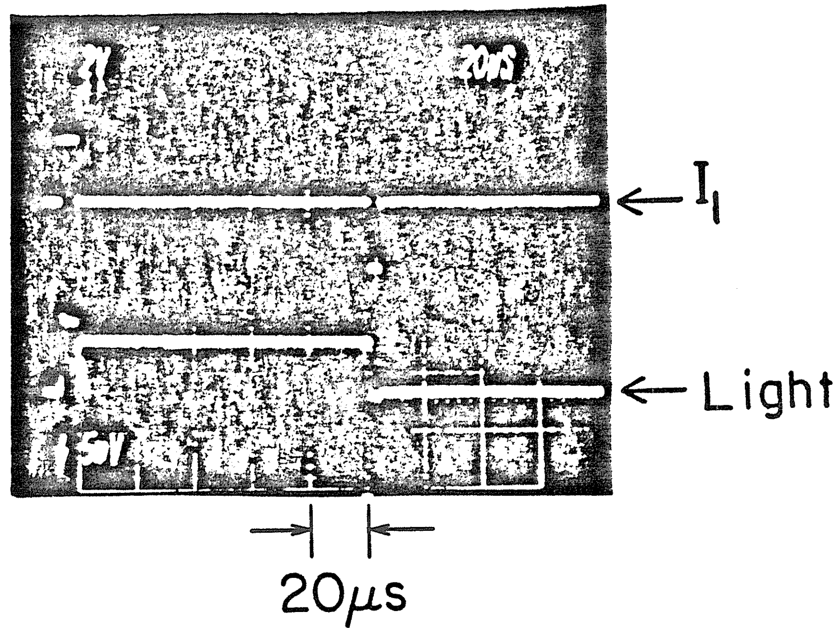

Figure 4.2.8. Gain-switching of the bistable laser. Top trace: Current I_1 through the gain section. Lower trace: Light output. Hor.: 20μs/div.

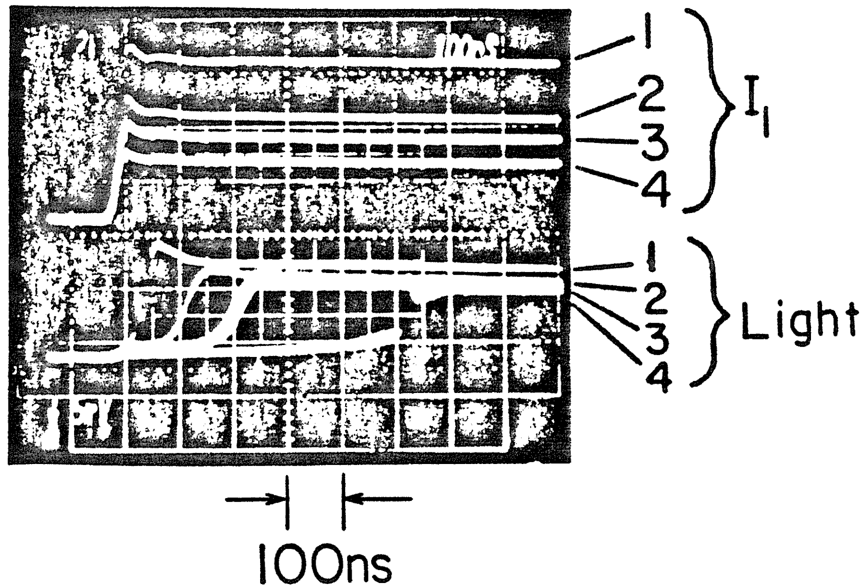

Figure 4.2.9a. Delay of the light output for four different trigger pulse amplitudes. Hor.: 100ns/div.

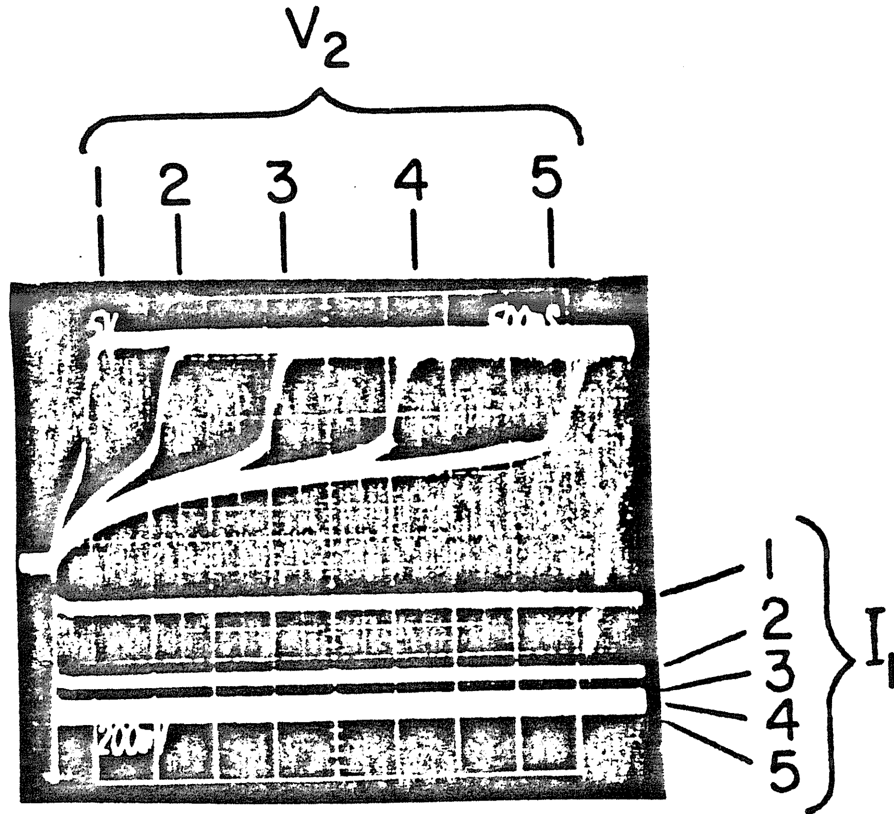

Figure 4.2.9b. Voltage change across the absorber section V_2 during the switch-on transient for five different trigger current amplitudes I_1 injected into the gain section. The five different traces of V_2 are marked at their points of switch-on. Hor.: 500ns/div

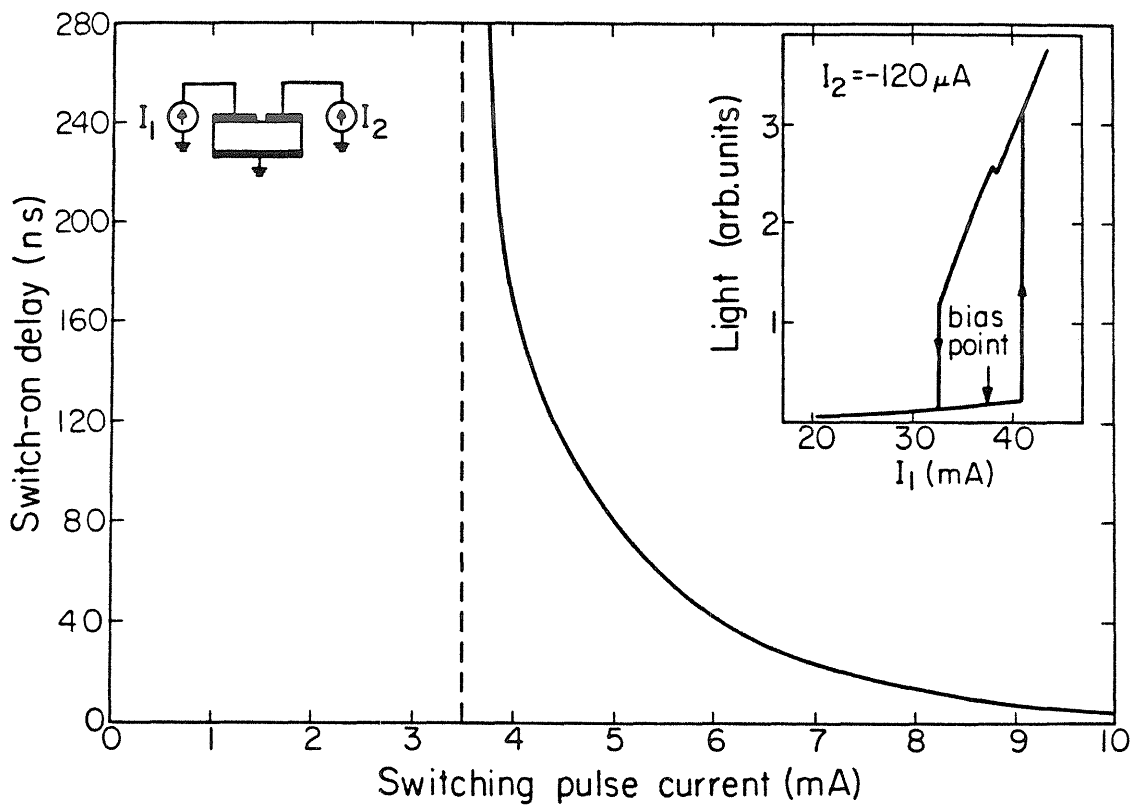

Figure 4.2.10. Switch-on delay time as function of the trigger pulse amplitude. The critical slowing down of the switch delay occurs for pulse amplitudes of 3.5mA.

the switch-on shows these interesting effects, the switch-off is usually fast and without delay. This arises from the fact that the switch-off process involves stimulated recombination of carriers at high density which is extremely fast. To observe the inherent switching behavior, the external parasitic capacitance at the absorbing section must be reduced to a minimum, since a switching of the device is accompanied by a change of the voltage, and thus charge, across the absorber section as can be seen in Fig. 4.2.2. In our experiment the diode was isolated from the capacitance of the current source by placing a 250kΩ resistance as close to the diode as possible.

Considerable insight into the switching dynamics can be gained by probing the voltages across the gain and absorber sections, thus in effect probing the carrier densities. The voltage V_2 across the absorber section is shown in Fig. 4.2.9b for five different trigger current amplitudes I_1. To illustrate the switching characteristics we discuss trace five, the smallest trigger current amplitude in Fig. 4.2.9b. Initially the laser is turned off, i.e. the total gain in the laser is smaller than one (the total gain is defined to be the sum of the gain in the gain section minus the losses in the absorber section and due to the mirrors). Increasing the current through the gain section, I_1, increases the carrier density and therefore the spontaneous (superluminescent) radiation increases also. Some fraction of this radiation is captured in the absorbing section and pumps there slowly the carrier density upwards, as can be seen from the voltage V_2, trace five, measured across the absorbing section. Increasing the carrier density reduces the amount of absorption (saturates the absorber) until the total round trip gain becomes larger than one. At this point the lasing action starts up extremely fast, within a few round trip times, bleaching the saturable absorber completely and the voltage V_2 jumps up to around 1.5V, the bandgap voltage of GaAs, as shown in Fig 4.2.9b. This externally measured voltage , which is equal

to the difference of the quasi-Fermi levels of the holes and electrons, corresponds to a carrier density at which the material is transparent. Increasing the trigger current amplitude I_1, decreases the time it takes to photopump the absorber to the point where the round trip gain becomes larger than one. This photopump time corresponds to the delay time of the switching as it is observed in Fig. 4.2.9a. The time it takes for the laser to switch on once the round trip gain has become larger than one is extremely fast and not strongly dependent on the trigger pulse amplitude.

Experiments on absorber switching (by injecting a current pulse into the absorber section) reveal a switch on delay in the hundreds of nanoseconds for moderate overdrives and of 20 ns for a large overdrive of 150μA corresponding to a delay power product of 20ns$\times$150μA$\times$2V=6pJ. Recently Dziura and Hall [27] calculated the characteristics of two semiconductor lasers coupled to an optical cavity and they predict bistability.

4.2.5 Static analysis

The purpose of this section is to analyze a simple model which explains the main features of a semiconductor laser with inhomogeneous current injection along the active region. This model emphasizes the relevant mechanisms and parameters responsible for the bistability and the negative differential resistance across the absorbing section. First the light-current characteristic is calculated using familiar rate equations. When we add equations describing the electrical aspect of the device a negative differential resistance is predicted. To clarify the intrinsic frequency limitation of this negative differential resistance a small signal analysis is performed and an electrical equivalent circuit is developed.

A set of three rate equations is the starting point of this analysis, one for the density of minority carriers in the gain section, one for those in the absorbing section and a third one for the density of photons in the lasing mode. The confinement of the injected carriers in a buried heterostructure laser to the small dimensions of the active region ($2\mu m \times 0.2\mu m$) justifies the characterization of the inversions by their average over these dimensions. Measurements show that the built in dielectric waveguide forces the laser to operate under all conditions in the fundamental transverse mode. In addition, when this laser is biased for stable operation, the light is emitted into one longitudinal mode. This simple optical behavior can be modeled by one rate equation for the density of photons in the lasing mode. The carrier and photon densities have been averaged over the length of the device to render the calculation tractable. This assumption is approximately correct at high photon densities when the absorber section is saturated and bleached. At low photon densities this assumption is violated due to superluminescent effects. A model which does not average the variables over the length and which includes superradiance will be discussed separately. The three equations are:

$$\frac{dN_1}{dt} = \frac{I_1}{eV_1} - B(N_1+N_A)N_1 - A(N_1-N_{tr})P \tag{4.2.1}$$

$$\frac{dN_2}{dt} = \frac{I_2}{eV_2} - B(N_2+N_A)N_2 - A(N_2-N_{tr})P \tag{4.2.2}$$

$$\frac{dP}{dt} = A(\alpha_1 N_1+\alpha_2 N_2-N_{tr})P - \frac{P}{\tau_P} + \beta B\left\{\alpha_1 N_1(N_1+N_A) + \alpha_2 N_2(N_2+N_A)\right\} \tag{4.2.3}$$

$V_1=\alpha_1 V$ is the volume of the active region with gain, N_1 is the inversion density of carriers in the gain region, and I_1 the current injected into it. V_2, α_2, N_2 and I_2, are the corresponding variables in the absorber section, ($\alpha_1+\alpha_2 = 1$). P is the photon density in the lasing mode, e is the electronic charge, τ_P is the photon

lifetime and β is the coupling coefficient for spontaneous emission into the lasing mode. Since the carrier densities vary over a large range it is not reasonable to assume a constant spontaneous lifetime τ_s. These rate equations incorporate a bimolecular recombination rate where B is the recombination constant and N_A is the doping concentration of the p-type background in the active region. A *linear* gain dependence on injected carrier density $G(N)=A(N-N_{tr})$ is used in these calculations in agreement with recent measurements of the gain in undoped or only slightly doped GaAs [28]. The same coefficients are used for the gain and absorbing section assuming equal conditions such as temperature and material in both sections.

It is crucial to appreciate the importance of the functional dependence of the gain on carrier density G(N) for the stability of a laser diode with inhomogeneous injection. It has been shown [13], [18], [19], that a *sublinear* gain dependence such as $G(N)=A(N-N_{tr})^{\alpha}$ with $\alpha< 1$, causes an inhomogenously pumped laser to pulsate due to a repetitively Q-switched mechanism. On the other hand a *superlinear* gain dependence such as $G(N)=A(N-N_{tr})^{\alpha}$ with $\alpha> 1$, has a stabilizing effect, suppressing pulsations and bistability. A laser with a *linear* gain dependence $G(N)=A(N-N_{tr})$ together with a bimolecular recombination rate displays a more complex behavior. In the following analysis it will be shown that for such a gain dependence a laser with inhomogeneous injection can be made to display bistability *or* self pulsations depending on the electrical biasing circuit.

The following values of the various parameters have been used: $\alpha_1=0.5$; $\alpha_2=1-\alpha_1=0.5$; $V=250\mu m\times 2\mu m\times 0.2\mu m$; $B=3\times 10^{10} cm^3/s$; $N_A=3\times 10^{17} cm^{-3}$; $A=2.34\times 10^{-6} cm^3/s$ corresponding to an absorption coefficient of $\alpha=-230 cm^{-1}$ at zero inversion; $N_{tr}=0.83\times 10^{18} cm^{-3}$; $\tau_p=1.5ps$ corresponding to waveguide and other distributed losses $\alpha=40 cm^{-1}$ and $\beta=10^{-4}$. To calculate the static light

set to zero. The solution shown in Fig. 4.2.11 displays the main features of the measurement (Fig. 4.2.2), linear characteristic under homogeneous excitation and a sizable hysteresis if the absorbing section is biased with a small negative current. Measured and calculated threshold currents agree if we take a current confinement factor of one half into account. Note that the calculation predicts a hysteresis for I_2=0. This is not observed, probably because the superradiance of the gain section is intense enough to saturate this weak absorption. Measurements reveal that the light coming out of the gain section facet is weaker than that from the absorber section [29]. The average light from both sides compares well with the calculated characteristic. The carrier densities in the gain section and absorber section are shown in Fig. 4.2.12 as function of I_1.

The rate equations (4.2.1) through through (4.2.3) model the device with given currents I_1 and I_2 being injected into the gain and absorber sections and are therefore sufficient for a complete description if the gain and absorber sections are biased with sources whose equivalent impedance is much larger than the impedance of the gain and absorber section. Although this condition is always true in the case of the gain section it is violated for the absorbing section which is typically only slightly forward-biased.

The external voltage V_2 across the absorbing section is given, using an approximation for the carrier density in a parabolic band [30] by:

$$V_2 = V_g + V_T\left(\ln\left(\frac{N_2(N_2+N_A)}{N_C N_V}\right) + \frac{N_2}{2\sqrt{2}}\left(\frac{1}{N_C}+\frac{1}{N_V}\right) + \frac{1}{2\sqrt{2}}\frac{N_A}{N_V}\right) \qquad (4.2.4)$$

In the expression above V_g=1.46V is the bandgap voltage, V_T=25.9mV the thermal voltage at room temperature kT/q and $N_C=4.7\times10^{17}cm^{-3}$ and $N_V=7\times10^{18}cm^{-3}$ are the effective conduction band and valence band density of states respectively. The calculated I_2–V_2 characteristic of the absorbing section obtained from the static solutions of equations (4.2.1) through (4.2.4) is shown in Fig. 4.2.13 and

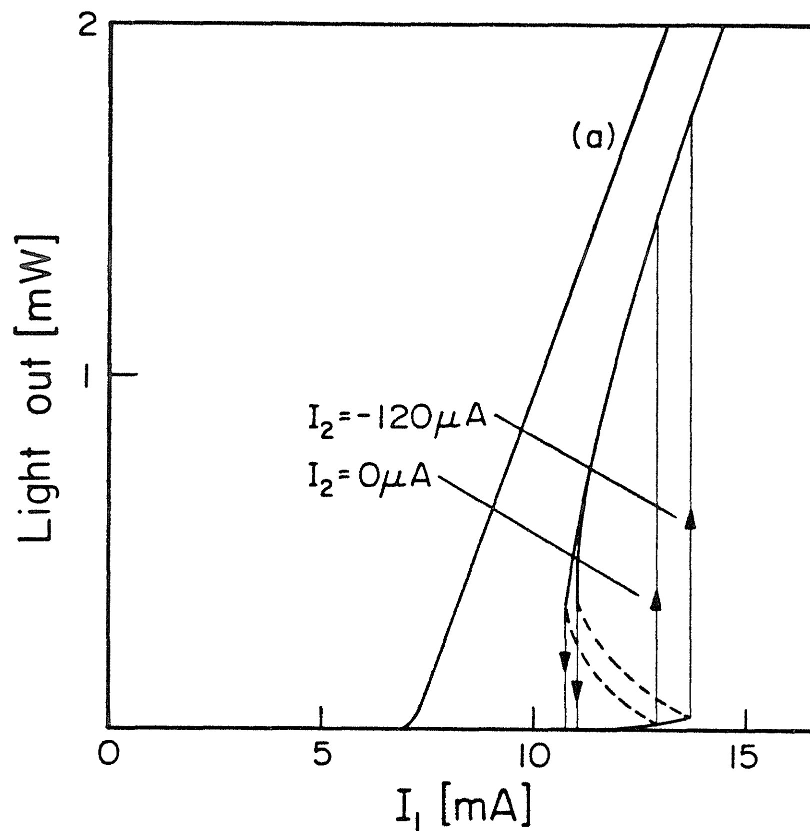

Figure 4.2.11. Calculated static light-current characteristic. For homogeneous pumping: curve (a). For inhomogeneous pumping: curve (b) for I_2=−120μA and curve (c) for I_2=0μA. Parameters of the model are given in the text.

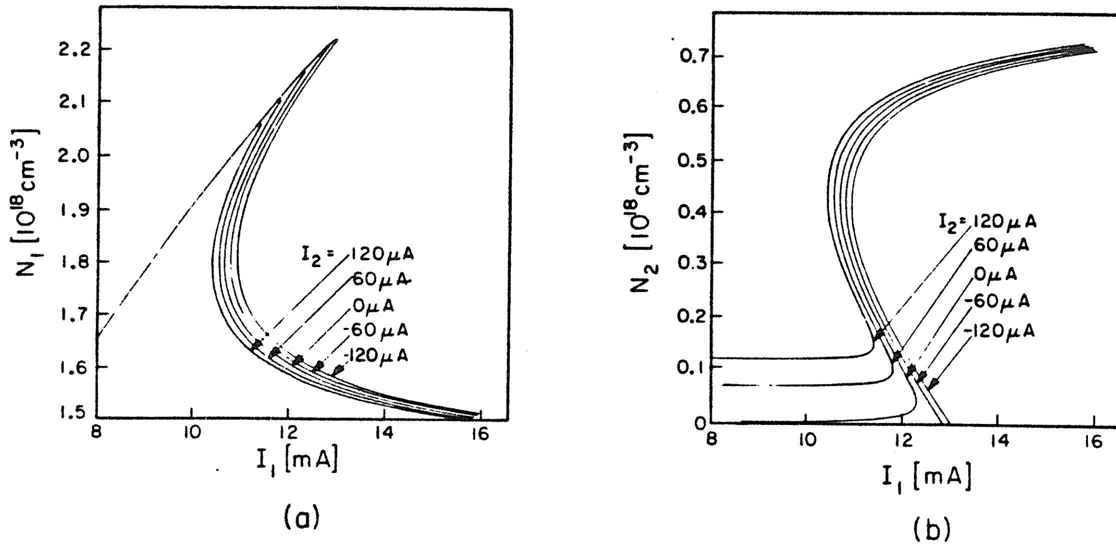

Figure 4.2.12. Calculated carrier concentration in the gain section (N_1) and in the absorber section (N_2) as function of I_1, the current through the gain section for a set of different bias-currents I_2 through the absorber section.

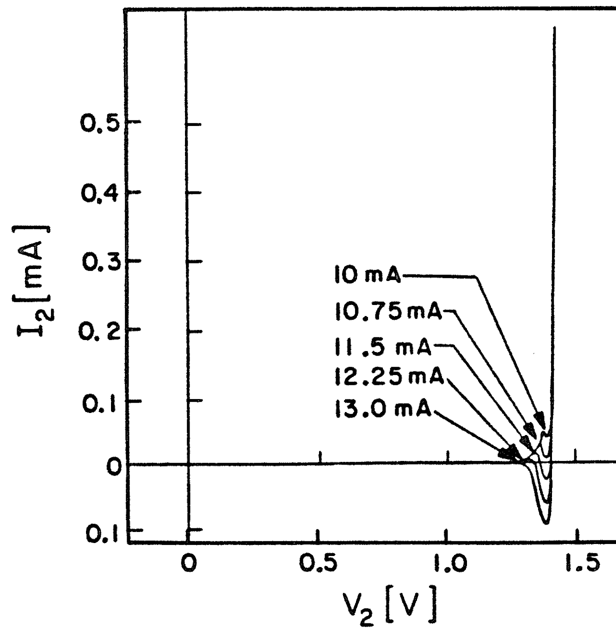

Figure 4.2.13. Calculated current-voltage characteristic (I_2–V_2) of the absorber section for different currents I_1 injected into the gain section.

static solutions of equations (4.2.1) through (4.2.4) is shown in Fig. 4.2.13 and displays a region of negative differential resistance between V_2=1.3V and V_2=1.4V. This negative differential resistance is obtained as the static solution of the conventional rate equations (4.2.1) through (4.2.4). Some of the difference between the measurements and the calculations is due to the neglected superluminesence, but it is believed that most is caused by the photoconductive effect, which is discussed in the next paragraph.

It has been assumed up to here that the gain and absorbing section are electrically insulated and that they only interact optically. However, there is an electrical coupling which consists of the following two parts: a constant parasitic resistance R_p due to the finite lateral conductance of the p-type top cladding layer which has been made so large (R_p=60kΩ), by doping this layer only slightly, that it can be neglected and a connection through carriers generated in the optical waveguide connecting gain and absorber section, to which we will refer to as photoconductive effect. When the bistable laser is switched off the resistance of this photoconductive path is very large (≥ 200kΩ) but if it is switched on the density within this photoconductor is increased to transparancy level and the resistance is estimated to drop to about 2kΩ. This photoconductive effect adds constructively to the opto-electronic effect in the I_2–V_2 characteristic and is probably responsible for the main differences between measurements and calculation.

4.2.6 Small signal analysis and equivalent circuit

The small signal rate equations are obtained from equations (4.2.1) through (4.2.3) by substituting $N_1=N_{10}+n_1$, $N_2=N_{20}+n_2$, $P=P_0+p$, $I_1=I_{10}+i_1$ and $I_2=I_{20}+i_2$.

$$\frac{dn_1}{dt} = \frac{i_1}{eV_1} - (\frac{1}{\tau_1} + AP_0)n_1 - A(N_{10} - N_{tr})p \tag{4.2.5}$$

$$\frac{dn_2}{dt} = \frac{i_2}{eV_2} - (\frac{1}{\tau_2} + AP_0)n_2 - A(N_{20} - N_{tr})p \tag{4.2.6}$$

$$\frac{dp}{dt} = \alpha_1 n_1(\frac{\beta}{\tau_1} + AP_0) + \alpha_2 n_2(\frac{\beta}{\tau_2} + AP_0) - A(N_{tr} + \frac{1}{A\tau_p} - \alpha_1 N_{10} - \alpha_2 N_{20})p \tag{4.2.7}$$

$$\tau_1 = \frac{1}{B(2N_{10} + N_A)} \tag{4.2.8}$$

$$\tau_2 = \frac{1}{B(2N_{20} + N_A)} \tag{4.2.9}$$

In the equations above N_{10} , N_{20} and P_0 are the static solutions obtained from equations (4.2.1) through (4.2.3) for I_{10} and I_{20}, and n_1 , n_2 , and p are the small signal responses of the carrier densities of the gain section, absorber section and photons, respectively, if the small signal currents i_1 and i_2 are injected into the gain and absorbing section.

Now consider the separate problem of the equivalent circuit as shown in Fig. 4.2.14a. This circuit is described by the following set of circuit equations.

$$\frac{dv_1}{dt} = \frac{i_1}{C_1} - \frac{v_1}{R_1C_1} - \frac{i_L}{C_1} \tag{4.2.10}$$

$$\frac{dv_2}{dt} = \frac{i_2}{C_2} - \frac{v_2}{R_2C_2} + k\frac{i_L}{C_2} \tag{4.2.11}$$

$$\frac{di_L}{dt} = \frac{v_1}{L} + \frac{v_2}{NL} - \frac{R_{se}}{L}i_L \tag{4.2.12}$$

where i_1 and v_1 are the small signal current and voltage at the gain section and i_2 and v_2 are the corresponding variables for the absorber section. Setting $N_1=N_{10}+n_1$ and $N_2=N_{20}+n_2$ in equation (4.2.4) yields the small signal relationships between carrier variation and voltage.

$$v_1 = m_1 V_T \frac{n_1}{N_{10}} \qquad m_1 = \frac{2N_{10}+N_A}{N_{10}+N_A} + \frac{N_{10}}{2\sqrt{2}}\left(\frac{1}{N_V}+\frac{1}{N_C}\right) \tag{4.2.13}$$

$$v_2 = m_2 V_T \frac{n_2}{N_{20}} \qquad m_2 = \frac{2N_{20}+N_A}{N_{20}+N_A} + \frac{N_{20}}{2\sqrt{2}}\left(\frac{1}{N_V}+\frac{1}{N_C}\right) \tag{4.2.14}$$

Comparing factors in equation (4.2.5)-(4.2.7) with (4.2.10)-(4.2.12) and using equations (4.2.13) and (4.2.14) leads to a proportionality between the current i_L and the optical small signal power p.

$$i_L = pA(N_{10}-N_{tr})eV_1 \tag{4.2.15}$$

The following values for the elements of the equivalent circuit are also obtained.

$$C_1 = \frac{eV_1 N_{10}}{m_1 V_T} \tag{4.2.16}$$

$$R_1 = \frac{1}{C_1\left(\frac{1}{\tau_1}+AP_0\right)} \tag{4.2.17}$$

$$C_2 = \frac{eV_2 N_{20}}{m_2 V_T} \tag{4.2.18}$$

$$R_2 = \frac{1}{C_2\left(\frac{1}{\tau_2}+AP_0\right)} \tag{4.2.19}$$

$$L = \frac{1}{C_1 \alpha_1 A(N_{10}-N_{tr})\left(\frac{\beta}{\tau_1}+AP_0\right)} \tag{4.2.20}$$

$$R_{se} = LA\left(N_{tr}+\frac{1}{A\tau_p}-\alpha_1 N_{10}-\alpha_2 N_{20}\right) \tag{4.2.21}$$

$$k = \frac{\alpha_2(N_{tr}-N_{20})}{\alpha_1(N_{10}-N_{tr})} \tag{4.2.22}$$

$$N = \frac{\alpha_1 m_2 N_{10}\left(\frac{\beta}{\tau_1}+AP_0\right)}{\alpha_2 m_1 N_{20}\left(\frac{\beta}{\tau_2}+AP_0\right)} \tag{4.2.23}$$

Fig. 4.2.14b shows the reduced equivalent circuit with the absorbing section

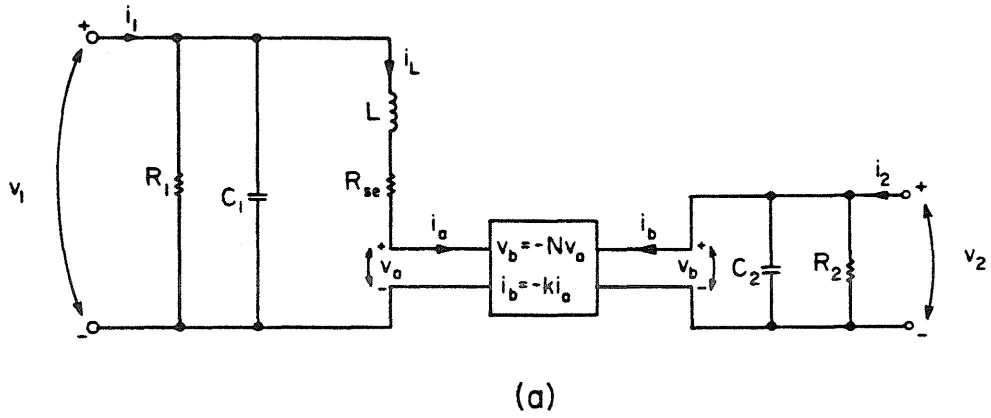

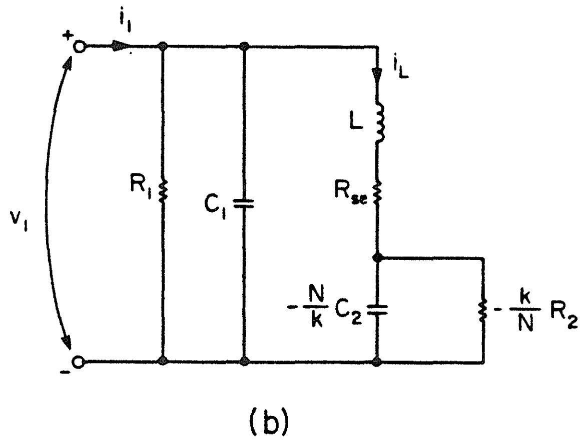

Figure 4.2.14. Equivalent electrical small signal circuit of the two segment laser. The values of the elements are given in the text: (a) full equivalent circuit, (b) reduced equivalent circuit.

represented by a negative resistance $-\frac{k}{N}R_2$ with $\frac{k}{N} > 0$. From this circuit it can be inferred that the useful small signal bandwidth of this gain element is limited to about $\frac{1}{R_2C_2} = \frac{1}{\tau_2} + AP_0$ (a few hundred megahertz) due to the shunting of R_2 by the capacitor C_2. The usefulness of the double contact laser as a negative resistance electrical circuit element [2], [31] is limited mainly by the contact resistance of the gain section which makes it difficult to couple $-\frac{k}{N}R_2$ to an electrical circuit. Since the gain element $-\frac{k}{N}R_2$ is not frequency selective the device will pulsate with a frequency given by a frequency selective mechanism, such as the relaxation resonance (represented by L and C_1) or the round trip time of an external optical cavity . A small signal analysis of a bistable laser in an external optical cavity shows that the negative resistance $-\frac{k}{N}R_2$ can be coupled very efficiently to the frequency selective mechanism of an external cavity and indeed measurements show that pulsations in an external optical cavity correspond to the round trip time and have harmonic contents up to the gigahertz range.

4.2.7 Small signal analysis of the critical slowing down

In this paragaph we develop a small signal interpretation of the critical slowing down. The stability of the laser can be investigated by calculating the roots of the charateristic equation of the Laplace transform of equations (4.2.10) to (4.2.12) with s as independent variable.

$$\left(s+\frac{1}{R_1C_1}\right)\left\{\left(s+\frac{1}{R_2C_2}\right)(R_{se}+sL) - \frac{k}{N}\frac{1}{C_2}\right\} + \frac{1}{C_1}\left(s+\frac{1}{R_2C_2}\right) = 0 \qquad (4.2.24)$$

The loci of the three roots in the complex s-plane are shown in Fig. 4.2.15 as a function of the power in the lasing mode. At low optical power all three roots

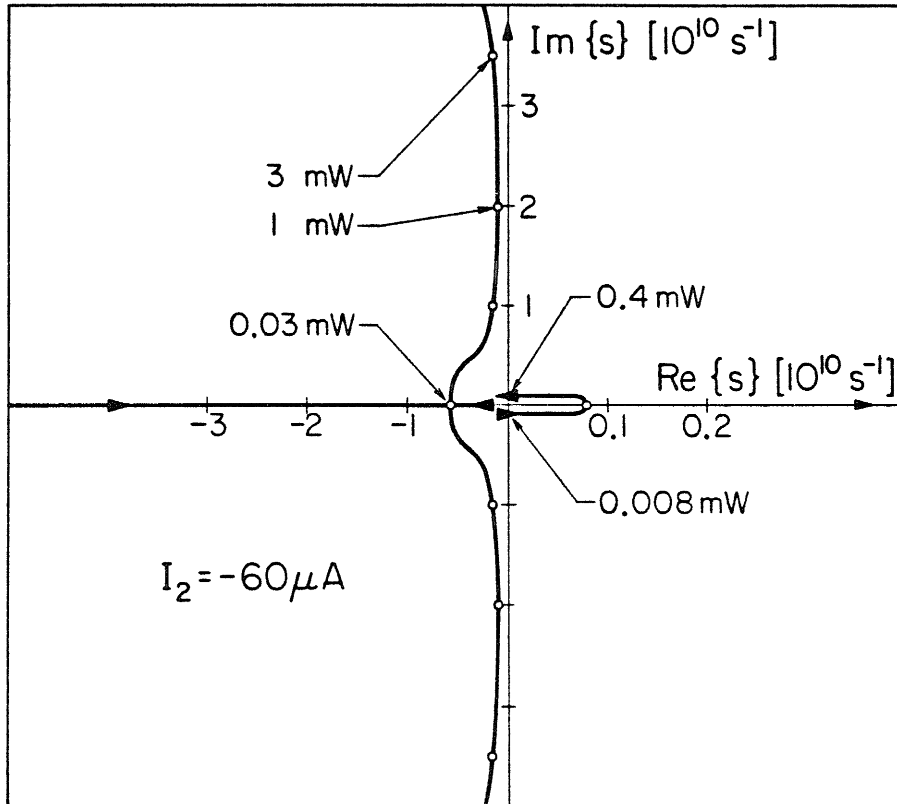

Figure 4.2.15. Location of the three roots of the characteristic equation as function of the optical power emitted. One root is at the origin at the transition points, P=0.008mW and P=0.4mW. Note that the scale of the positive real axis is expanded.

are on the negative real axis and the laser is therefore stable. Increasing the power causes two roots to split off the negative real axis into the complex left half plane. The third zero moves on the real axis towards the right, crosses the origin and remains on the positive real axis for biasing conditions where the light current characteristic has a negative slope. At high optical power densities this root returns to the negative real axis. At the transition points (switch-on P=0.008 mW and switch-off P=0.4mW) of the bistable laser this root of the characteristic equation is right at the origin. A root at the origin of the s-plane signifies an infinite long response time to any pertubation which results in a dead time. This corresponds to the critical slowing down [20] of the delay time at the transition points as observed.

4.2.8 External optical cavity

The typical experimental arrangement of the device in an external optical cavity is shown in Fig. 4.2.16. Also shown is the light versus current through the gain section I_1 characteristic curve at a constant current through the absorber section I_2. A shift of the hysteresis under optical feedback is apparent. The amount of light fed back into the laser is estimated from the shift of the threshold current to be around 50%. To switch the bistable laser on and off by varying the optical feedback it is necessary that the hystereses with and without feedback do not overlap. This can be achieved by adjusting the current through the gain section, I_1, and through the absorber section I_2 as shown in Fig. 4.2.17. A good combination is I_1=29.5mA and $I_2=-78\mu A$ [18] and the resulting light versus feedback characteristic is shown in Fig. 4.2.18. The voltage V_2 across the absorbing section (also shown in Fig. 4.2.18) depends on the feedback in a manner similar to that of the light output. The switching of the voltage V_2 through a control of the amount of feedback can be utilized, for example, in

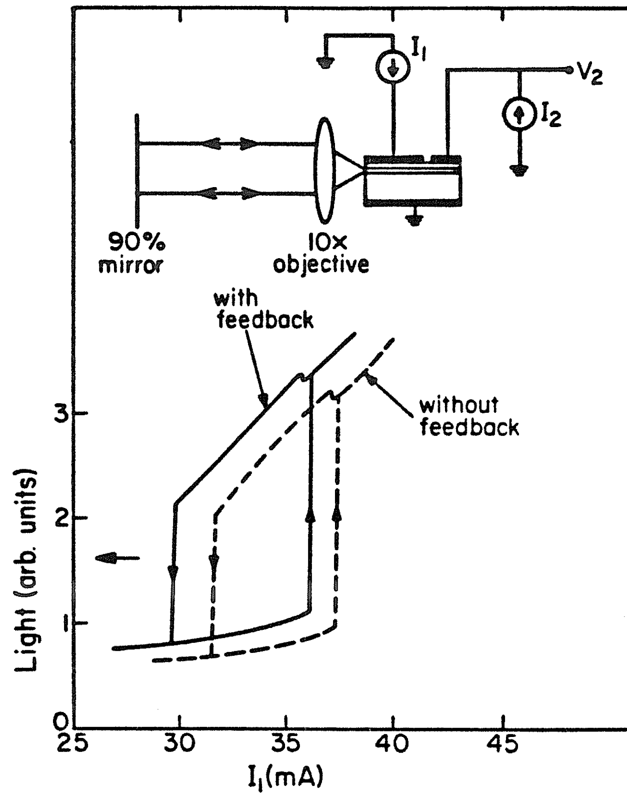

Figure 4.2.16. Typical experimental set-up of the bistable laser in an external optical cavity. Measured light versus current I_1 through the gain section characteristic without (solid line) and with (dashed line) optical feedback for I_2=−110μA. The amount of feedback is about 50%.

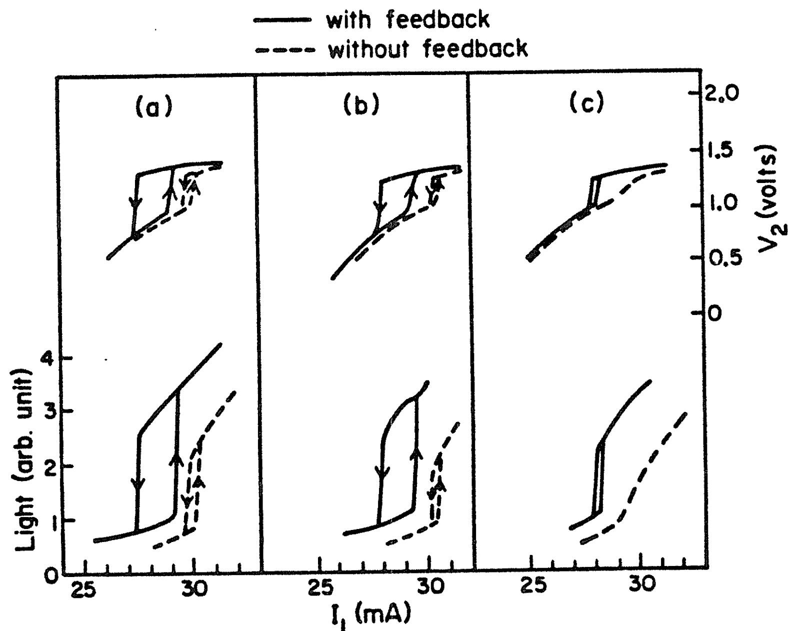

Figure 4.2.17. Light versus current I_1 characteristics where the hysteresis curves with (solid) and without (dashed) optical feedback do not overlap. (a) I_2 = − 80μA, (b) I_2 = − 70μA, (c) I_2 = − 60μA.

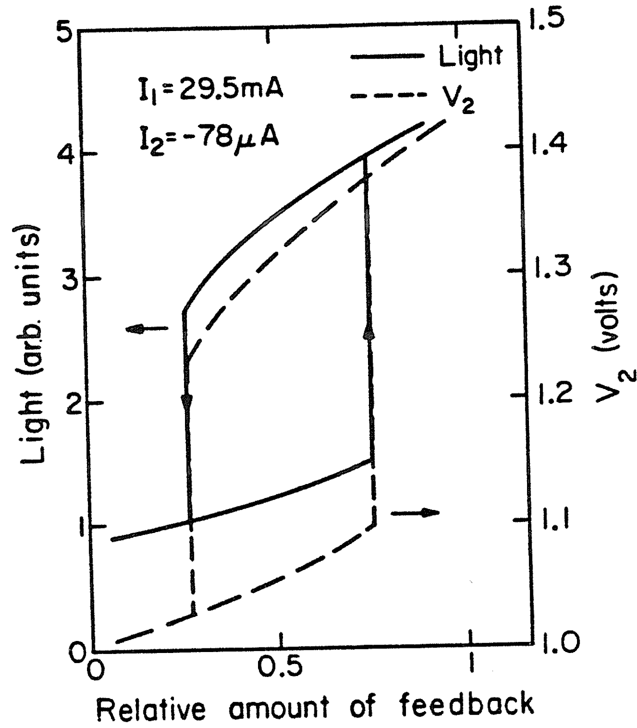

Figure 4.2.18. Hysteresis in the light versus relative feedback characteristic (solid line). Hysteresis in the voltage V_2 across the absorber section versus relative feedback characteristic (dashed line). A relative feedback of 1 corresponds to a total feedback of 50%.

optical disk readout, in which a rotating disk, carrying binary information as reflective spots is placed into the optical feedback path as shown in Fig. 4.2.19. The bistable laser serves as an integrated source detector combination. A larger flexibility in controlling the amount of optical feedback is achieved if one facet of the bistable laser is antireflection (AR) coated. Unlike the previous case with no AR-coating (Fig. 4.2.16) it is not necessary to maintain the bias currents I_1 and I_2 within a small range [4].

This application of the bistable laser as an optical stylus was simulated in our experiment by inserting a mechanical chopper in the external cavity. The measured voltage V_2, the output signal of the optical stylus , is shown in Fig. 4.2.20. The signal amplitude is very large V_{pp}=400mV, which is some three orders of magnitude larger than the signal of conventional self coupled detectors [32] which is only a few hundred microvolts. The slow rise (fall) in the voltage preceding the fast switch on (switch off) is caused by the finite transversal time of the chopper blade through the optical beam. The switching time is measured to be less than 70ns, consistent with that obtained by electrical switching of this bistable laser. Faster switching (< 20ns) can be achieved electrically by raising the switching pulse overdrive, an option not available in optical feedback switching. Critical slowing down similar to that in electrical switching of up to several μs is observed when the amount of feedback is just barley sufficient to cause switching. Using a bistable laser as an optical stylus in disk readout has the following advantages. The optical system can be kept simple, the signal to noise ratio is very good due to the optical schmidt-trigger characteristic and the detector output signal is a few hundred millivolts large. The switching speed is compatible with audio-disk applications.

The results above were obtained with the device operated in the bistable regime, by driving the absorber section with a high impedance source. No

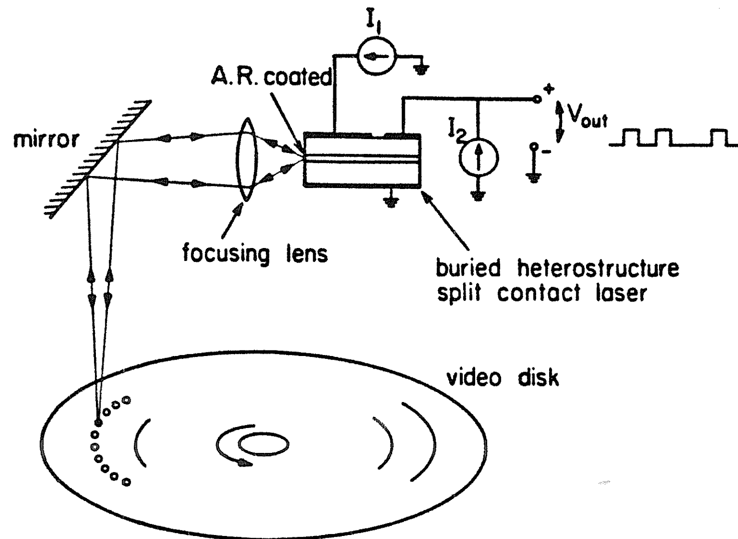

Figure 4.2.19. Application of the bistable laser as an optical stylus. The bias currents I_1 and I_2 are held at a constant value and the bistable laser is switched on and off by the light reflected back from the optical disk. The detector output signal V_2 is very large, $V_{2\,pp}$=400mV.

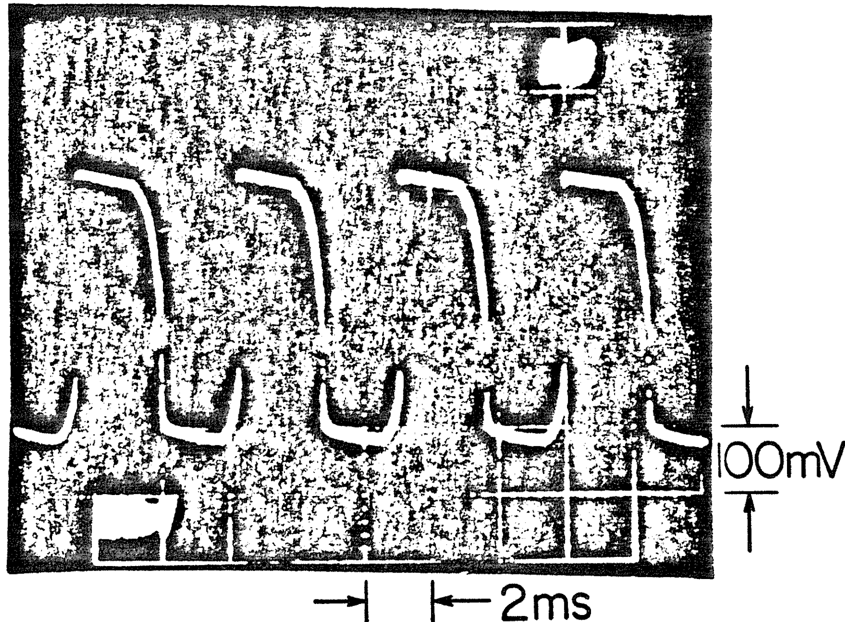

Figure 4.2.20. Measured detector output signal V_2 of the optical stylus shown in Fig. 18. The optical feedback is modulated by a rotating chopper disk in the optical feedback path. Hor.: 2ms/div, Ver.: 100mV/div.

pulsations can be observed within the detector bandwith of 5 GHz. As discussed above, and treated extensively in chapter five, the laser can be made to pulsate and have a very narrow hysteresis when it is biased with a low impedance source. Without optical feedback the electrical and optical pulsations occur at the relaxation resonance. With optical feedback the external cavity becomes the dominant frequency selective element and the laser is observed to pulsate at the roundtrip time of the external optical cavity. Note that such pulsations do not occur when the absorber section is driven with a current source in marked contrast to the results obtained using aged or damaged lasers [33], [34], [35]. This indicates that even though the intrinsic absorption of the semiconductor laser does not saturate more easily than the gain, the presence of inhomogeneous excitation in GaAs lasers can still produce pulsations. This can be understood by taking the electrical aspect of the injection laser into account as pointed out above.

4.2.9 Conclusions

We have found that double contact injection lasers can be made to display a large hysteresis in the light-current characteristic when the gain and absorber section are well insulated from each other. A negative differential resistance, which is opto-electronic in origin, is observed across the absorber section. Depending on the load impedance biasing the absorber section, this negative resistance can lead to (i) bistability with a very large hysteresis in the light-current characteristic without selfpulsations or (ii) a narrow hysteresis (or a light jump) with self pulsations at microwave frequencies. These results indicate that in the absence of side effects, such as local heating [36] or proton bombardment induced defects [24], the intrinsic absorption of GaAs does not saturate more easily than the gain and therefore will not produce pulsations

due to repetitive Q-switching [36]. The presence of inhomogeneous excitation caused by nonuniform contacts or centers of nonradiative recombination can however produce light-jumps and pulsations through a different mechanism involving the electrical aspect of the device as illustrated in section 3 and 5.

The dynamic switching characteristic of the bistable injection laser was investigated in some detail. While the switch off is usually fast, the switch on delay shows critical slowing down. The delay can be reduced to less than 20ns by increasing the trigger pulse overdrive. Switch delays between a few and a few hundred nanoseconds and power delay products between a few and a few hundred picojoules are obtained depending on the switch mechanism and the trigger pulse overdrive.

A simple model was analyzed which displays the main features of a semiconductor laser with inhomogeneous current injection, namely a large hysteresis in the light current characteristic and a negative differential resistance across the absorber section. A small signal analysis of this model leads to an equivalent electrical circuit which clarifies the frequency limitations of this negative differential resistance. This analysis also leads to a small signal interpretation of the observed critical slowing down at the transition points.

Experiments on interactions of this laser with an external optical cavity show that the behavior depends on the load impedance at the absorber section. A large load resistance produces bistability and a small one produces pulsations at the round trip time of the optical cavity with harmonics up to several GHz. In bistable operation, the switching can also be achieved by varying the amount of optical feedback. The associated switching in the voltage across the absorber section can be utilized in a digital disk readout. We showed that a bistable laser with an AR coating on one facet is even more suitable for this task. The switch-

ing speed is compatible with the application of this device as an optical stylus for audio-disk readout.

4.3 Outlook

From an application oriented point of view it is important to know if the switching speed of a few nanoseconds and the switch energy of a few picojoules (as measured in chapter 4.2. on practical devices) can be improved, how one would design such an optimized device and what are the basic limitations. The topic of the basic speed and power delay products (switching energies) of optical circuits (optical computers) is a very controversial one [37]. It is often claimed [37] that optical circuits have an inherent power delay advantage since an optical capacitance does not exist. We believe this to be wrong. We can see this easily by comparing the basic electrical and optical memory cells. An electrical memory cell is typically a capacitor which stores charge, nowadays around a few thousand electrons at 1 volt; a total energy of roughly 1 keV. The number of stored electrons cannot be decreased much below this level since this would increase the soft error rate above a tolerable level. It has been projected [37], that an optimized optical bistable device needs around one thousand photons, stored in a cavity or used up to saturate an absorber. At visible wavelengths this also corresponds to around 1keV. The bistable laser presented in chapter 4.2. is between a factor of 10^3 to 10^4 away from this ultimate limit. Similar energy arguments apply for interconnections since it does not really matter if we send 1000 electrons down a transmission line or 1000 photons through a waveguide.

In this paragraph we will investigate the switching energies of the bistable laser presented above. We can distinguish two different switching regimes [3], one for strong trigger pulses and one for moderate trigger pulses. In the case of

a strong trigger pulse the switch energy is given by the power delay product of a normal semiconductor laser, between 10^5 to 10^7 eV, depending on the laser structure. In the case of a moderate trigger amplitude the switching energy is given by the number of photons which are needed to saturate the absorber. In GaAs typical carrier densities for transparency are around $10^{18}cm^{-3}$. The switching energy is given by density × volume × energy = $10^{18}cm^{-3} \times 0.2 \times 2 \times 50 \mu m^3 \approx 3 \times 10^7 eV \approx 5pJ$. This value compares with the measured values quoted in section 4.2. which are a factor of two to ten times larger, probably due to parasitic loading. The switching energy scales with the geometrical size and it could be made smaller by two to three orders of magnitude by fabricating a laser the size of a few optical wavelenghts.

The accurate analysis of a bistable laser [38], [39], [25], [40] is rather complex and extremely difficult to apply to a practical laser system. The simple rate equations as used in section 4.2. provided for our purposes a model which was very useful and sufficient to explain most of the observed static and dynamic features.

A very interesting thermodynamic approach develops an analogy between second order phase transitions and the threshold behavior of lasers [41], [42]. This model has been extended to an analogy between first order phase transitions and bistable lasers. These analogies are very useful because the Landau free energy description of phase transitions relies implicitly upon the assumption of thermal equilibrium whereas the laser is explicitly a non equilibrium system. Thus much of the intuitive understanding of equilibrium physics may be borrowed to provide insight into non-thermal systems and vice versa.

4.4 References

1. Ch. Harder, K. Y. Lau, and A. Yariv, Appl. Phys. Lett. , vol. 39, p. 382 (1981).

2. Ch. Harder, K. Y. Lau, and A. Yariv, Appl. Phys. Lett. , vol. 40, p. 124 (1982).

3. K. Y. Lau, Ch. Harder, and A. Yariv, Appl. Phys. Lett. , vol. 40, p. 198 (1982).

4. K. Y. Lau, Ch. Harder, and A. Yariv, Appl. Phys. Lett. , vol. 40, p. 369 (1982).

5. Ch. Harder, K. Y. Lau, A. Yariv, IEEE J. Quantum Electron., vol. 18, p. 1351 (1982).

6. Ch. Harder, K. Y. Lau, A. Yariv, invited paper FC1, Integrated and guided wave optics conference, Pacfic Grove, California, January 1982.

7. Ch. Harder, K. Y. Lau, A. Yariv, invited paper TU6, 12th International quantum electronics conference, Munchen, Germany, June 1982.

8. G. J. Lasher, Solid-State Electron. , vol. 7, p. 707 (1964).

9. M. I. Nathan, J. C. Marinace, R. F. Rutz, A. E. Michel, and G. J. Lasher, J. Appl. Phys. , vol. 36, p. 473 (1965).

10. H. Kawaguchi, G. Iwane, Electron. Lett. , vol. 17, p. 167 (1981).

11. H. Kawaguchi, Electron. Lett. , vol 17, p. 741 (1981).

12. J. K. Carney and C. G. Fonstad, Appl. Phys. Lett. , vol 38, p. 303 (1981).

13. T. P. Lee, and R. H. R. Roldan, IEEE J. Quantum Electron. , vol. QE-6, p. 339 (1970).

14. N. G. Basov, IEEE J. Quantum Electron. , vol. QE-4, p. 855 (1968).

15. H. Ito, N. Onodera, K. Gen-ei, H. Inaba, Electron. Lett. , vol. 17, p. 15 (1981).

16. K. Hanamitsu, T. Fujiwara, and M. Takusagawa, Appl. Phys. Lett. , vol. 39, p. 14 (1981).

17. J. K. Carney, C. G. Fonstad, IEEE J. Quantum Electron., vol. 19, p. 22 (1983).

18. R. W. Dixon, W. B. Joyce, IEEE J. Quantum Electron. , vol. QE-15, p.470 (1979).

19. T. Ohmi, S. Yamazaki, IEEE J. Quantum Electron. , vol. QE-9, p. 366 (1973).

20. R. Bonifacio, P. Meystre, Opt. Commun. , vol. 29, p. 131 (1979).

21. E. Garmire, J. H. Marburger, S. D. Allen, and H. G. Winful, Appl. Phys. Lett. , vol. 34, p. 374 (1979).

22. N. Bar-Chaim, J. Katz, I. Ury, A. Yariv, Electron. Lett. , vol. 17, p. 108 (1981).

23. C. H. Henry, R. A. Logan, and K. A. Bertness, J. Appl. Phys. , vol. 52, p. 4457 (1981).

24. J. F. Scott, M. Sargent III, C. D. Cantrell, Opt. Commun. , vol. 15, p. 13 (1975).

25. L. A. Lugiato, P. Mandel, S. T. Dembinski, A. Kossakowski, Phys. Rev. A , vol. 18, p. 238 (1978).

26. H. Kressel, J. K. Butler, Semiconductor Lasers and Heterojunction LEDs. Academic Press, (1977).

27. T. G. Dziura, D. G. Hall, IEEE J. Quantum Electron., vol. 19, p. 433 (1983).

28. C. H. Henry, R. A. Logan, F. R. Merritt, J. Appl. Phys. , vol. 51, p. 3042 (1980).

29. D. Marcuse, F. R. Nash, IEEE J. Quantum Electron. , vol QE-18, p. 30 (1982).

30. W. B. Joyce and R. W. Dixon, Appl. Phys. Lett. , vol. 31, p. 354 (1977).

31. T. L. Paoli, IEEE J. Quantum Electron. , vol. QE-16, p. 1248 (1980).

32. Y. Mitsuhashi, J. Shimada, and S. Mitsutsuka, IEEE J. Quantum Electron. , vol. QE-17, p. 1216 (1981).

33. K. Y. Lau, L. Figueroa, and A. Yariv, IEEE J. Quantum Electron. , vol. QE-16, p. 1329 (1980).

34. J. P. van der Ziel, W. T. Tsang, R. A. Logan, and W. M. Augustyniak, Appl. Phys. Lett. , vol. 39, p. 376 (1981).

35. J. P. van der Ziel, W. T. Tsang, R. A. Logan, R. M. Mikulyak, and W. M. Augustyniak, Appl. Phys. Lett. , vol. 39, p. 525 (1981).

36. C. H. Henry, J. Appl. Phys. , vol. 51, p. 3051 (1980).

37. D. A. B. Miller, Laser Focus, p. 79 (1982).

38. T. Erneux, P. Mandel, Z. Phys. B.-Condensed Matter, vol. 44, p. 353 (1981).

39. T. Erneux, P. Mandel, Z. Phys. B.-Condensed Matter, vol. 44, p. 365 (1981).

40. L. A. Lugiato, P. Mandel, S. T. Dembinski, A. Kossakowski, Phys. Rev. A, vol. 18, p. 1145 (1978).

41. H. Haken, Synergetics, B. G. Teubner (1973).

42. H. Haken, Rev. Mod. Phys., vol. 47, p. 67 (1975).

Chapter 5

Mode locking

5.1 Introduction

The technique of phase locking the different modes of a laser has been extensively used to generate ultrashort high intensity pulses and pulse lengths as short as 90 femtoseconds have been reported [1]. This technique was first analyzed by A. Yariv [2] and an excellent introduction can be found in his textbook [3]. There are essentially two methods to phaselock the different longitudinal modes; active mode locking and passive mode locking. In the first case the coupling is obtained by modulating a laser parameter, such as loss, gain or index of refraction, at a frequency corresponding to the intermode spacing. This modulation generates sidebands which coincide with the the neighboring longitudinal modes. The phases of the different longitudinal modes are locked together through interaction with each other through these sidebands. In this chapter we will address the case of passive mode locking which is achieved by placing a nonlinear element (such as a saturable absorber) in the cavity of a multimode laser causing the different longitudinal modes to interact now through this nonlinear element. Their phases will become only locked if the nonlinear element fulfills specific requirements. We will address these conditions in section 5.2 and discuss them extensively in section 5.3.

The repetition rate of the pulses emitted by a mode locked laser corresponds to the longitudinal mode spacing, that is, to the round trip time of an optical

pulse in the laser cavity. Since semiconductor lasers are typically around 0.3 mm long the repetition rate would be extremely fast, 4.3 picoseconds, and it would also be extremely difficult to lock the modes which are spaced by 233 GHz. Making the semiconductor lasers much longer is technologically difficult and this will remain so until long, low loss waveguides (with losses less than 1 cm^{-1}) can be fabricated on GaAs.

Lately, the rigor of the term " mode locking " has eroded somewhat and it is also used in cases where the phases of different modes are only partially locked. We will use in the following this expanded definition. In chapter 4 we have seen that a semiconductor laser with two contacts has a negative differential resistance, causing the laser to be unstable and to oscillate. Since the negative differential resistance is not frequency selective such a laser will oscillate at a frequency dictated by an external tank circuit, be it an electrical tank circuit (an LC combination) or an optical tank circuit such as an external optical cavity. Since the bandwidth of the negative electrical resistance is given essentially by the stimulated carrier lifetime, (see chapter 4), it is not expected that the pulses become extremely short, i.e. not shorter than 20 ps for typical parameters of our lasers. In section 5.2 we present experimental results of such a laser with a split contact which has been coupled to an external cavity [4]. In section 5.3 the requirements on the absorber for passive mode locking are derived and an improved laser structure to obtain extremely short pulses is proposed.

5.2 Passive mode locking of buried heterostructure lasers with nonuniform current injection

5.2.1 Introduction

Ultrashort optical pulses generated with semiconductor lasers are of great interest for applications such as very fast optical signal processing and high bit rate communication. Pulses in the picosecond range have been obtained by such diverse methods as microwave current injection [5], pumping with short electrical pulses [6] or by mode locking the lasers in an external optical cavity. Mode locking has been achieved either by modulating the gain at a frequency corresponding to the cavity round trip time (active mode locking [7-16]) or by placing a nonlinear element such as a saturable absorber in the cavity (passive mode locking [17-21]) and the shortest pulses to date have been generated by the passive mode locking technique [19], [21]. The usually quoted necessary condition to obtain passive mode locking with an homogeneously broadened laser is that the absorbing medium saturate much more easily with optical intensity than the gain medium [22]. In order to passively mode lock a semiconductor laser one has to place an absorber with this desired characteristic in the external optical cavity. It seems promising to use unpumped GaAs as the absorber i.e. to pump only part of the semiconductor laser and to use the unpumped section as the absorber. Unfortunately measurements of the gain as a function of the carrier density in GaAs lasers [23] indicate that the absorption in unpumped GaAs does not saturate more easily than the gain. However, an absorber with the desired characteristic can be obtained by damaging the GaAs crystal and introducing defects. These defects are optically absorbing and can be saturated very easily. One method for obtaining such defects (dark line defects) is to age a laser to the point of severe degradation. Pulses as short as

1.3 picoseconds have been achieved with this technique [21]. Unfortunately the concentration of these defects increases at this stage rapidly and short pulses are only obtained with lasers at the verge of failure. Another method is to introduce these saturable defects by damaging the crystal near one mirror through proton bombardment [24]. 15 picosecond long bursts of sub-picosecond pulses have been generated by this technique [19].

In this section we report on a different method for producing picosecond pulses which does not rely on any damage of the crystal and which is consequently inherently more reliable. The picosecond pulses are generated by a laser with nonuniform current injection obtained through a split contact structure [25]. We have shown that for a complete description of such an opto-electronic device the electrical aspect has to be included and that the necessary condition for small signal instability is less restrictive than the one quoted above; indeed, we have shown that a nonuniform pumped laser (with a linear gain dependence on carrier density and a bimolecular recombination rate) can either be bistable or pulsating depending on the biasing condition.

5.2.2 Short pulse generation

The GaAlAs buried heterostructure lasers with a split contact were fabricated in our laboratory as described earlier [25]. Under the usual operating conditions one section is heavily forward biased (gain section) and the other section is only slightly biased thus introducing loss (absorber section). An SiO anti reflection (AR) coating was applied to one mirror facet in order to facilitate the coupling to the external optical cavity and to suppress the effects of the short cavity. The gain section was pumped with a constant current (I_1) and the absorbing section was biased with a voltage source (V) with a resistor in series (R_2) as shown in Fig. 5.2.1. The external optical cavity consisted of a 0.3 n.a.

microscope objective which collimated the light and a dielectric mirror with a reflectivity of 90%. The light emitted from the AR coated facet was reinjected into the active region by careful adjustment of the mirror and the lens. The degree of reinjection was monitored by measuring the voltage across the absorbing section which greatly facilitated the alignment procedure. The optical cavity length was varied between 10cm and 30cm corresponding to a pulsation frequency between 500MHz and 1.5GHz. From the changes in the threshold current of the uniform pumped laser we estimated that the mirror reflectivity was reduced to around 1% to 3% after deposition of the AR coating and that the effective mirror reflectivity in the external cavity was around 6%. The light emitted from the back facet of the laser was collimated and focused on a wide bandwidth avalanche photodiode (AEG-Telefunken S 171P) with a calibrated risetime of 120ps. The width of the optical pulses were measured with an autocorrelator employing phase matched second harmonic generation in a $LiIO_3$ crystal [26]. A photomultiplier tube was used to detect the relatively weak frequency doubled signal which was of the order of a few femtowatts at a wavelength of 440 nm.

The average light output as a function of current through the gain section (I_1) is shown in Fig. 5.2.2. As reported earlier [27] the charcteristic depends dramatically on the biasing resistor R_2 which is in series with the absorber section. When R_2 is large (R_2=200kΩ), a condition to which we will refer as current biasing, the pump rate is constant and the device displays bistability with a large hysteresis. When R_2 is small (R_2=330Ω), i.e. voltage biasing, the carrier density in the absorber section is clamped and the device displays a region with a very high differential quantum efficiency (light jump). It is a unique feature of semiconductor diode lasers that the carrier density inside the active region can be clamped from the outside by biasing the diode with a constant voltage

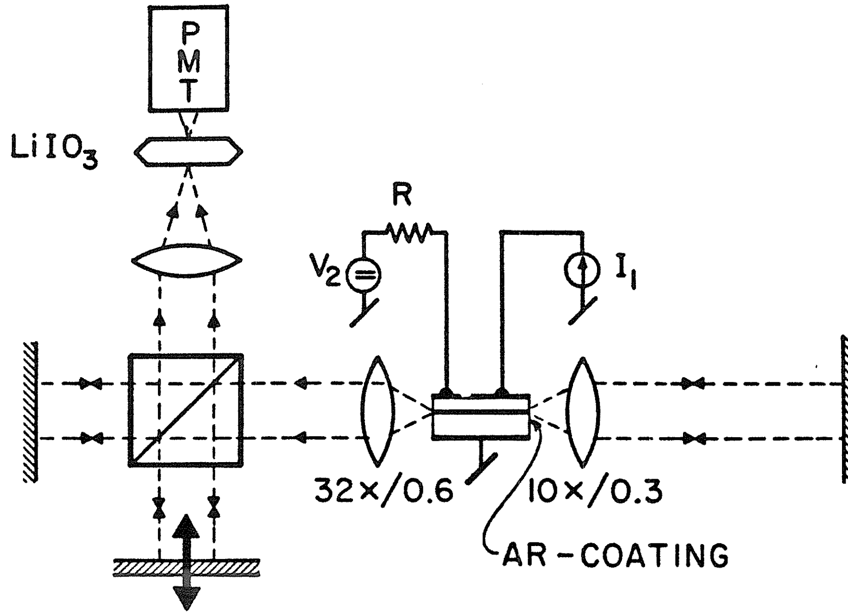

Figure 5.2.1. Experimental arrangement of a double contact laser which is passively mode locked in an external optical cavity. Also shown is the pulse measurement system consisting of an avalanche photodiode (APD) and an autocorrelator employing a 3mm long $LiIO_3$ crystal as the nonlinear medium.

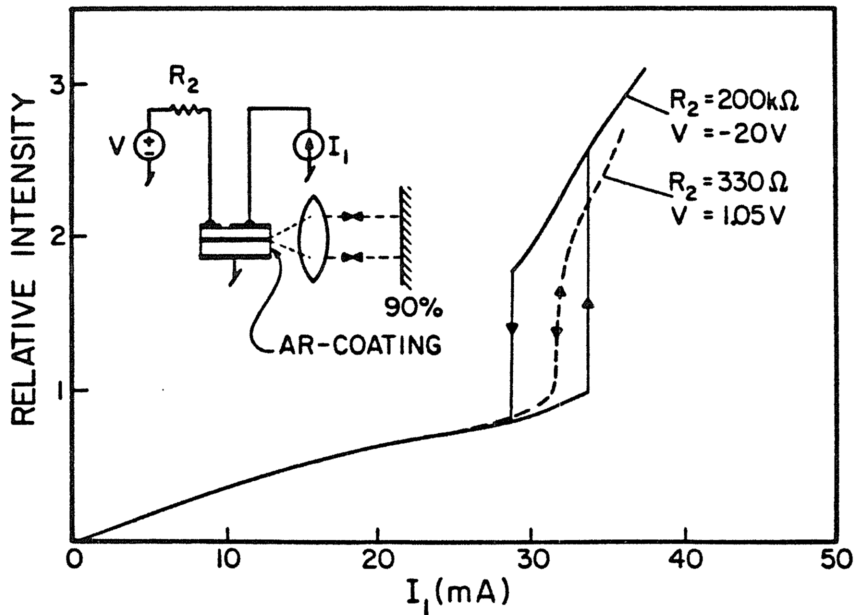

Figure 5.2.2. Light-current characteristic of a double contact laser in an external optical cavity for current biasing (R_2=200kΩ ; V=−20V) and voltage biasing (R_2=300Ω ; V=1.05V) as measured with the avalanche photodiode (APD).

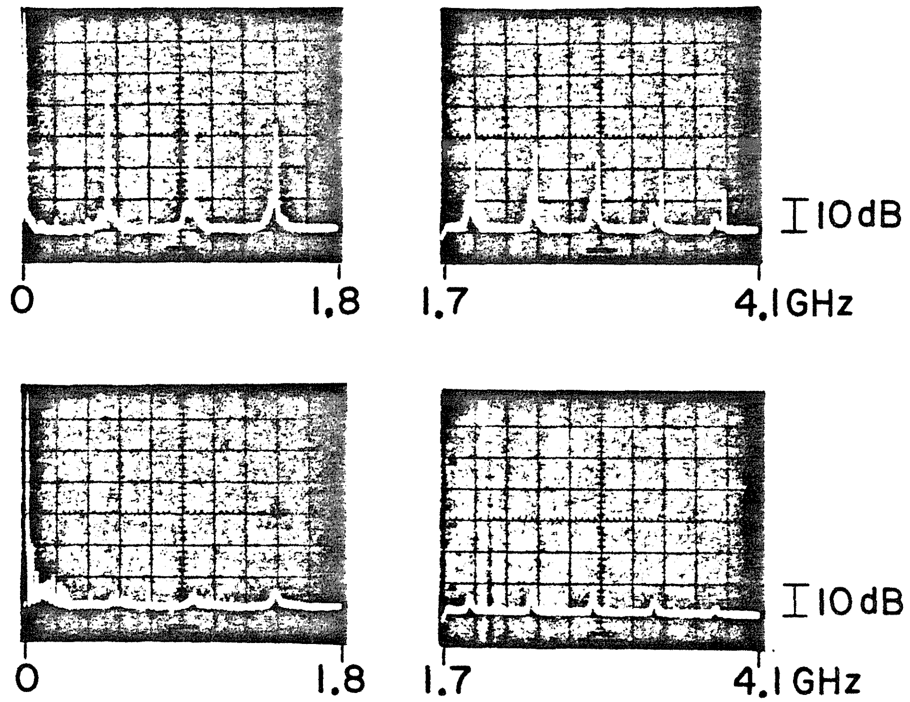

Figure 5.2.3. Typical microwave spectrum of the optical output as measured with the avalanche photodiode (APD) for voltage biasing (top half) and current biasing (lower half) for a cavity length of 30cm.

source. We have shown earlier [25] that through this voltage biasing the laser can be forced into operating points not attainable with current biasing. Fig. 5.2.3 shows the microwave spectrum of the photocurrent generated in the avalanche photodiode for voltage biasing (upper half) and current biasing (lower half). In the current biasing mode the laser light output is stable and only some small noise peaks can be seen at multiples of the frequency corresponding to the round trip time. Through voltage biasing the laser can be forced to operate in an unstable regime where it self pulsates [25]. The pulsation rate is around 500 MHz for this specific case corresponding to a cavity length of 30cm. This rate is fairly stable having a linewidth of less than 20KHz. Harmonics up to 4 GHz can be observed and they are limited by the bandwidth of the photodiode. The shortest pulses were observed when the laser was biased just above the light jump and the pulses observed with a sampling oscilloscope were detector limited 150ps long with a modulation depth close to 100%.

A typical second order correlation trace is shown in Fig. 5.2.4. The laser is voltage biased and operated at a current I_1 just above the light jump in a cavity with a length of 30cm. The correlation trace consists of a relatively broad peak with a width of $\Delta\tau_1$=53ps upon which is superimposed a series of extremely sharp spikes with a width of $\Delta\tau_2$=1.4ps and a separation of t_2=5.5ps. Since the second order correlation has an intensity ratio of 1:2:3 this trace corresponds in the time domain to a pulse with some noisy periodic substructure [28]. Assuming gaussian shapes and transform limited pulses we obtained a FWHM of Δt_1=37ps and a spectral width of $\Delta\nu_1$=12GHz ($\Delta\lambda_1$=0.3Å). This means that around twenty longitudinal modes of the external cavity are phase locked. The separation t_2 between the spikes corresponds to the round trip time in the semiconductor cavity (L=200μm). Under stable operating condition these lasers typically emitted all their power into one single longitudinal mode. After applying

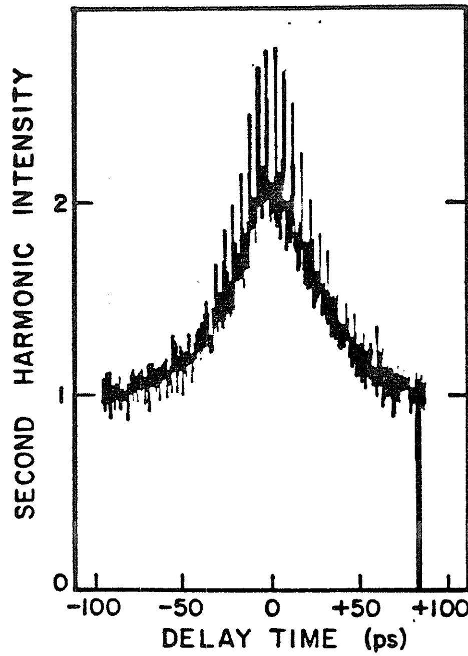

Figure 5.2.4. Auto correlation trace of the passively mode locked diode laser. FWHM of the pulse is around 35ps.

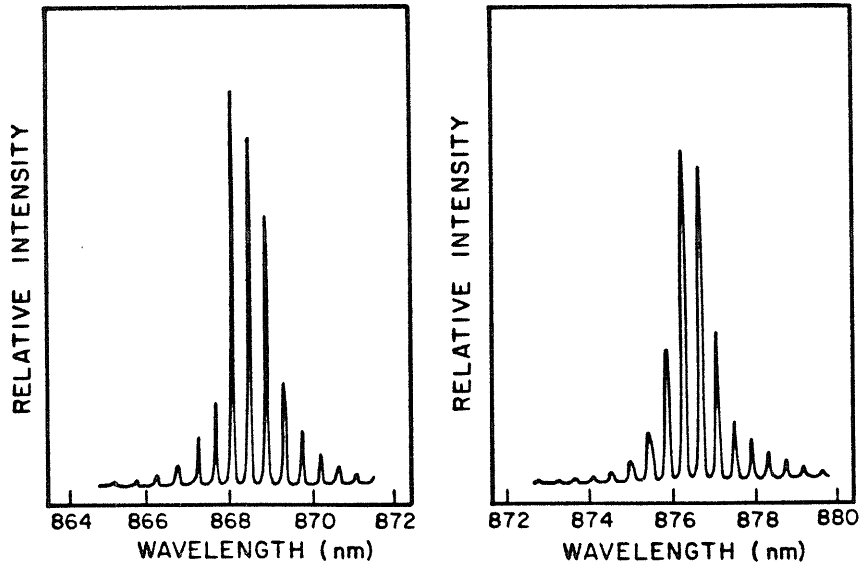

Figure 5.2.5. Optical spectrum of the laser with a segmented contact placed into an external cavity. On the left side is the spectrum shown when the absorber section is current biased (stable output) and on the right side is the spectrum shown with the absorber section voltage biased (pulsating output).

the AR coating they operated multilongitudinal as shown in Fig. 5.2.5 on the left side with a separation of 4.5Å corresponding to the semiconductor length L. The width of the modes was 0.3Å, limited by the resolution of the spectrometer. Under mode locking conditions the modes broadened appreciably to around 0.9Å as can been seen in Fig. 5.2.5 on the right half. Even if we take the finite resolution of the spectrometer into account the modes are broader than expected from transform limitations. This could be explained by a frequency chirp due to the variation of the carrier density in the active region during one pulse. The separation of the clusters of locked modes corresponds to the separation in time (5.5ps) of the fine structure of the second order correlation and the overall width of the spectrum (10Å) corresponds to the width of the fine structure.

5.2.3 Conclusion

We have shown in this section 5.2 that nonuniform pumping of a semiconductor laser is an excellent means of introducing saturable absorption in a controllable way. This absorption can lead to bistability or pulsations depending on the biasing conditions. We utilized this scheme to generate picosecond pulses by passively mode locking this device in an external optical cavity. This passive mode locking technique is inherently more reliable since it does not rely on absorption introduced by damaging the GaAs crystal. By using a large optical cavity structure the coupling to the external cavity could be made stronger and easier and by introducing a bandwidth limiting element [17], [29] transform limited pulses should be obtained.

5.3 Large signal analysis of pulsations

The usually quoted necessary condition for passive mode locking of a homo-

geneously broadened laser is that the absorbing medium saturate much more easily with optical intensity than the gain medium [22]. It has been shown [30] that the condition for self sustained pulsations is exactly the same. In this section we will derive this condition for pulsations. We start with the rate equations for a laser with two sections, a gain section (with the subscript 1) and an absorber section (with the subscript 2). The gain occupies the fraction α of the laser cavity and the absorber section the fraction $(1-\alpha)$.

$$\frac{dN_1}{dt} = J_1 - R(N_1) - \frac{c}{n} g(N_1)\, P \qquad (5.3.1)$$

$$\frac{dN_2}{dt} = J_2 - R(N_2) - \frac{c}{n} g(N_2)\, P \qquad (5.3.2)$$

$$\frac{dP}{dt} = \frac{c}{n} (\alpha g(N_1) + (1-\alpha) g(N_2) - \frac{n}{c\tau_p})\, P \qquad (5.3.3)$$

N is the carrier density, R(N) is the spontaneous recombination rate of the carriers, g(N) is the gain in cm^{-1} and $\frac{c}{n}$ is the group velocity of the light. It is assumed that the optical pulse is long compared to the laser cavity length and that the photon density P can be assumed to be uniform in the cavity, an approximation which is good for pulses longer than 2ps in a laser which is 0.3 mm long. The photon lifetime is τ_p. For the following discussion it is very useful to introduce the phase plane with the coordinates N_1 (carrier density in the gain section) and N_2 (carrier density in the absorber section). We can solve in the static case equation (5.3.3) for N_1 as a function N_2, to obtain the equilibrium condition.

$$N_1 \equiv f(N_2) = g^{-1}(\frac{1}{\alpha}(\frac{n}{c\tau_p} - (1-\alpha) g(N_2))) \qquad (5.3.4)$$

This equilibrium line is plotted in Fig. 5.3.1A. Below this equilibrium line $\dot{P} < 0$ (the dot stands for the derivative with respect to time), i.e. the photon popula-

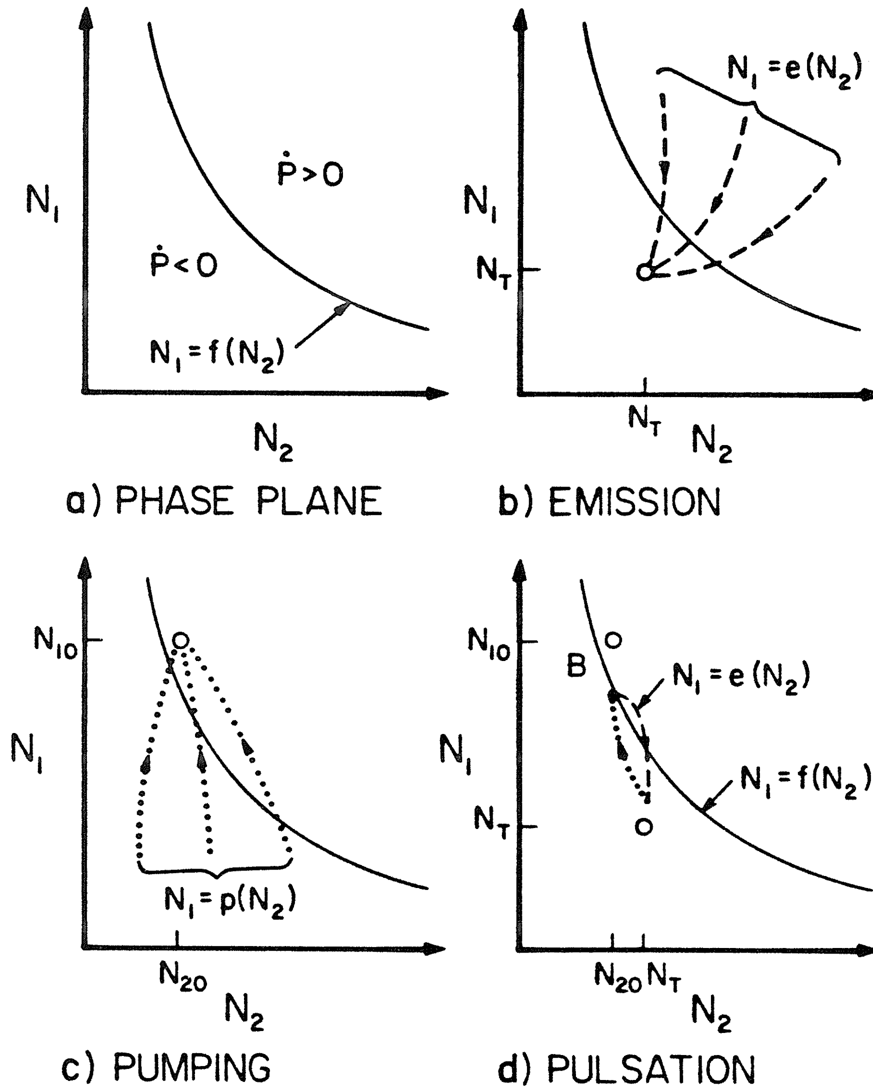

Figure 5.3.1. Derivation of the condition for pulsations.

tion decreases. Above this equilibrium line $\dot{P} > 0$, i.e. the light output increases.

When we analyze one cycle of the pulsations we can distinguish two subcycles, emission (when the light pulse is emitted) and pumping (when the light pulse is over and the laser is pumped back to its initial value). During the emission subcycle gain and absorber are getting saturated and the state in the phase plane moves towards the point $N_1 = N_T$, $N_2 = N_T$ as shown in Fig. 5.3.1b along the curve $N_1 = e(N_2)$, where N_T is defined as the transparency carrier density; $g(N_T) \equiv 0$. During the pumping subcycle it is assumed that the photon density P=0 and the state moves as shown in Fig. 5.3.1c towards the point $N_1 = N_{10}$, $N_2 = N_{20}$, along $N_1 = p(N_2)$, where by definition $R(N_{10}) \equiv J_1$ and $R(N_{20}) \equiv J_2$. A complete pulsing cycle is shown in Fig. 5.3.1d. During the pumping subcycle the state which moves along $N_1 = p(N_2)$ hits the equilibrium line $N_1 = f(N_2)$ at the point B and the emissive subcycle starts moving along $N_1 = e(N_2)$. A pulse builds only up if the emissive path starts from the point B to the right of the equilibrium line $N_1 = f(N_2)$ into the region with $\dot{P} > 0$. This gives the condition for pulsations.

$$\frac{de(N_2)}{dN_2}\Big|_B \geq \frac{df(N_2)}{dN_2}\Big|_B \tag{5.3.5}$$

By dividing equation (5.3.1) through (5.3.2) we obtain:

$$\frac{de(N_2)}{dN_2}\Big|_B = \frac{dN_1}{dN_2}\Big|_B = \frac{J_1 - R(N_1) - \frac{c}{n} g(N_1) P}{J_2 - R(N_2) - \frac{c}{n} g(N_2) P}\Big|_B \tag{5.3.6a}$$

Now we assume that the photon density P is very large, as it is the case during the emissive cycle and we get from (5.3.6a):

$$\frac{de(N_2)}{dN_2}\Big|_B = \frac{g(N_1)}{g(n_2)}\Big|_B \tag{5.3.6b}$$

From equation (5.3.4) we obtain:

$$\frac{df(N_2)}{dN_2}\Big|_B = \frac{dg^{-1}(\frac{1}{\alpha}(\frac{n}{c\tau_p}-(1-\alpha)g(N_2)))}{dN_2} = -\frac{1-\alpha}{\alpha}\frac{g'(N_2)|_B}{g'(N_1)|_B} \tag{5.3.7}$$

where we defined $g'(N) \equiv \frac{dg(N)}{dN}$. Plugging equations (5.3.6b) and (5.3.7) in (5.3.5) we obtain the pulsation condition:

$$\frac{g'(N_1)|_B}{g'(N_2)|_B} \leq \frac{1-\alpha}{\alpha}\frac{-g(N_2)|_B}{g(N_1)|_B} \equiv \eta_{tr} \tag{5.3.8a}$$

$$\eta_{tr} \equiv \frac{1-\alpha}{\alpha}\frac{-g(N_2)|_B}{g(N_1)|_B} = \frac{\text{loss in saturable absorber}}{\text{total loss in laser}} \tag{5.3.8b}$$

The transport efficiency η_{tr} is equal to the probability that a photon emitted in the gain section is captured in the absorber section and is used to saturate loss. The transport efficiency depends on the geometry and other laser parameters and is always smaller than one.

The gain as a function of carrier density as measured in intrinsic GaAlAs [23] is shown in Fig. 5.3.2a. Indicated are also the typical operating points of the gain section (point 1) and the absorber section (point 2). It can be seen immediately that this gain dependence does not fulfill the large signal pulsation condition as stated in (5.3.8), i.e. that the steepness of g(n) at point 2 is larger by at least a factor $\frac{1}{\eta_{tr}}$ than the steepness of g(n) at point 1. The more subtle small signal analysis, as developed in chapter 4, is appropriate for stability considerations in this case.

In Fig. 5.3.2b the gain curve of damaged GaAlAs is shown. The absorption due to line or point defects is expected to be easily saturable. A laser with such parameters fulfills the pulsation condition (5.3.8) and will self pulsate or can be passively mode locked. The defects can be introduced by proton bombarding the GaAlAs or by operating the laser for a short time at excessive current or optical intensity levels as discussed in section 5.2.

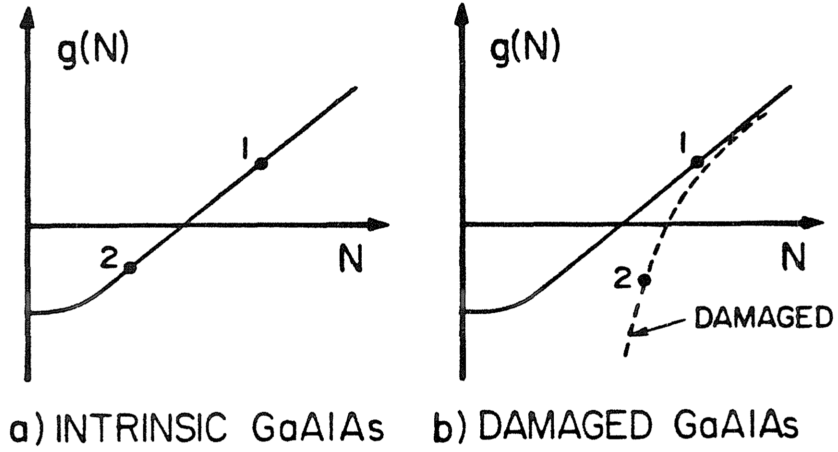

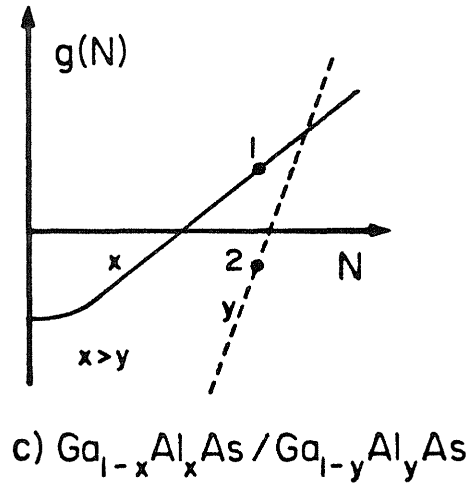

Figure 5.3.2. Gain as a function of the carrier density: a) intrinsic GaAlAs, b) damaged GaAlAs, c) $Ga_{1-x}Al_xAs$ for two different aluminium concentrations.

Fig. 5.3.2c shows the gain curve for GaAlAs with two different aluminium concentrations x and y [23]. Lasers with nonuniform aluminum concentration in the active region along the cavity length can be easily fabricated [31]. Such an injection laser with two sections, a gain section with a larger aluminium concentration than in the absorber section is expected to be a reliable device to produce ultra short pulses.

5.4 References

1. R. L. Fork, B. I. Greene, C. V. Shank, Appl. Phys. Lett. 38, 671 (1981).

2. A. Yariv, J. Appl. Phys. 36, 388 (1965).

3. A. Yariv, " Quantum Electronics", 2nd edition, John Wiley and Sons, 1975, chapter 11.

4. Ch. Harder, J. S. Smith, K. Y. Lau, A. Yariv, Appl. Phys. Lett. 42, *** (1983).

5. J. P. van der Ziel, R. A. Logan, IEEE J. Quantum Electron. 18, 1340 (1982).

6. P. L. Liu, C. Lin, I. P. Kaminow, J. J. Hsieh, IEEE J. Quantum Electron. 17, 671 (1981).

7. P. T. Ho, L. A. Glasser, E. P. Ippen, H. A. Haus, Appl. Phys. Lett. 33, 241 (1978).

8. L. A. Glasser, Electron. Lett. 14, 725 (1978).

9. P. T. Ho, Electron. Lett. 15, 526 (1979).

10. J. P. van der Ziel, R. M. Mikulyak, J. Appl. Phys. 51, 3033 (1980).

11. H. Ito, H. Yokoyama, H. Inaba, Electron. Lett. 16, 620 (1980).

12. D. J. Bradley, M. B. Holbrook, W. E. Sleat, IEEE J. Quantum Electron. 17, 658 (1981).

13. J. P. van der Ziel, J. Appl. Phys. 52, 4435 (1981).

14. J. P. van der Ziel, R. A. Logan, R. M. Mikulyak, Appl. Phys. Lett. 39, 867 (1981).

15. M. B. Holbrook, W. E. Sleat, D. J. Bradley, Appl. Phys. Lett. 37, 59 (1980).

16. J. C. AuYeung, A. R. Johnston, Appl. Phys. Lett. 40, 112 (1982).

17. E. P. Ippen, D. J. Eilenberger, R. W. Dixon, Appl. Phys. Lett. 37, 267 (1980).

18. L. Figueroa, IEEE J. Quantum Electron. 17, 1074 (1981).

19. J. P. van der Ziel, W. T. Tsang, R. A. Logan, R. M. Mikulyak, W. M. Augustyniak, Appl. Phys. Lett. 39, 525 (1981).

20. H. Yokoyama, H. Ito, H. Inaba, Appl. Phys. Lett. 40, 105 (1982).

21. E. P. Ippen, D. J. Eilenberger, R. W. Dixon, in Picosecond Phenomena II, edited by R. Hochstrasser, W. Kaiser, C. V. Shank (Springer, New York 1980).

22. H. A. Haus, IEEE J. Quantum Electron. 12, 169 (1976).

23. C. H. Henry, R. A. Logan, F. R. Merritt, J. Appl. Phys. 51, 3042 (1980).

24. J. P. van der Ziel, W. T. Tsang, R. A. Logan, W. M. Augustyniak, Appl. Phys. Lett. 39, 376 (1981).

25. Ch. Harder, K. Y. Lau, A. Yariv, IEEE J. Quantum Electron. 18, 1351 (1982).

26. E. P. Ippen, C. V. Shank, in Picosecond Phenomena, edited by C. V. Shank, E. P. Ippen, S. L. Shapiro (Springer, New York 1978).

27. K. Y. Lau, Ch. Harder, A. Yariv, Appl. Phys. Lett. 40, 369 (1982).

28. H. A. Pike, M. Hercher, J. Appl. Phys. 41, 4562 (1970).

29. H. A. Haus, P. T. Ho, IEEE J. Quantum Electron. 15, 1258 (1979).

30. R. W. Dixon, W. B. Joyce, J. Appl. Phys. 15, 470 (1979).

31. S. Yamamoto, H. Hayashi, T. Hayakawa, N. Miyauchi, S. Yano, T. Hijikata, Appl. Phys. Lett. 42, 406 (1983).

Chapter 6

Amplitude noise in semiconductor laser diodes

6.1 Introduction

An ideal monochromatic radiation field can be represented by

$$\varepsilon_{ideal}(t) = E_0\cos(\omega_0 t) \tag{6.1.1}$$

where E_0 is the field amplitude and ω_0 is the optical frequency and both are constant. A real radiation field of a laser undergoes random amplitude and phase fluctuations and the field is of the form:

$$\varepsilon_{real}(t) = E(t)\cos(\omega_0 t+\Phi(t)) \tag{6.1.2}$$

where $E(t)$ and $\Phi(t)$ change only by a small fraction during one optical period. Many mechanisms in a practical laser cause the random fluctuation in amplitude and phase and most of them can be eliminated (at least theoretically) by various improvements such as eliminating temperature fluctuations and mechanical disturbances. However, there remain intrinsic fluctuations of the radiation field which are quantum mechanical in origin. The exact theoretical analyses [1], [2] which treat the whole laser system (light and matter) quantum mechanically are very complex and extremely difficult to apply to a practical laser system. The basic results of these treatments can also be obtained by simplified theories, the most prominent two being the Van der Pol treatment [3], [4], [5] and the Langevin approach which adds noise source terms to the rate

equations [6].

In the first method the laser is treated as an oscillator with saturable gain which is driven by noise, i.e. spontaneous emission. The resulting equation for the radiation field is of the Van der Pol form and can be solved to yield expressions for amplitude and phase fluctuations. Recently this method has been modified by Vahala and Yariv [5] to include the carrier density as a dynamical variable.

Very often only amplitude fluctuations are of interest, i.e. if the light is measured by a square law detector, such as a photodiode or a photomultiplier. The signal i(t) is then given by:

$$i(t) \propto E^2(t) \tag{6.1.3}$$

McCumber developed a laser theory to calculate these amplitude fluctuations by adding noise sources to the standard rate equations to account for quantum mechanical fluctuations. These noise sources are obtained in a Langevin model which associates a noise impulse of unit integrated intensity with each change in the electron or photon population. The beauty of this shot noise model is that it provides a simple physical explanation of the origin of the intrinsic quantum fluctuations and that it permits us to infer the magnitude of the quantum noise sources by an inspection of the rate equations. In this chapter we implement these shot noise sources in the electrical equivalent circuit [7]. This equivalent circuit allows a straightforward calculation of the noise and modulation characteristics of a laser diode which is combined with electronic components.

6.2 Noise equivalent circuit of a semiconductor laser diode

6.2.1 Introduction

Modeling of semiconductor laser diodes combined with other electronic components requires an accurate representation of the laser. As a first step a small signal electrical circuit of a laser has been developed [8], [9]. The purpose of this work is to extend the model to include noise sources. The extended equivalent circuit allows a straightfoward calculation of the modulation and noise characteristics of a laser and the dependence on the extrinsic elements, such as the driving source and the parasitic elements.

Intrinsic intensity fluctuations in semiconductor laser diodes are caused by quantum-statistical photon generation and electron-hole recombination within the lasing medium. The intensity noise spectrum for laser light was first calculated by McCumber for a four level laser system using rate equations with Langevin noise sources [6]. A quantum-mechanical justification of such an approach has been given by Lax [10]. Later, this model was adapted to semiconductor lasers [11], [12]. In early GaAs diode lasers the intrinsic light fluctuations were masked by excess noise due to inadequate transverse mode control, but measurements in stripe contact lasers were nevertheless able to confirm the basic features of the theory, namely large fluctuations at the onset of stimulated emission and a high frequency noise peak at the resonance frequency of the laser [13].

Recently it has been verified experimentally [14], [15], that mode stabilized lasers, such as the channeled-substrate planar and the buried heterostructure, operate at the quantum noise limit, in excellent agreement with McCumber's noise theory. These intrinsic intensity fluctuations are usually very small and the noise performance of an optical communication system is normally

determinded by the receiver, but in some specific applications, the quantum noise may significantly reduce the signal to noise ratio [16].

6.2.2 Intensity noise of a single mode laser diode

The spectral intensity of the quantum fluctuations of the photon and electron population can be found by adding to the familiar rate equations Langevin source terms for electrons $f_N(t)$ and for photons $f_S(t)$, assumed to have shot noise character [6], [11].

$$\frac{dn}{dt} = \frac{i}{q} - \frac{n}{\tau_s} - (E_{CV} - E_{VC}) s + f_N \qquad (6.2.1a)$$

$$\frac{ds}{dt} = (E_{CV} - E_{VC}) s + \beta \frac{n}{\tau_s} - \frac{s}{\tau_{ph}} + f_S \qquad (6.2.1b)$$

n and s are the total number of electrons in the gain medium and photons in the single lasing mode. The pump rate is $\frac{i}{q}$, τ_s is the spontaneous and τ_{ph} the photon lifetime. E_{CV} s is the downward stimulated rate (stimulated emission) and E_{VC} s is the upward stimulated transition rate (stimulated absorption). The gain g, which is by definition the net stimulated emission, is $g = E_{CV} - E_{VC}$. $\beta \frac{n}{\tau_s}$ is the spontaneous emission coupled into the lasing mode. By setting $\langle f_N \rangle = \langle f_S \rangle = 0$, where $\langle \, \rangle$ denotes the time average, the equations for the average rates are obtained.

$$\frac{i_0}{q} - \frac{n_0}{\tau_s} - g_0 s_0 = 0 \qquad (6.2.2a)$$

$$- \frac{s_0}{\tau_{ph}} + g_0 s_0 + \beta \frac{n_0}{\tau_s} = 0 \qquad (6.2.2b)$$

For a given dc pump current i_0 and gain dependence on injected carriers $g(n)$, we can calculate using equations (6.2.2) the resulting average electron population n_0, average gain $g_0=g(n_0)$ and the average number of photons s_0 in the lasing mode.

Following the treatment of McCumber [6], each change in the photon or electron population is associated with a noise impulse of unit integrated intensity. The spectral intensities of the Langevin noise sources f_N and f_S and the cross spectral density are therefore given by the shot noise expression [17], [18] and can be written by inspection of the particle rates entering and leaving the electron and photon reservoir as displayed in Fig. 6.2.1.

$$\langle F_N^2(f)\rangle = \sum r_n^+ + \sum r_n^- = E_{VC}s_0 + E_{CV}s_0 + \frac{n_0}{\tau_s} = \frac{i_0}{q} + 2E_{VC}s_0 \qquad (6.2.3a)$$

$$\langle F_S^2(f)\rangle = \sum r_s^+ + \sum r_s^- = \beta\frac{n_0}{\tau_s} + E_{VC}s_0 + E_{CV}s_0 + \frac{s_0}{\tau_{ph}} = 2\frac{s_0}{\tau_{ph}} + 2E_{VC}s_0 \qquad (6.2.3b)$$

$$\langle F_S(f)F_N(f)\rangle = -[\sum r_{ns} + \sum r_{sn}] = -[E_{CV}s_0 + \beta\frac{n_0}{\tau_s} + E_{VC}s_0] \qquad (6.2.3c)$$

$$= -[\frac{s_0}{\tau_{ph}} + 2E_{VC}s_0]$$

where r_n^+ and r_n^- are the rate of entering and leaving the electron reservoir (gain medium) and r_s^+ and r_s^- are the corresponding rates for the photon reservoir (lasing mode). The rates of exchange between electron and photon reservoir are denoted by r_{ns} and r_{sn}. The equations (6.2.2) have been used to simplify the expressions in (6.2.3). The pump term $\frac{i_0}{q}$ does not enter directly into equation (6.2.3a), in agreement with the noise treatment of a semiconductor diode [18]. The reason for the term $E_{VC}s_0$ is that the sum of the uncorrelated emission and

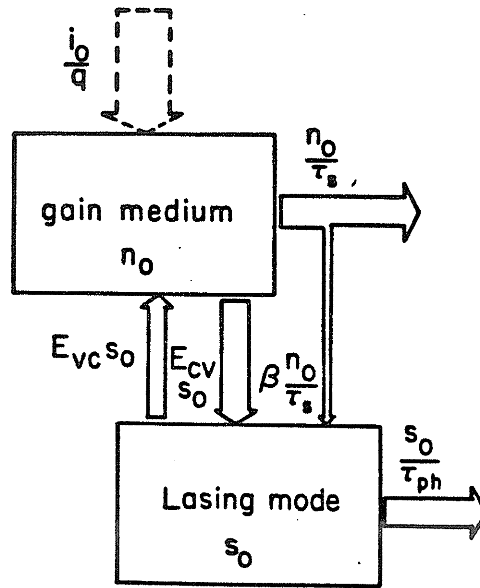

Figure 6.2.1. Model for the shot noise of a semiconductor laser. Each change in the electron (n_0) or photon (s_0) population is associated with a noise impulse of unit integrated intensity.

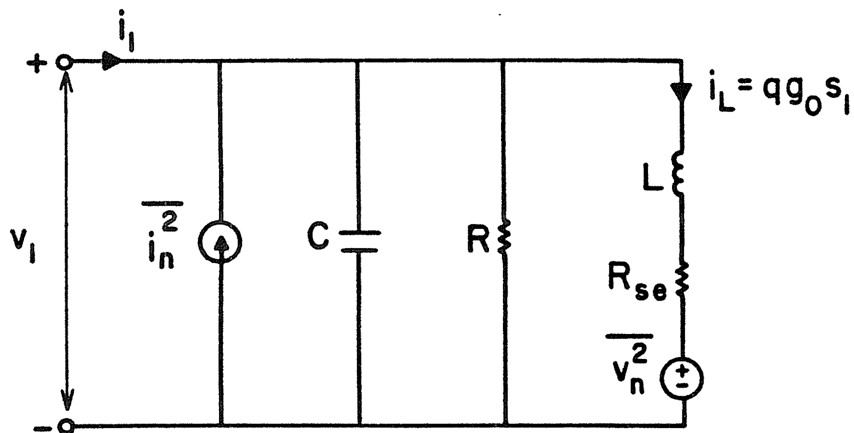

Figure 6.2.2. Small signal model of a semiconductor laser diode. The input signal is the modulation current i_1 or the modulation voltage v_1. The optical output signal is directly proportional to i_L. The values of the components R, C, L, and R_{se} are given in Fig. 6.2.3. The intrinsic shot noise is modeled by the voltage and current noise sources.

absorption rates contributes to noise, while only the difference enters into the gain expression.

6.2.3 Electrical equivalent circuit

A small signal analysis of the rate equations (6.2.1) gives the following relations for small photon (s_1), electron (n_1) and pump (i_1) variations.

$$\frac{dn_1}{dt} = \frac{i_1}{q} - [\frac{1}{\tau_s} + As_0]n_1 - g_0 s_1 + f_N \qquad (6.2.4a)$$

$$\frac{ds_1}{dt} = [\frac{\beta}{\tau_s} + As_0]n_1 - \beta\frac{n_0}{s_0\tau_{ph}} s_1 + f_S \qquad (6.2.4b)$$

A is defined as differential gain slope $A = \frac{dg}{dn}$. The small signal junction voltage v_1 is introduced by the following boundary condition.

$$v_1 = mV_T\frac{n_1}{n_0} \qquad V_T = \frac{kT}{q} \qquad (6.2.5a)$$

$$m = 2 + \frac{n_0}{Vol\ 2\sqrt{2}}[\frac{1}{N_V} + \frac{1}{N_C}] \qquad (6.2.5b)$$

m in equation (6.2.5b) is given by an approximation of the Fermi-Dirac distribution [19], where N_V and N_C are the effective valence- and conduction band densities. V_T is the thermal voltage, k is Boltzman's constant, q is the electron charge and T is the absolute temperature. Anticipating the resulting equivalent electrical circuit of the diode a new variable, i_L, is introduced.

$$i_L = qg_0 s_1 \qquad (6.2.6)$$

Now consider the separate problem of the equivalent circuit shown in Fig. 6.2.2. The equations describing v_1 and i_L of the equivalent circuit can be written

by inspection.

$$\frac{dv_1}{dt} = -\frac{v_1}{RC} + \frac{i_1}{C} - \frac{i_L}{C} + \frac{i_n}{C} \tag{6.2.7a}$$

$$\frac{di_L}{dt} = \frac{v_1}{L} - \frac{R_{se}}{L} i_L - \frac{v_n}{L} \tag{6.2.7b}$$

Equations (6.2.4) and (6.2.7) are identical in form and by comparing constants and using the definitions (6.2.5) and (6.2.6) one obtains the values of the equivalent electrical circuit as function of n_0, g_0 and s_0 given by equations (6.2.2).

$$C = \frac{q}{mV_T} n_0 \tag{6.2.8}$$

$$R = \frac{mV_T}{qn_0[As_0 + \frac{1}{\tau_s}]} \tag{6.2.9}$$

$$L = \frac{mV_T}{qn_0g_0[As_0 + \frac{\beta}{\tau_s}]} \tag{6.2.10}$$

$$R_{se} = \frac{mV_T\beta}{q\tau_s s_0 g_0[As_0 + \frac{\beta}{\tau_s}]} \tag{6.2.11}$$

C is the usual diffusion capacitance resulting from the storage effect of the injected carriers. R is a modified differential diode resistance which approaches the conventional mV_T/i_0 expression in the absence of photons.

In Fig. 6.2.3 we plot the elements of the equivalent circuit using equations (6.2.8) to (6.2.11) with the following laser parameters. Volume of the active

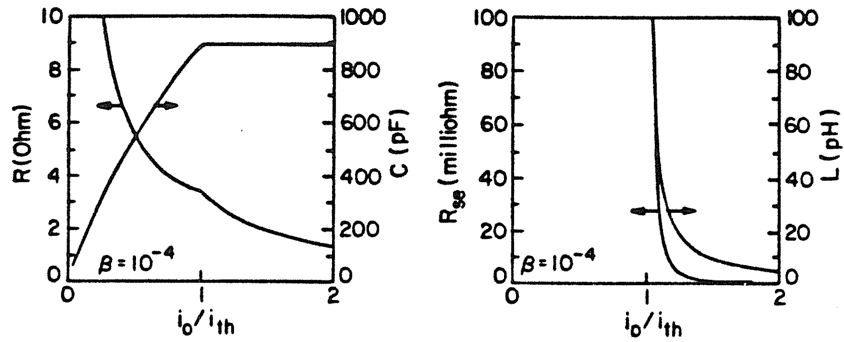

Figure 6.2.3. Values of the elements of the equivalent circuit as a function of the bias point. The parameters of the modeled laser are given in the text.

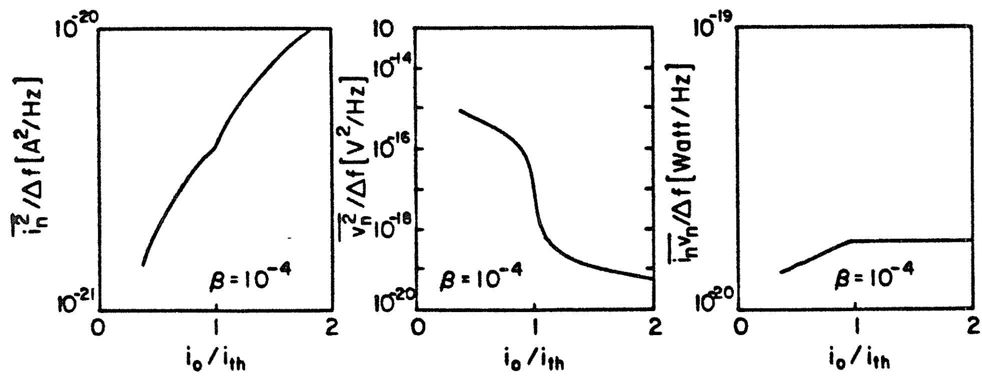

Figure 6.2.4. Spectral intensities of the noise sources of the equivalent circuit as a function of the normalized bias-current $\frac{i_0}{i_{th}}$.

region, Vol = 300x5x0.2 μm^3; spontaneous lifetime, τ_s=3ns; photon lifetime, τ_{ph}=2ps; gain, $g_0=A(n_0-n_{nom})$; $A=\frac{5x10^{-7}cm^3s^{-1}}{Vol}=1.7x10^3s^{-1}$; n_{nom} = $5x10^{17}cm^{-3}xVol=1.5x10^8$; threshold current $i_{th}=\frac{q}{\tau_s}(n_{nom}+\frac{1}{A\tau_{ph}})$=24mA. The small signal current in the inductive branch, earlier arbitrarily defined as i_L in (6.2.6), is directly proportional to the optical signal.

The spectral intensities S_{ii} and S_{vv} of the current and voltage noise source and the cross spectral intensity S_{iv} do not depend on frequency and are given by comparing the fourier transforms of equations (6.2.4) and (6.2.7).

$$S_{ii} = \frac{\overline{i_n^2}}{\Delta f} = 2C^2[\frac{mV_T}{n_0}]^2\langle F_N^2(f)\rangle = 2qi_0+4q^2E_{VC}s_0 \qquad (6.2.12a)$$

$$S_{vv} = \frac{\overline{v_n^2}}{\Delta f} = 2L^2[qg_0]^2\langle F_S^2(f)\rangle = 4\frac{[mV_T]^2}{[n_0[As_0+\frac{\beta}{\tau_s}]]^2}[\frac{1}{\tau_{ph}}+E_{VC}]s_0 \qquad (6.2.12b)$$

$$S_{iv} = \frac{\overline{i_n v_n}}{\Delta f} = -2LC\frac{mV_T}{n_0}qg_0\langle F_N(f)F_S(f)\rangle = 2\frac{mV_Tq}{n_0[As_0+\frac{\beta}{\tau_s}]}[\frac{1}{\tau_{ph}}+2E_{VC}]s_0 \qquad (6.2.12c)$$

An additional factor of 2 has been included, because we changed from the double sided to the more common single sided noise spectrum. The current noise source i_n in parallel with the junction represents mainly the fluctuation in electron population. The first term on the right side of equations (6.2.12a) is the usual shot noise term $2qi_0$ of a nonlasing diode. The second term is resulting from the fact that the noise is determined by the sum of emission and absorption, whereas the net gain corresponds to the difference of the rates.

The fluctuation of the photon population is due mainly to the shot noise of the gain mechanism, that is, due to the voltage noise source v_n. The sources i_n

and v_n are partially correlated due to the coupled rates and their cross spectral intensity is given by (6.2.12c). The spectren of the noise sources $\frac{\overline{i_n^2}}{\Delta f}$, $\frac{\overline{v_n^2}}{\Delta f}$ and $\frac{\overline{i_n v_n}}{\Delta f}$, given by the equations (6.2.12), are plotted in Fig. 6.2.4 as a function of the pump current, where a simple model has been used to calculate E_{VC}.

6.2.4 An application of the formalism

From the intrinsic equivalent circuit and the knowledge of the extrinsic parameters (series resistance, parasitic capacitance and inductance, the impedance of the modulating source) the noise and modulation characteristics of the laser diode can be calculated. We limit ourselves in the following example to the intrinsic case and current modulation. The following properties of the laser diode are calculated: $Z(\omega)$, the diode impedance; $H(\omega)$, the photon modulation transfer function; $\frac{\overline{v_l^2}}{\Delta f}$, the junction voltage noise spectrum and $\frac{RIN}{\Delta f}$, the relative intensity noise spectrum.

$$Z(\omega) = \frac{V_1(\omega)}{I_1(\omega)} = \frac{1}{LC}\frac{[R_{se}+j\omega L]}{D} \qquad (6.2.13a)$$

$$H(\omega) = \frac{S_1(\omega)}{I_1(\omega)} = \frac{1}{LCqg_0D} \qquad (6.2.13b)$$

$$\frac{\overline{v_l^2}(\omega)}{\Delta f} = \frac{\overline{i_n^2}[R_{se}^2+[\omega L]^2]+\overline{v_n^2}+2\overline{v_n i_n}R_{se}}{[LC]^2DD^*}\frac{1}{\Delta f} \qquad (6.2.13c)$$

$$\frac{RIN(\omega)}{\Delta f} = \frac{S_s(\omega)}{s_0^2} = \frac{\overline{i_n^2}+\overline{v_n^2}[\frac{1}{R^2}+[\omega C]^2]-2\overline{v_n i_n}\frac{1}{R}}{[LC]^2DD^*[qg_0]^2}\frac{1}{\Delta f} \qquad (6.2.13d)$$

$$D = -\omega^2+j\omega[\frac{R_{se}}{L}+\frac{1}{RC}]+\frac{1}{LC}[1+\frac{R_{se}}{R}]$$

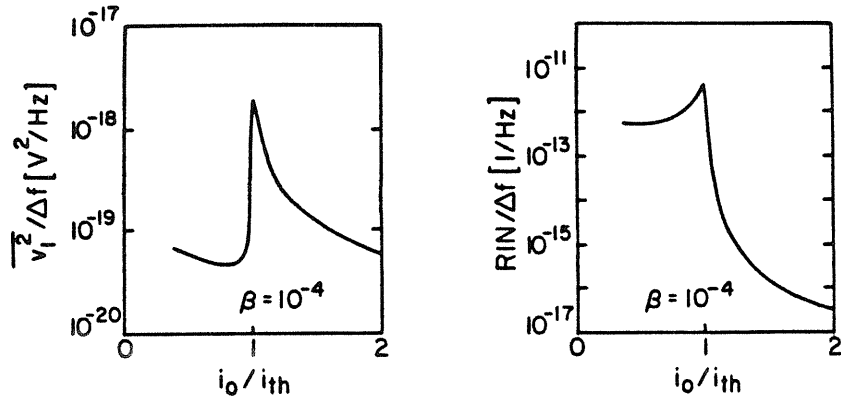

Figure 6.2.5. The junction voltage noise spectrum $\frac{\overline{v_1^2}}{\Delta f}$ of a laser diode driven by a current source at low frequencies as a function of the normalized biascurrent $\frac{i_0}{i_{th}}$. $\frac{RIN}{\Delta f}$ is the relative intensity noise spectrum. Both noise spectra show a peak at the onset of stimulated emission.

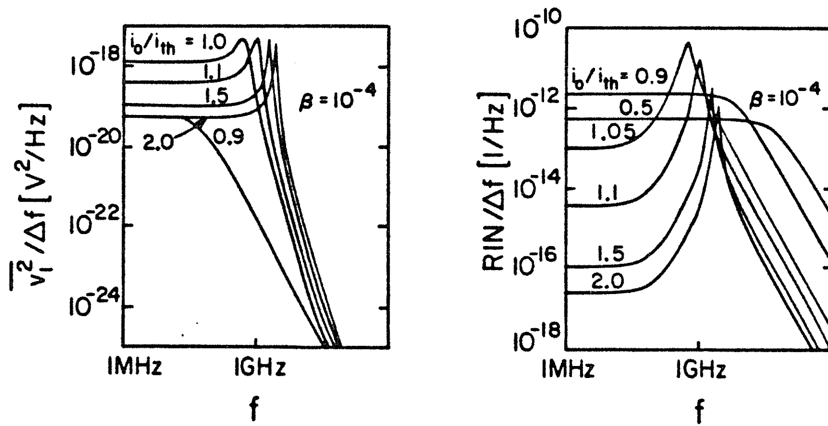

Figure 6.2.6. Frequency dependence of the junction voltage noise spectrum $(\frac{\overline{v_1^2}}{\Delta f})$ and the relative intensity noise spectrum $(\frac{RIN}{\Delta f})$ as a function of the normalized biascurrent $\frac{i_0}{i_{th}}$. Both spectra show a resonance at the relaxation frequency of the laser.

(6.2.13e)

$$S_s(\omega) = 2\int_{-\infty}^{\infty}\left[\int_{-\infty}^{\infty} s(t)s(t+\tau)dt\right]e^{-j\omega\tau}d\tau \qquad \omega \geq 0 \qquad (6.2.13f)$$

where $S_s(\omega)$ is the photon noise spectrum. Fig. 6.2.5 and Fig. 6.2.6 show the calculated dependence of $\frac{\overline{v_i^2}}{\Delta f}$ and $\frac{RIN}{\Delta f}$ on current and frequency and display the characteristic noise peak at onset of lasing and the high frequency resonance. The frequency dependence of $Z(\omega)$ is shown in Fig. 6.2.7 for different pump levels.

6.2.5 Noise of the multi-mode laser

The rate equations for a laser emitting radiation into n longitudinal modes are.

$$\frac{dn}{dt} = \frac{I}{q} - \sum_{k=1}^{k=n} g_k s_k - \frac{n}{\tau_s} + f_N \qquad (6.2.14a)$$

$$\frac{ds_k}{dt} = g_k s_k - \frac{s_k}{\tau_{phk}} + \beta_k \frac{n}{\tau_s} + f_{Sk} \qquad k=1..n \qquad (6.2.14b)$$

An analysis analogous to that above yields the equivalent circuit shown in Fig. 6.2.8. Each optical mode contributes a parallel branch to the circuit with a current i_{Lk} corresponding to the photons of the signal in the mode k. The capacitance modeling the injected carriers remains unchanged. Taking the gain of the k-th mode as $g_k = g_{0k} + A_k n_{1k}$ the values of the components are.

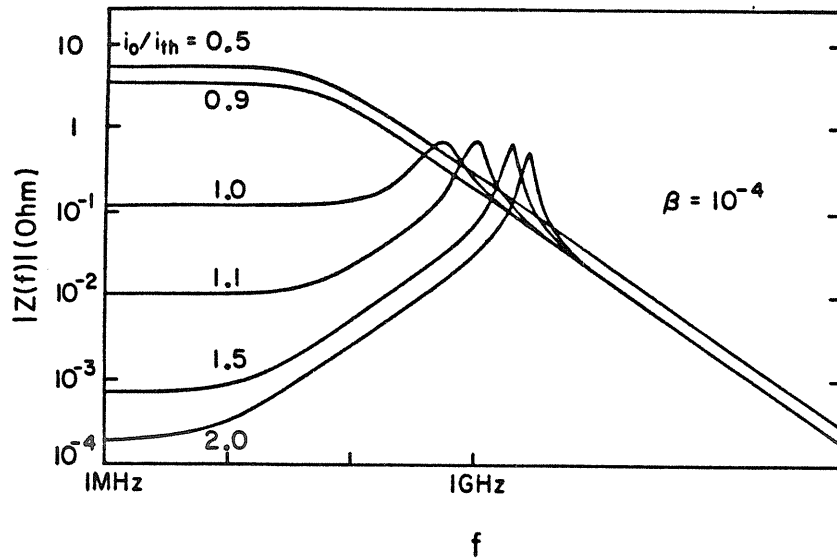

Figure 6.2.7. Frequency dependence of the impedance of a diode laser as function of the normalized biascurrent $\frac{i_0}{i_{th}}$.

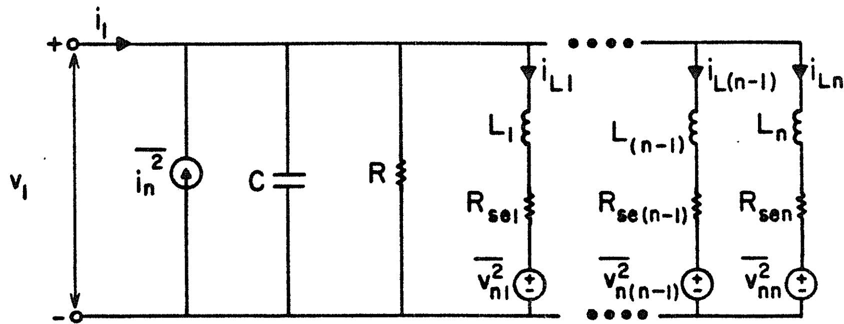

Figure 6.2.8. Noise equivalent circuit of a multilongitudinal semiconductor laser diode. Each optical mode contributes a parallel branch to the circuit with a current i_{Lk} proportional to the photons of the signal in the mode k.

$$R = \frac{mV_T}{qn_0} \frac{1}{\sum_{k=1}^{k=n} A_k s_{0k} + \frac{1}{\tau_s}} \tag{6.2.15a}$$

$$L_k = \frac{mV_T}{qn_0} \frac{1}{g_{0k}[A_k s_{0k} + \frac{\beta_k}{\tau_s}]} \tag{6.2.15b}$$

$$R_{sek} = \frac{\beta n_0}{\tau_s s_0} \frac{mV_T}{qn_0} \frac{1}{g_{0k}[A_k s_{0k} + \frac{\beta_k}{\tau_s}]} \tag{6.2.15c}$$

And the noise power spectra are

$$\frac{\overline{i_n^2}}{\Delta f} = 2qi_0 + 4q^2 \sum_{k=1}^{k=n} E_{VCk} s_{0k} \tag{6.2.15d}$$

$$\frac{\overline{v_{nk}^2}}{\Delta f} = 4 \frac{[mV_T]^2}{[n_0[A_k s_{0k} + \frac{\beta_k}{\tau_s}]]^2} [\frac{1}{\tau_{phk}} + E_{VCk}] s_{0k} \tag{6.2.15e}$$

$$\frac{\overline{v_{nk} i_n}}{\Delta f} = 2 \frac{mV_T q}{n_0[A_k s_{0k} + \frac{\beta_k}{\tau_s}]} [\frac{1}{\tau_{phk}} + 2E_{VCk}] s_{0k} \tag{6.2.15f}$$

$$\overline{v_{nm} v_{nl}} = 0 \qquad m \neq l \tag{6.2.15g}$$

This noise analysis of a multimode laser neglecting the phase relations between the modes is justified if the beat frequencies of the longitudinal modes lie outside the spectrum of interest. The model above predicts that the relative intensity fluctuations of one isolated mode of a multimode laser are several orders of magnitude larger than the relative intensity fluctuations of all the modes together [14]. The intensity fluctuations of different modes are negatively

correlated because the different modes are competing for gain from the same electron reservoir. This so called competition noise may significantly deteriorate the signal to noise ratio in communication systems which have mode selective elements, such as material dispersion or interference effects [16].

6.2.6 Conclusions

The small signal model of a semiconductor laser has been extended to include the effects of the intrinsic noise by adding current and voltage noise sources. The current noise source represents the shot noise of the recombination of the carriers and the voltage noise source the random process of stimulated emission. The intensity fluctuation of the light is dominated by the stimulated emission process. The usefulness of the noise equivalent circuit in modeling an electronic circuit with an injection laser as one of its elements is demonstrated by calculating the modulation and noise characteristic of a current driven laser diode. In addition, the model has been generalized to the multimode case.

6.3 Shotnoise and thermal noise

An interesting introduction to shot noise and thermal noise is given by D. K. C. McDonald [20] and an excellent treatment of fluctuations from the nonequilibrium steady state has been written by M. Lax [21]. It is known from the Nyquist theorem [20] that fluctuations in a system at *thermal equilibrium* are intimately related to the transport properties; i.e. a resistor R produces a noise voltage with a spectral power density $\frac{\overline{v_n^2}}{\Delta f} = 4kTR$. The total noise of a more complex electrical circuit (containing resistors, capacitors, inductors etc.) can be obtained by inspection, namely by attaching to each resistor a noise voltage

$\frac{\overline{v_n^2}}{\Delta f} = 4kTR$ in series and by calculating their effects on the output terminals by any conventional network analysis.

We have seen in chapter 6.2 that the fluctuations in a ***nonequilibrium steady state*** can be obtained by inspection of the rate equations, by associating a noise impulse of unit integrated intensity with each change in the electron or photon population, i.e. each steady state current I (electrical or particle current) produces a noise with a spectral power density of $\frac{\overline{i_n^2}}{\Delta f} = 2eI$. The total noise power at the output ports of such a system is obtained by attaching to each steady state current I a shotnoise $\frac{\overline{i_n^2}}{\Delta f} = 2eI$ and by superimposing their effects by standard network methods as has been done in chapter 6.2.

In the course of this work we encountered [22] an interesting connection between shotnoise (fluctuations around a nonequlibrium steady state) and thermal noise (fluctuations in a system at thermodynamic equilibrium). We will first derive the shotnoise formula. Assume we have two baths A and B separated by a membrane as shown in Fig. 6.3.1. Each bath is composed of particles which carry one quantum of "something", where "something" could be energy, mass or charge. We assume that each particle carries e of "something". The membrane permits only transfer of particles from bath A to B and a steady current is assumed to flow from the left side to the right side. The current I is defined as the number of units of e which pass through the membrane per unit time. Since the membrane is assumed to be infinitely thin the current as function of time I(t) is a series of randomly spaced δ functions as shown in Fig. 6.3.2:

$$I(t) = \sum_n e\delta(t-t_n) \tag{6.3.1}$$

The average current is given by:

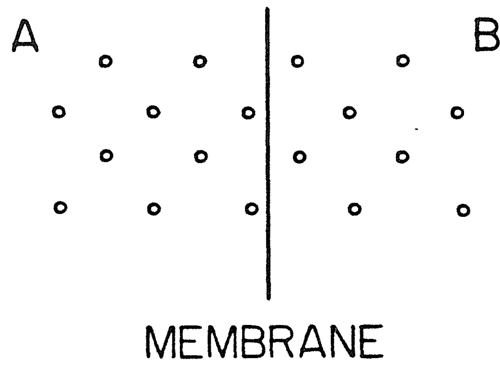

Figure 6.3.1. Particles separated by a unidirectional membrane

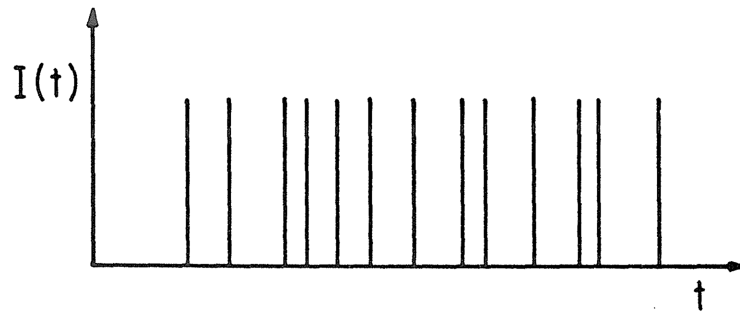

Figure 6.3.2. Current due to particles crossing the semi-permeable membrane

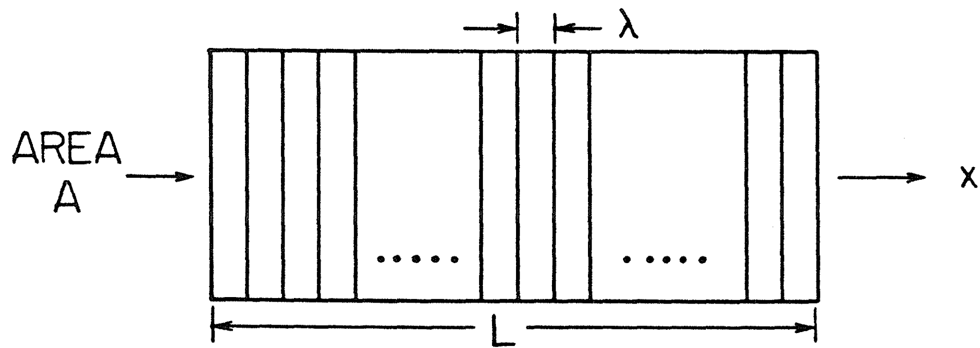

Figure 6.3.3. A resistor R sliced into short sections with the mean free path length

$$\bar{I} = eR \qquad (6.3.2a)$$

$$R = \lim_{T\to\infty} \frac{1}{2T} \int_{-T}^{+T} \sum_n \delta(t-t_n) \equiv \langle \sum_n \delta(t-t_n) \rangle \qquad (6.3.2b)$$

The autocorrelation of I(t) is given by:

$$\langle I(t+\tau) I(t) \rangle = e^2 R \delta(\tau) \qquad (6.3.3)$$

Using the Wiener-Khintchine theorem this gives the spectral density of the current

$$\frac{\overline{i_n^2}}{\Delta f} = S_I = 2e^2 R = 2e\bar{I} \qquad (6.3.4)$$

where the 2 comes from considering only positive frequencies in the spectral space. If the transit time through the membrane is finite then the spectral density of the current is no longer white but rolls off past a "knee" frequency corresponding to the transit time. A vacuum or semiconductor diode is an element which is a close realisation of such a membrane.

The argument up to now has been fairly straightforward since the transport of particles was very simple, i.e. crossing a thin membrane in one direction without scattering. We now consider a more complicated case where particles are scattered very often and as a consequence are moving randomly with only a small drift component. This corresponds, for example, to the case of Johnson noise across a resistor where the particles are electrons with charge e. We will derive the well known formulas for current noise spectral density $\frac{\overline{i_n^2}}{\Delta f} = \frac{4kT}{R}$ and voltage noise spectral density $\frac{\overline{v_n^2}}{\Delta f} = 4kTR$ using shot noise arguments on a microscopic scale. These equations are forms of the fluctuation dissipation theorem which relates fluctuations (diffusion) to dissipation (drift) in a random walk problem [20].

To begin we must identify at which length scale the shot noise arguments are valid. Over distances for which electrons are not scattered, i.e. a mean free path length, the transport of carriers behaves as in the case discussed above. We consider therefore a resistor which has been sliced into segments whose length is one mean free path λ as shown in Fig. 6.3.3. The current along the x-axis consists of two opposing thermal currents I_T , both of which are contributing independently to the shot noise. Therefore in one slice l of the resistor the fluctuations are:

$$\frac{\overline{i_{n,l}^2}}{\Delta f} = 2eI_T + 2eI_T = 4eI_T \tag{6.3.5}$$

If n is the carrier density, v_{th} is the thermal velocity ($v_{th}^2 = \frac{3kT}{m}$) and A the cross section of the resistor, then I_T is given by:

$$I_T = \frac{1}{\sqrt{6\pi}} Aenv_{th} = \frac{1}{6\pi} Aen(\frac{3kT}{mv_{th}}) \tag{6.3.6}$$

where the factor $\frac{1}{6\pi}$ enters because it is assumed that the velocity distribution is isotropic. Substituting equation (6.3.6) in (6.3.5) yields:

$$\frac{\overline{i_{n,l}^2}}{\Delta f} = 4e(\frac{1}{\sqrt{6\pi}} Aen(\frac{3kT}{mv_{th}})) \tag{6.3.7}$$

Now consider the resistance r_l of the slice l which is defined as the total resistance R divided by the number of slices of the resistor.

$$r_l = R \times \frac{\lambda}{L} = \frac{\rho L}{A} \times \frac{\lambda}{L} = \sqrt{\frac{3\pi}{8}} \times \frac{m}{Ae^2 n} \times v_{th} \tag{6.3.8}$$

where the factor $\sqrt{\frac{3\pi}{8}}$ enters because a constant mean free path has been assumed to calculate the resistivity. Substituting equation (6.3.8) in (6.3.7) gives:

$$\frac{\overline{i_{n,l}^2}}{\Delta f} = \frac{4kT}{r_l} \times \sqrt{\frac{27}{48}} \approx \frac{4kT}{r_l} \tag{6.3.9}$$

where the factor $\sqrt{\frac{27}{48}}$ is close enough to unity for our purposes to be dropped. Using Thevenins theorem:

$$\frac{\overline{v_{n,l}^2}}{\Delta f} = 4kTr_l \tag{6.3.10}$$

Now adding all the noise sources of the slices which make up the whole resistor and recalling that $\sum_l r_l = R$ we obtain the Johnson noise expression of the spectral density of the fluctuations of a resistor in thermal equilibrium.

$$\frac{\overline{v_n^2}}{\Delta f} = 4kTR \tag{6.3.11}$$

6.4 References:

1. M. Sargent III, M. O. Scully, W. E. Lamb Jr., " Laser Physics", Adison-Wesley Publishing Company, 1974.

2. H. Haken, "Light and Matter", Encyclopedia of Physics, Springer Verlag, 1970.

3. A. Yariv, W. M. Caton, IEEE J. Quantum Electron., vol. 10, p. 509, 1974.

4. K. Vahala, A. Yariv, IEEE J. Quantum Electron., vol. 19, June 1983.

5. K. Vahala, A. Yariv, IEEE J. Quantum Electron., vol. 19, June 1983.

6. D. E. McCumber, Phys. Rev. , vol. 141, pp. 306-322, Jan. 1966.

7. Ch. Harder, J. Katz, S. Margalit, J. Shacham, A. Yariv, IEEE J. Quantum Electron., vol. 18, p. 333, 1982.

8. M. Morishita, T. Ohmi, and J. Nishizawa, Solid-State Electron. , vol. 22, pp. 951-962, Nov. 1979.

9. J. Katz, S. Margalit, Ch. Harder, D. Wilt, and A. Yariv, IEEE J. Quantum Electron. , vol. QE-17, pp. 4-7, Jan. 1981.

10. M. Lax, IEEE J. Quantum Electron. , vol. QE-3, pp. 37-46, Feb. 1967.

11. H. Haug, Phys. Rev. , vol. 184, pp. 338-348, Aug. 1969.

12. D. J. Morgan and M. J. Adams, phys. stat. sol. (a), vol. 11, pp. 243-253, 1972.

13. T. L. Paoli and J. E. Ripper, Phys. Rev. A, 2, pp. 2551-2555, 1970.

14. H. Jackel, Diss. ETH Nr. 6447, Zurich 1980.

15. H. Melchior, Topical meeting on integrated and guided-wave optics. , Jan. 1980, paper MA2.

16. G. Arnold, K. Petermann, Optical and Quantum Electronics, vol. 12, pp. 207-219, 1980.

17. S. O. Rice, Bell System Tech. J. , vol. 23, pp. 282-332, July 1944, and vol. 24, pp. 46-156, Jan. 1945.

18. A. Van der Ziel, London, Butterworths Scientific Publications, 1959.

19. W. B. Joyce and R. W. Dixon, Applied Physics Letters, vol. 31, pp. 354-356, Sept. 1977.

20. D. K. C. McDonald, John Wiley and Sons, 1962.

21. M. Lax, Review of Mod. Phys., vol. 32, p. 25, 1960.

22. K. Vahala, private communication.

Chapter 7

Phase noise in semiconductor laser diodes

7.1 Introduction

The radiation field of a laser undergoes random amplitude and phase fluctuations and the field $\varepsilon_{real}(t)$ is of the form:

$$\varepsilon_{real}(t) = E(t)\cos(\omega_l t + \Phi(t)) \tag{7.1.1}$$

In the previous chapter we investigated the amplitude fluctuations E(t) which are responsible for the noise in a quadratic (intensity) detector. In this chapter we will address the phase fluctuations $\Phi(t)$ which are of utmost importance in applications that utilize the coherence properties of the laser such as heterodyne detection schemes of the optical signal. We will investigate the field spectrum (or in short: spectrum) of injection lasers [1]. This spectrum is obtained, for example, as the output of a very narrow Fabry-Perot resonator which is slowly scanned over the lasing line. Clearly, the spectrum is centered around the lasing frequency ω_l and it will have a finite width. An analysis by Schawlow-Townes [2], [3] predicts the spectrum to be Lorentzian in shape with a full width at half maximum Δf of

$$\Delta f = \frac{R}{2\,P_m} \tag{7.1.2}$$

where R is the rate of spontaneous emission into the lasing mode and P_m is the total number of photons in this mode. In Fig. 7.1.1 the measured spectrum of

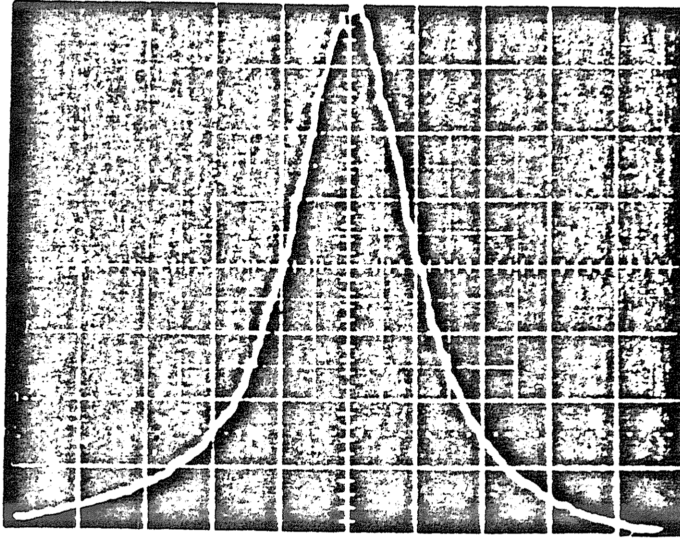

Figure 7.1.1. Field spectrum of a BOG laser at an output power per facet of 1mW measured with a scanning Fabry-Perot. The linewidth is around Δf =70MHz.

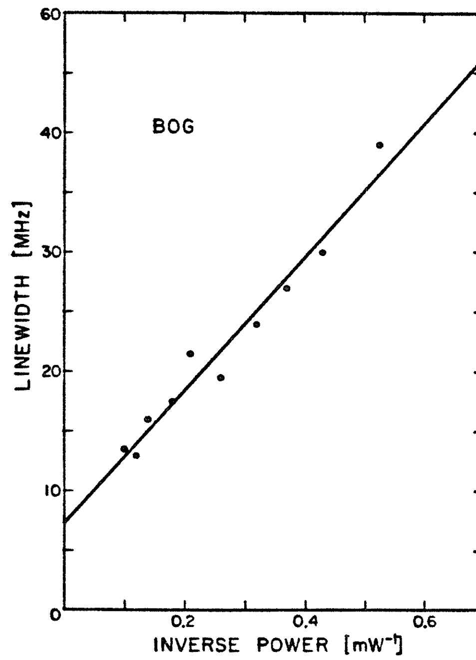

Figure 7.1.2. Linewidth Δf as a function of the inverse output power.

an injection laser is shown, and it is, within the experimental accuracy, Lorentzian. The linewidth equation (7.1.2) can be recast in a more practical form by using the relation between spontaneous and stimulated emission (equation 2.2.5) and between the mode population number P_m and the output power per mirror P_{out} (equation 2.3.26).

$$\Delta f = \frac{{v_{gr}}^2 \, h\nu \, g \, n_{sp} \alpha_{mir}}{8\pi P_{out}} \tag{7.1.3}$$

where v_{gr} is the group velocity of the light, $h\nu$ is the lasing energy, g is the gain, n_{sp} is the spontaneous emission factor [4], and α_{mir} is the mirror loss. Fig. 7.1.2 shows a measurement of the linewidth Δf as a function of the inverse output power. As predicted, the linewidth is inversely proportional to the output power. However, there are two discrepancies between measured and calculated values. First, an extrapolation of the measurement to obtain the linewidth in the limiting case of infinite output power shows that there remains a residual linewidth [5] whereas the theory predicts that the linewidth continues to narrow without limit as long as the power increases. This so called power independent linewidth is still a topic of active research [6]. And secondly, the theory, for example, predicts a linewidth $\Delta f = 4.1\text{MHz}$ at an output power of $P_{out} = 1\text{mW}$, using the typical numerical values, $v_{gr} = \frac{c}{n_{gr}}$, $n_{gr} = 4.3$, $h\nu = 1.5\text{eV}$, $g = \alpha_L + \alpha_{mir}$, $\alpha_L = 45\text{cm}^{-1}$, $\alpha_{mir} = 39\text{cm}^{-1}$ and $n_{sp} = 2.7$ [4]. However, measurements yield a spectral width which is much larger [7] by a factor between 10 and 50. From our measurement in Fig. 7.1.2 the spectral width is $\Delta f = 70\text{MHz}$ at an output power of 1mW. The measured linewidth is wider by about a factor of 20 than the calculated one.

Injection lasers differ markedly from other laser systems in some respects and approximations which have been made in deriving the classical linewidth

formula (7.1.1) cannot be made in the case of semiconductor lasers. Recently, Henry [8] presented a model of the linewidth of single mode semiconductor lasers, which takes line broadening due to the coupling of phase and intensity into account. Independently, Vahala and Yariv [9] developed a semiconductor laser noise theory which treats the carrier density as a dynamic variable and which includes the carrier density dependence of the index of refraction. Both treatments predict a spectral linewidth Δf of the modified Schawlow-Townes form:

$$\Delta f = \frac{v_{gr}^2 \, h\nu \, g \, n_{sp} \alpha_{mir}}{8\pi P_{out}} (1+\alpha^2) \qquad (7.1.4)$$

where α is the linewidth enhancement factor [8], [9]. α is defined as the ratio of the change in the real index of refraction $\Delta N_{ind,r}$ divided by the change of the imaginary index of refraction $\Delta N_{ind,i}$ when the carrier density fluctuates, $\alpha \equiv \frac{\Delta N_{ind,r}}{\Delta N_{ind,i}}$. Until now no direct measurement of this important device parameter was available and its approximate value had to be estimated from frequency shift measurements [10], [11], from gain measurements [10] or from gain calculations [12], [13] and a subsequent Kramers-Kronig analysis.

7.2 Measurement of the linewidth enhancement factor α

The purpose of this section is twofold: first, we derive the relationship between the small signal modulation characteristic of a semiconductor laser and the linewidth enhancement factor α, and second, we apply this result to measure α through a high frequency modulation experiment. We can then calculate the quantum mechanical limit of Δf.

$$\Delta f = \frac{v_{gr}^2\, h\nu\, g\, n_{sp}\alpha_{mir}}{8\pi P_{out}}(1+\alpha^2) \qquad (7.2.1)$$

This small signal analysis is based on the electromagnetic field equation of a laser as derived by Lamb [14] and is applied to the case of index guided single mode lasers with a spatially inhomogeneous carrier density. The polarization $\vec{P}(\vec{r},t)$ due to the carriers injected into the semiconductor material is given as a function of the electric field $\vec{E}(\vec{r},t)$ by:

$$\vec{P}(\vec{r},t)=\varepsilon_0\chi(n(\vec{r},t),\vec{r})\vec{E}(\vec{r},t) \qquad (7.2.2)$$

where $\chi=\chi_r+i\chi_i$ is the complex susceptibility which is an explicit function of the carrier density and of the position (in the case where the material is inhomogeneous).

The equation for the time evolution of the cavity mode $E_m(t)$ is obtained by substituting the polarization $\vec{P}$, as given by equation (7.7.2), into the electromagnetic field equation [14].

$$\frac{d^2}{dt^2}\left[(1+\frac{\chi_m(t)}{N^2})E_m(t)\right]+\frac{1}{\tau_p}\frac{d}{dt}E_m(t)+\omega_m^2E_m(t) = -\frac{1}{\varepsilon_0 N^2}\frac{d^2P_{sp,m}}{dt^2} \qquad (7.2.3.a)$$

$$\vec{E}(\vec{r},t) \equiv E_m(t)\vec{e}_m(\vec{r}) \qquad (7.2.3.b)$$

$$\chi_m \equiv \int_V \chi(n(\vec{r},t),\vec{r})\vec{e}_m(\vec{r})\cdot\vec{e}_m(\vec{r})dV \qquad (7.2.3.c)$$

$$\tau_p \equiv \frac{1}{v_{gr}(\alpha_{sc}+\frac{1}{L}\ln(\frac{1}{R}))} \qquad (7.2.3.d)$$

$$N^2 \equiv \frac{\varepsilon}{\varepsilon_0} \qquad (7.2.3.e)$$

$$\omega_m \equiv 2\pi\frac{c}{2LN}m \qquad (7.2.3.f)$$

The optical mode profile is given by $e_m^2(\vec{r})$ and χ_m is the effective susceptibility for the mode m. τ_p, N and ω_m are the photon lifetime, index of refraction, and

resonance frequency respectively, of the cold cavity, that is, of the cavity when the effects of the lasing transition are removed. The spontaneous emission can be taken into account by adding a driving term $P_{sp,m}$ [9]. The explicit form can be obtained from a Langevin noise source treatment which is pretty tedious. Fortunately, there is a simpler way to obtain the effects of $P_{sp,m}$ since we are only interested into its average contribution. It is a basic result of quantum mechanics that the ratio of stimulated emission to average spontaneous emission into the lasing mode is equal to the number of photons in the mode, P_m . The average effect of $P_{sp,m}$ can therefore be accounted for in a small signal analysis by changing the second term (the lossterm) in the field equation (7.2.3.a) from $\frac{1}{\tau_p}\frac{dE}{dt}$ to $\frac{1}{\tau_p}(1-\frac{n_{sp}}{P_m})\frac{dE}{dt}$, where n_{sp} is equal to the ratio of the total to the net stimulated emission rate.

For the small signal analysis the mode $E_m(t)$ and the mode susceptibility $\chi_m(t)$ are assumed to be of the following form:

$$E_m(t) = E_0(1+\delta(t)) \cos(\omega_l t+\varphi(t)) \tag{7.2.4.a}$$

$$\chi_m(t) = \chi_{m,0}+\chi_{m,1}(t) = \chi_{m,0,r}+\chi_{m,1,r}(t)+i\left[\chi_{m,0,i}+\chi_{m,1,i}(t)\right] \tag{7.2.4.b}$$

The solution for the operating point shows that the mode gain $\chi_{m,0,i}$ is clamped and the lasing frequency ω_l is shifted slightly from the cold cavity resonance ω_m.

$$\chi_{m,0,i} = \frac{N^2}{\omega_l \tau_p}(1-\frac{n_{sp}}{P_m}) \tag{7.2.5a}$$

$$\omega_l^2 = \frac{\omega_m^2}{(1+\frac{\chi_{m,0,r}}{N^2})} \tag{7.2.5b}$$

The small signal behavior is given by the solution of:

$$\dot{\varphi}(t)+\frac{1}{2}\frac{\chi_{m,1,r}(t)}{N^2}\omega_1 = 0 \qquad (7.2.6a)$$

$$\dot{\delta}(t)+\frac{1}{2\tau_p}\frac{n_{sp}}{P_m}\delta(t)-\frac{1}{2}\frac{\chi_{m,1,i}(t)}{N^2}\omega_1 = 0 \qquad (7.2.6b)$$

In the experiments described below the semiconductor laser is biased above threshold and a small sinusoidally varying current at the frequency Ω is superimposed. Therefore the steady state sinusoidally modulated solution of the field $E_m(t)$ is of interest. To obtain it we substitute

$$E_m(t) = E_0(1+\frac{m}{2}\cos(\Omega\, t))\,\cos(\omega_1 t+\beta\cos(\Omega\, t+\Phi)) \qquad (7.2.7)$$

into equation (7.2.6a) and (7.2.6b), where m and β are the intensity and phase modulation indices, respectively. For large modulation frequencies Ω ($\Omega >> \frac{n_{sp}}{P_m}\frac{1}{\tau_p}$) the solution is:

$$\beta = -\frac{1}{2}\alpha_m m \qquad (7.2.8a)$$

$$\Phi = 0 \qquad (7.2.8b)$$

$$\alpha_m(\Omega) \equiv \frac{\chi_{m,1,r}}{\chi_{m,1,i}} = \frac{\int_V \frac{\partial\chi_r(n)}{\partial n}\Big|_{n=n_0(\vec{r})} N_1(\vec{r},\Omega)\, e_m^2(\vec{r})\,dV}{\int_V \frac{\partial\chi_i(n)}{\partial n}\Big|_{n=n_0(\vec{r})} N_1(\vec{r},\Omega)\, e_m^2(\vec{r})\,dV} \qquad (7.2.8c)$$

As can be seen from equation (7.2.8a), the phase and intensity modulation indices are proportional to each other, independent of the bias point and optical confinement factor. This result suggests a simple way to obtain the exact value of α_m through a measurement of the ratio of intensity and phase modulation depths, two relatively straightforward measurements as will be shown below. The factor $\alpha_m(\Omega)$ is defined in equation (7.2.8c), where $n_0(\vec{r})$ is the quiescent carrier density at location $\vec{r}$, $N_1(\vec{r},\Omega)$ is the small signal frequency dependent carrier density fluctuation at position $\vec{r}$, and $e_m^2(\vec{r})$ is the normalized photon den-

sity. If the susceptibilty $\chi(n,\vec{r})$ is linear in n and does not depend on $\vec{r}$, then it can be seen from equation (7.2.8c), that α_m is independent of Ω. Using the relation between the index of refraction N_{ind} and the susceptibility χ, $\varepsilon_0 N_{ind}^2 \equiv 1+\chi$, one obtains that in this case α_m is equal to the linewidth enhancement factor α as defined by Henry [8].

$$\alpha_m = \frac{\frac{\partial \chi_r}{\partial n}}{\frac{\partial \chi_i}{\partial n}} = \frac{\Delta N_{ind,r}}{\Delta N_{ind,i}} = \alpha \qquad (7.2.8d)$$

Please note that in this linear case α_m is totally independent of the spatial distribution of the carrier density modulation, (e.g. the incomplete carrier clamping in the wings of the optical mode, or diffusion effects do not enhance the phase modulation as suggested in [15]). However, if the susceptibility $\chi(n,\vec{r})$ is not linear in the carrier density or depends on the location (e.g. the optical field penetrates into a material with a different bandgap [10]), then the factor α_m is dependent on the modulation frequency and its value measured at high frequencies cannot be used to infer the linewidth broadening factor α.

The experimental arrangement for measuring the intensity and phase modulation index is shown in Fig. 7.2.1 The semiconductor laser is biased above threshold and a small sinusoidally varying current at frequency Ω is superimposed. The intensity and spectral density of the radiation field are given by:

$$\text{Intensity} \sim E_0^2(1+m\cos\Omega t) \qquad (7.2.9a)$$

$$\text{Spectrum: centerline at } \omega_1\text{: } E_0^2(J_0^2(\beta)+m^2 J_1^2(\beta)) \qquad (7.2.9b)$$

$$1^{st} \text{ sidebands at } \omega_1 \pm \Omega\text{: } E_0^2(J_1^2(\beta)+(\frac{m}{2}(J_2(\beta)-J_0(\beta)))^2) \qquad (7.2.9c)$$

where $J_n(\beta)$ are n-th order Bessel functions. Note that the calculated spectrum is symmetric.

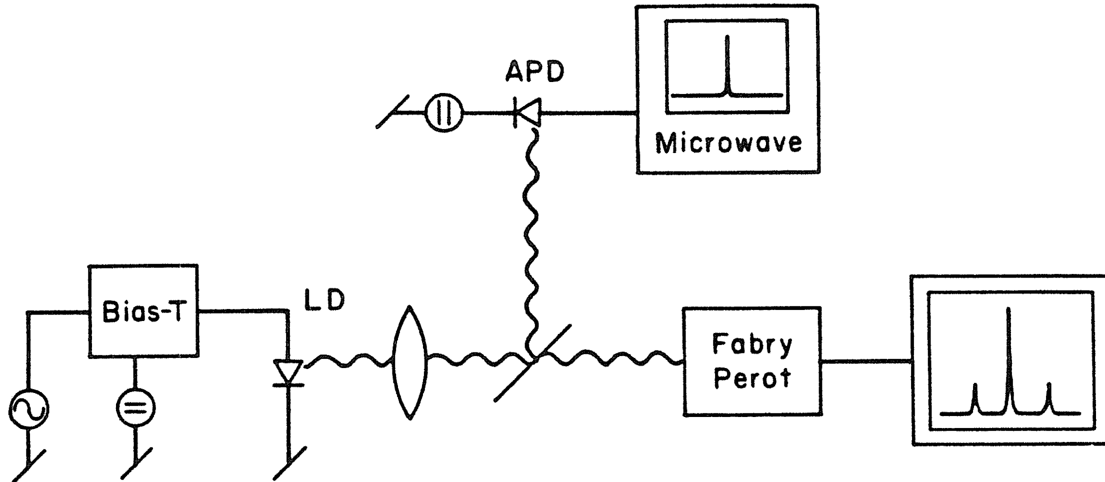

Figure 7.2.1. Set-up for measuring the intensity and phase modulation index. The laser diode (LD) is biased well above threshold and a small signal current at frequency Ω is superimposed. The intensity modulation depth is measured with an avalanche photodiode (APD) and the spectral density with a scanning Fabry-Perot.

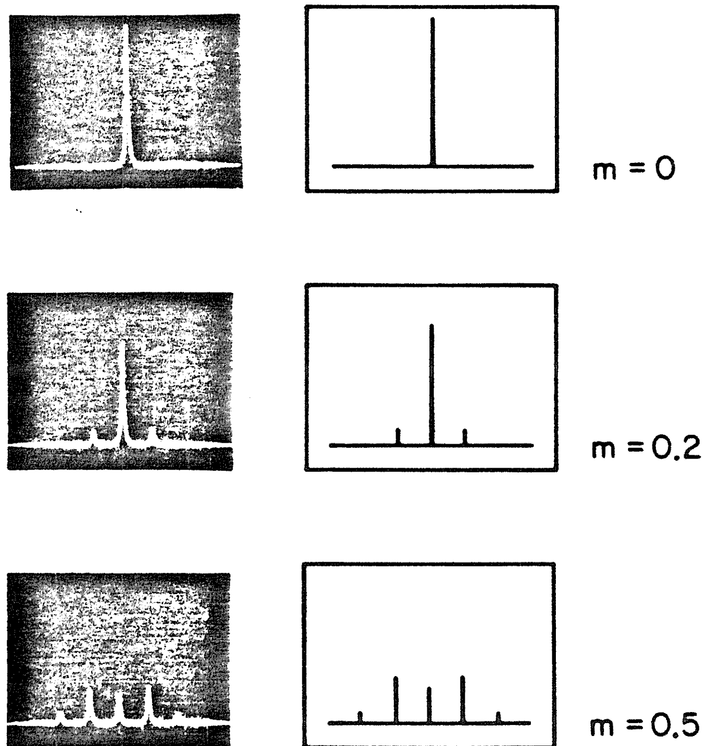

Figure 7.2.2. Measured and calculated optical spectra of a laser diode with an intensity modulation m = 0, 20% and 50%. The modulation frequency is $\Omega = 1\text{GHz}\cdot 2\pi$.

The intensity modulation index m was measured with an avalanche photodiode (S171P Telefunken) calibrated in the measurement set-up from DC to 3.5 GHz to an accuracy of ± 1 dB. The optical spectrum was measured with a confocal scanning Fabry-Perot (Tropel 240). Care was taken to avoid any back reflection into the laser. In a typical measurement as shown in Fig. 7.2.2 the modulation current at frequency Ω was adjusted to produce a desired intensity modulation depth m, which was measured with the photodiode. The phase modulation index β can be found by measuring the relative sideband strength and using equation (7.2.9.b) and (7.2.9.c). The factor α_m is then obtained as, $\alpha_m = -2 \frac{\beta}{m}$. Since only the absolute value of β can be measured, the sign of α_m must be obtained by other means. A measurement of the α_m of a buried optical guide laser (BOG Hitachi 3400, λ = 816nm) at Ω =2 GHz, a bias level of 1.3 times threshold, and an intensity modulation depth of 10%, gave $|\alpha_m|$ = 4.5. Repetition of this measurement for about 50 different conditions (Ω varied between 1 GHz and 3.5 GHz, bias level varied between 1.3 and 1.9 times threshold, and modulation depth varied between 10% and 30%) gave $|\alpha_m|$ = 4.6 ± 0.5. This value has an additional uncertainty of ± 10% due to the inaccuracy of the photodiode calibration. A simple structure such as the BOG laser is expected to have the required simple form of the susceptibility so as to render α_m as given by equation (7.2.8c) frequency independent. Indeed our measurements of α_m could not detect any dependence on Ω in the range from 1 GHz to 3.5 GHz. Therefore we conclude that for this BOG laser $|\alpha|$ = 4.6± 1.0.

Attempts to measure α in a channeled substrate planar laser (CSP) failed because the measured α_m was strongly dependent on the modulation frequency Ω. To understand this we must consider the details of the modified CSP structure which is shown in Fig. 3.5.1. The transverse mode is guided through a

dielectric waveguide which is obtained through the specific shape of the active layer. The active layer is relatively thick $0.2\mu m$ in the center and tapers off towards the sides. This structure is fabricated by making clever use of the dynamics of the crystal growth by liquid phase epitaxy on substrates with an etched channel. The tendency of the equilibrium growth mechanism to smooth out the topology fills the channel etched into the substrate. The CSP lasers which we use in these experiments have a fair amount of aluminium in the active region to shift the lasing wavelength to 820nm. During the crystal growth the aluminium concentration in the melt becomes depleted (proportional to the growth rate) and as a consequence the active layer has a smaller aluminium concentration in the center (where the growth rate is faster) and a larger one towards the wings [16]. The transverse mode guide is formed by this lateral change of the aluminium concentration and the change of the thickness of the active layer. As discussed above the susceptibility in such a case (when the optical field is in a material with a varying bandgap) is no longer of the required simple form to render equation (7.2.8c) frequency independent.

In conclusion, we have developed a model for calculating the amplitude and phase modulation of the radiation field of the family of index guided, single mode semiconductor lasers with an inhomogeneous carrier density. In the model amplitude and phase are coupled through the complex susceptibility of the gain medium. We have shown that this coupling constant can be obtained by measuring the ratio of amplitude to phase modulation at high frequencies. Since the same coupling mechanism causes the spectral linewidth broadening, this method enables us to measure directly the linewidth enhancement factor α. Our measurements confirmed the model and we measured a linewidth enhancement factor $|\alpha| = 4.6 \pm 1.0$ for a buried optical guide laser.

7.3 Observation of the relaxation resonance effects in the field spectrum of semiconductor lasers

Standard treatments on semiconductor laser noise [17] model the laser as a first order system and predict that its field spectrum is Lorentzian. When carrier dynamics are included, however, the model is second order and accounts for effects such as the relaxation resonance [18]. As a consequence the laser field spectrum predicted by the second order model is not an exact Lorentzian. Instead, the field spectrum consists of the main lasing line surrounded by subsidiary maxima (sidebands) spaced at intervals of the relaxation resonant frequency. These sidebands have been observed in certain semiconductor laser diodes [19], but were not explained completely. We have observed field spectrum sidebands and in this section present data which show they are a consequence of the relaxation resonance.

Hitachi HLP 3400 Buried Optical Guide (BOG) and HLP 1400 Channeled Substrate Planar (CSP) GaAlAs lasers with threshold currents of 20mA and 57mA at room temperature were measured. The bias current to the lasers was passed through a low pass filter. To prevent instabilities due to optical feedback a neutral density filter (ND5) was inserted at an angle between the test laser and a microscope objective which collimate the beam into a scanning Fabry Perot interferometer. The severely attenuated output signal was detected using a photomultiplier. Both lasers exhibited fundamental inverse power field linewidth broadening when measured using a scanning Fabry Perot interferometer with a 1500MHz free spectral range and an instrumental bandwidth of approximately 12MHz. Predominately single mode operation was achieved for bias points a few milliamps above threshold, other modes being two to three orders of magnitude smaller than the lasing mode. The field spectrum sidebands were measured using a monochromator in tandem with a scanning Fabry Perot with a free

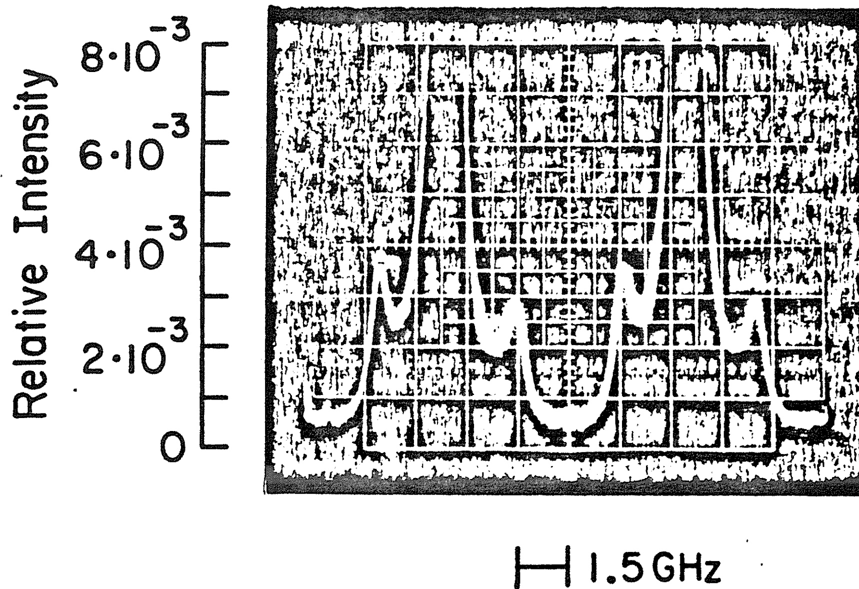

Figure 7.3.1. Fabry-Perot scan covering two free spectral ranges. The vertical scale is normalized to line center.

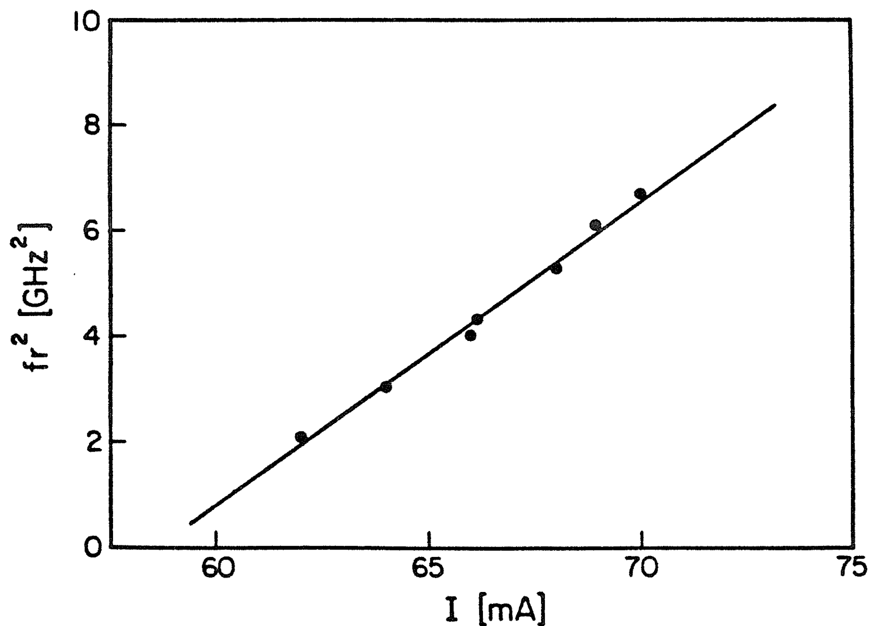

Figure 7.3.2. Square of the sideband frequency spacing versus bias current measured for the CSP laser.

spectral range of 7.5GHz and an instrumental bandwidth of 70MHz. The monochromator served as a wide bandpass, preventing weakly excited longitudinal modes from obscuring observations. Scan rates were adjusted so that any distortion caused by the detection time constant was not noticeable. The output of the photomultiplier drove the y axis of an oscilloscope whose sweep was synchronized to the Fabry Perot interferometer.

Fig. 7.3.1 is a typical output which shows the lasing lineshape twice. This photograph was taken using the CSP biased at 66mA, which corresponds to 16% above threshold and an optical output power of 2.0mW. The vertical magnification is 100× that normally used for viewing the field spectrum. This has caused the center lobe to be clipped. The first order sidebands are clearly visible and are separated from the line center by 1.7GHz. The sideband amplitude at this bias point is roughly 1% of the lasing peak amplitude and its absolute strength was observed to decrease with increasing power. Sidebands observed on the BOG exhibited the same amplitude power dependence, but their relative size was an order of magnitude smaller than those observed on the CSP.

It is well known that the square of the relaxation frequency varies linearly with current above threshold. To show that the frequency separation between the lasing line center and the first order sidebands is indeed the relaxation resonant frequency we have plotted the square of the measured separation versus current in Fig. 7.3.2 for the CSP. It can be seen that the dependence is linear and that the horizontal axis intercept is within experimental error the threshold current. We observed the same dependence for the BOG. We also observed the resonance in the power fluctuation spectrum using a silicon avalanche photodiode (AEG-Telefunken S171P). Values of the resonant frequency at various bias points were in close agreement with the sideband frequency separation measured in the field spectrum.

Sideband asymmetry was observed at all bias points and always took the form shown in Fig. 7.3.1 (i.e. lower frequency sideband larger than the upper sideband). Attempts to misalign the monochromator and the Fabry Perot resulted in attenuation of the signal, but did not change the form of the asymmetry. We believe this asymmetry results from coherence between amplitude and phase fluctuations. Since carrier fluctuations are tied to phase fluctuations through the refractive index, all shot noise sources which involve creation (annihilation) of a photon and simultaneous annihilation (creation) of a carrier would lead to coherence between the ensuing phase and amplitude fluctuations. To test this hypothesis we calculated the field spectrum sidebands using the results given in [18]. We present here only the calculated results in Fig. 7.3.3 on the exact structure of the lineshape and we refer to a paper by Vahala, Harder and Yariv [20] for the calculations. Compared to the theoretical sidebands in Fig. 7.3.3 the observed sidebands in Fig. 7.3.1 are somewhat smeared. We attribute this to the instrumental broadening of the Fabry Perot. Although its resolution is roughly 70MHz, the effective resolution is drastically reduced because of the main lobe's presence. To account for this effect we convolved the theoretical sideband spectrum and a Lorentzian with a FWHM equal to our instrumental bandwidth. The result is shown in Fig. 7.3.1 as the dashed curve and it resembles closely the observed field spectrum.

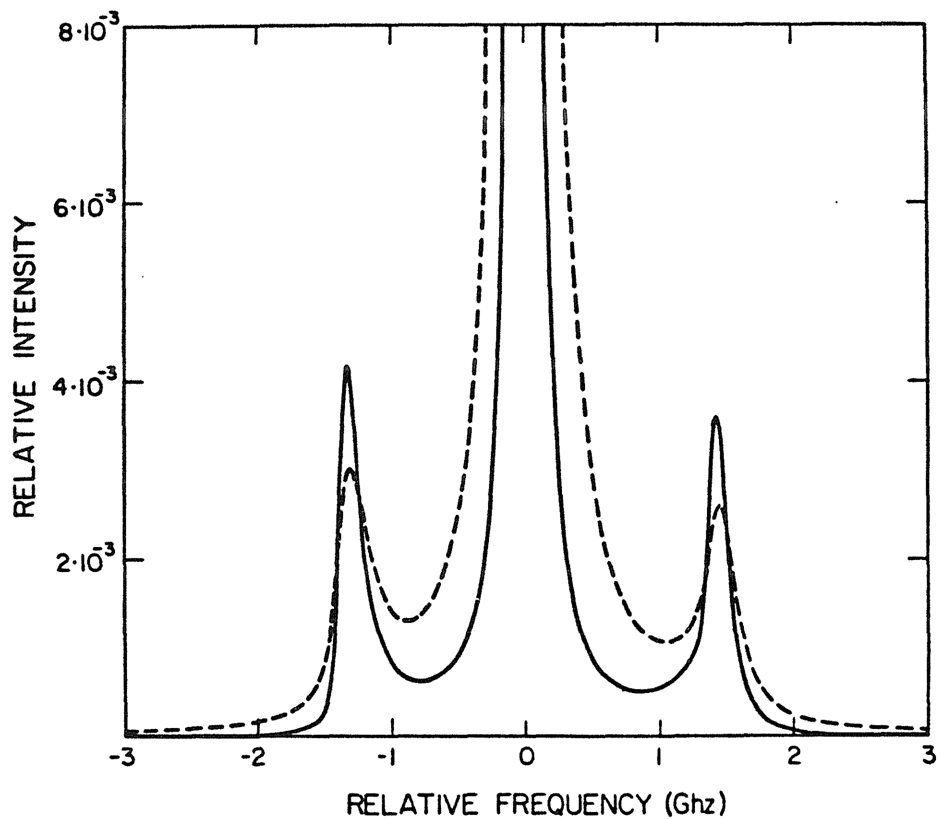

Figure 7.3.3. Solid curve: calculated field spectrum of a CSP laser at 2mW output power per facet. Vertical scale is normalized to line center. Dashed curve: solid curve convolved with instrumental bandwidth.

7.4 References

1. A. Yariv, W. M. Caton, IEEE J. Quantum Electron., vol. 10, p.509 (1974).

2. J. P. Gordon, H. J. Zeiger, C. H. Townes, Phys. Rev., vol. 99, p. 1264 (1955).

3. A. L. Schawlow, C. H. Townes, Phys. Rev., vol. 112, p. 1940 (1958).

4. H. Haug and H. Haken, Z. Phys. 204, 262 (1967).

5. M. W. Fleming, A. Mooradian, Appl. Phys. Lett., vol. 38, p. 511 (1981).

6. K. Vahala, A. Yariv, to be published in Appl. Phys. Lett. (1983).

7. D. Welford, A. Mooradian, Appl. Phys. Lett., vol. 40, p. 865 (1982).

8. C. H. Henry, IEEE J. Quantum Electron. QE-18, 259 (1982).

9. K. Vahala and A. Yariv, to be published in IEEE J. Quantum Electron.

10. C. H. Henry, R. A. Logan and K. A. Bertness, J. Appl. Phys. 52, 4457 (1981).

11. D. Welford and A. Mooradian, Appl. Phys. Lett. 40, 865 (1982).

12. J. G. Mendoza-Alvarez, F. D. Nunes and N. B. Patel, J. Appl. Phys. 51, 4365 (1980).

13. F. Stern, Phys. Rev. A133, 1653 (1964).

14. W. E. Lamb, Jr., Phys. Rev. 134, A1429 (1964).

15. S. Kobayashi, Y. Yamamoto, M. Ito, T. Kimura, IEEE J. Quantum Electron. QE-18, 582 (1982).

16. Y. Yamamoto, H. Hayashi, T. Hayakawa, N. Miyauchi, S. Yano, T. Hijikata, Appl. Phys. Lett., vol. 42, p. 406 (1983).

17. K. Vahala, A. Yariv, to be published in IEEE J. Quantum Electron.

18. K. Vahala, A. Yariv, to be published in IEEE J. Quantum Electron.

19. J. M. Osterwalder, IEEE J. Quantum Electron., vol. 18, p. 364 (1982).

20. K. Vahala, Ch. Harder, A. Yariv, Appl. Phys. Lett., vol. 42, p. 211 (1983).

Chapter 8

Monolithic integration

8.1 Introduction

At present, semiconductor lasers are exclusively fabricated as discrete elements. The lasers are typically driven from a 50 Ω line which is contacted through a bondwire to the laser diode. While it is possible to obtain satisfactory high speed modulation by driving the laser from a 50 Ω line, we have shown in chapter three that a laser integrated with one or several MESFET's is a very attractive alternative and makes a compact transmitter which can be easily interfaced to the electrical system as shown in Fig. 3.5.7b.

Similary, optical receivers are nearly exclusively built as hybrid circuits, consisting of a photodiode connected through a bondwire to the input of an amplifier. It has been shown [1] that the signal to noise ratio of an optical receiver depends critically on the input capacitance C_{in}, and the performance is proportional to the so called quality factor $\frac{g_m}{C_{in}^2}$, (g_m is the transconductance of the first amplifying element). It is imperative for a high quality receiver to have an input capacitance as small as possible and a large transconductance.

Integrating the photodiode monolithically with the first amplifying element reduces the total input capacitance C_{in} and thus increases the quality of the receiver dramatically. Such a circuit is, for example, a pin-photodiode MESFET combination [2] and these circuits are expected to outperform their hybrid

counterparts.

Heterojunction GaAlAs/GaAs bipolar transistors [3] have attractive features such as a high current amplification, (an amplification of 1600 has been measured [4]) and a projected gain bandwidth product of f_T = 100GHz [5]. A combination of a pin-photodiode and a bipolar transistor is expected to be able to compete with its MESFET counterpart and we will analyze now such an integrated pin-bipolar receiver.

The photodiode of an integrated receiver should have an area which is large enough to accommodate the incoming light spot, i.e. the photodiode should be at least as large as the core of the optical fiber, 10μm to 50μm, depending on the type of the fiber. The depletion width of the diode has to be large enough to keep the capacitance of the photodiode small. Bipolar transistors have the best high frequency performance (the highest f_T) when they run at very high current densities, just below the critical current at which the base pushout effect degrades the current amplification and the high frequency performance [6].

A quick noise analysis (neglecting base spreading and emitter resistors) yields the total shotnoise $\frac{I_n^2}{\Delta f}$ at the input in parallel to the photodiode [7]:

$$\frac{I_n^2}{\Delta f} = 2e(I_{Ph} + V_T 2\pi f C_{in} \sqrt{\frac{1}{\beta} + \frac{f}{f_T}}) \tag{8.1.1}$$

when the transistor is run at the optimum collector current I_C

$$I_C = \frac{V_T 2\pi f C_{in}}{\sqrt{\frac{1}{\beta} + \frac{f}{f_T}}} \tag{8.1.2}$$

I_{Ph} is the average photocurrent, V_T is the thermal voltage, e is the unit of charge, f is the signal frequency, C_{in} is the total capacitance at the input node, β is the current amplification and f_T is the gain bandwidth product of the transistor.

For typical values, $C_{in} = 0.5pF$, $f = 1GHz$, $f_T = 20GHz$, $\beta = 100$ we obtain: $\frac{I_n^2}{\Delta f} = 2e(I_{Ph} + 40\mu A)$ at $I_C = 0.34mA$ and the transconductance is $g_m = 12mmoh$. We can infer from equation (8.1.1) that a good noise performance is obtained for a small input capacitance, C_{in} and a large f_T. The optimum collector current is relatively small, $I_C = 0.34mA$, and in order to operate the transistor at a reasonable current density, which is necessary for a large f_T, its dimensions have to be extremely small, i.e. a $3\mu m \times 3\mu m$ emitter window results in a current density of around $4kA/cm^2$, a nominal value. The noise performance is degraded by the thermal noise of the base resistor $r_{bb'}$ and emitter resistor r_e if they are too large, i.e. the sum of the resistors has to be small, $(r_{bb'} + r_e) \leq \frac{1}{2\pi f_T C_{in}}$ which is in our example $\approx 16\Omega$. In order to satisfy this condition the emitter contact resistivity has to be smaller than $1.5 \times 10^{-6}\Omega\ cm^2$, a value which pushes the technological limit and the base has to be highly conductive.

We summarize: a receiver should have a photodiode large enough to accommodate the incoming light, an input capacitance as low as possible and a transistor with a very small emitter window, an extremely good emitter contact and a small base resistance. A phototransistor incorporates both elements, the photodiode and the transistor, but it is difficult to achieve an independent optimization of the elements; the collector diode area (photodiode) has to be large while the emitter base area has to be kept small. Also, from a circuit point of view, the photodiode capacitance is multiplied by the Miller effect which degrades the frequency response unless the collector of the bipolar transistor drives a very small impedance. A phototransistor can be easily integrated, but a photodiode bipolar transistor combination can be tailored to have a superior performance.

8.2 Monolithic integration of a GaAlAs buried heterostructure laser and a bipolar phototransistor

A complete optical repeater consists of three different circuits. A receiver, which interfaces the optical fiber to the digital electronics, a digital signal processing unit and a transmitter which interfaces the electronics to the optical fiber. These circuits have three key elements, optical detectors which transform the incoming light into an electrical signal, transistors (bipolar or fieldeffect) which amplify and reshape the electrical signal and which perform digital processing and switching of datastreams, and lasers which transform the electrical signal back into an optical one. Monolithic receivers [2], transmitters [8], [9] and even a very simple version of a repeater [10] have been demonstrated. The level of integration which can be achieved depends critically on the power dissipation of each element, which has to be kept as low as possible. The buried heterostructure (BH) laser is a prime candidate for a low power laser; threshold currents as low as 10mA are routinely obtained and BH lasers operate at much lower power level than the more simple stripe lasers. However, the technology of fabricating BH lasers is more complicated and two successive liquid phase epitaxy (LPE) steps are necessary. In this work we have employed for the first time the superior BH laser as the light source to be integrated with a bipolar transistor, using the second growth to form both, the bipolar transistor and the cladding layers for the laser waveguide [11]. The schematic diagram of this optoelectronic circuit is shown in Fig. 8.2.1. We demonstrate for the first time that high quality lasers can be fabricated monolithically with photodiodes and bipolar transistors, all the key elements which are necessary for a complete optoelectronic circuit.

The cross section of the device is schematically shown in Fig. 8.2.2. The first LPE growth, which involves the laser section consists of four layers: n-GaAs

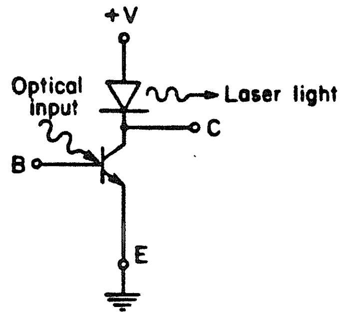

Figure 8.2.1. Schematic diagram of the circuit

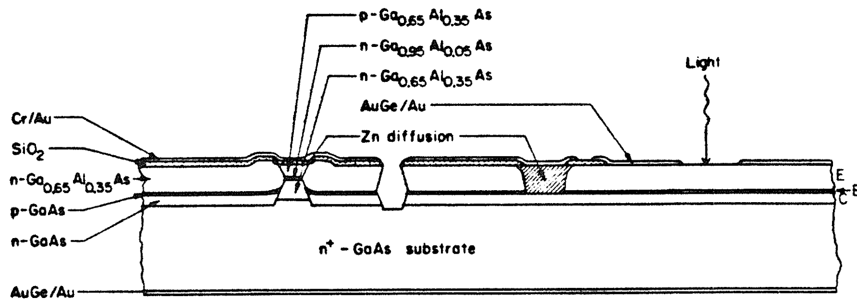

Figure 8.2.2. Cross section of the circuit (not drawn to scale).

(4μm, 4×10^{17}cm^{-3}), n$-Ga_{0.65}Al_{0.35}As$ (1.5$-$2μm, 10^{17}cm^{-3}), undoped $Ga_{0.95}Al_{0.05}As$ (0.25μm), and p-$Ga_{0.65}Al_{0.35}As$ (1.5$-$2μm, 10^{17}cm^{-3}). After etching mesa stripes down to the n-GaAs layer (stripe width 4μm) with H_2SO_4:H_2O:H_2O_2 (1:8:8) in the $\langle 1\bar{1}0 \rangle$ direction (inverted trapeziodal shape) the second LPE growth is performed in order to obtain the bipolar transistor structure. The regrown layers are n-GaAs (0.5μm, undoped), p-GaAs (0.3μm, 10^{18}cm^{-3}), and n$-Ga_{0.65}Al_{0.35}As$ (5×10^{16}cm^{-3}). The wafer is then coated with SiO_2 and two Zn diffusion processes are performed from a $ZnAs_2$ source: a shallow diffusion into the p-GaAlAs layer on top of the mesa (to improve the p contact of the laser) and a deep diffusion down through the emitter to the p-GaAs regrown layer (which serves as the base contact of the transistor). Finally the contacts are applied by thermal evaporation and alloying: Cr-Au for laser anode and transistor base and Au-Ge/Au for the laser cathode (which serves also as the collector of the npn transistor) and the transistor emitter. The laser is isolated from the transistor by etching a narrow stripe in the wafer down in the n-GaAs layer, which serves as the collector.

The threshold current of the laser is 30mA for 300 μm cavity length, and the external differential quantum efficiency is $\approx$50% from both facets. Since the stripe width is 3μm the laser does not operate in the fundamental lateral mode. The bipolar transistors have typical common emitter current gains of β in the range of 100-400, at collector current levels of several milliamperes. The thin base layer (0.3μm) and the high bandgap-emitter contribute to the high current gain and a high f_T by reducing the minority carrier transit time and increasing the injection efficiency. Since the laser and the transistor are connected in series as shown in Fig. 8.2.1 the laser output can be easily modulated by the transistor.

The measured gain bandwidth product is f_T = 25MHz at a collector current of I_C = 25mA, corresponding to a current density of $\frac{25mA}{300\mu m \times 200\mu m} = 40A/cm^2$.

The transistor can also be operated as a photodetector. This is achieved by removing the emitter contact from a 50μm diameter circular area and inserting light from a fiber coupled to a GaAlAs laser source (λ = 0.82μm). The phototransistor responsivity was measured to be 50 to 75A/W at collector currents larger than 15mA. Figure 8.2.3. shows a typical dependence of the light responsivity R and the common emitter current gain β on the collector current I_C. For currents above 20mA, the values of both R and β remain essentially constant.

The characteristic of this phototransistor can be improved by reducing the emitter base diode area. This can be achieved simply by changing the mask for the deep Zn diffusion down to the base. The Zn diffusion should cover the the whole transistor, except a small circular area with a few microns diameter, the emitter. The light can be coupled through the high bandgap base into the reverse biased base collector diode. And by growing this structure on semiinsulating substrate the devices can be completely isolated.

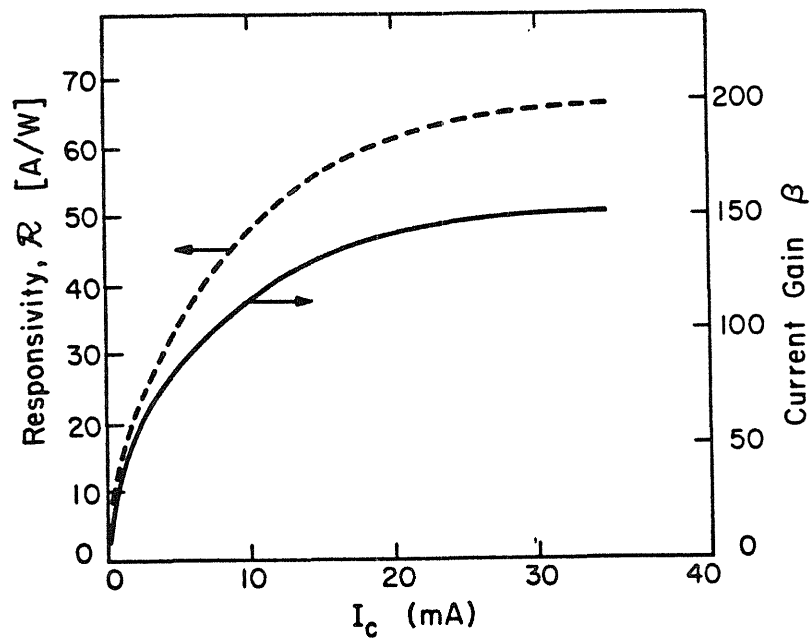

Figure 8.2.3. Phototransistor responsivity R and common emitter current gain β as a function of the collector current I_C.

8.3 References

1. R. G. Smith, S. D. Personic,"Semiconductor devices for optical communication", edited by H. Kressel, Springer Verlag, Berlin (1980).

2. R. F. Leheny, R. E. Nahory, M. A. Pollack, A. A. Ballmon, E. O. Beebe, J. C. DeWinter, R. J. Martin, Electron. Lett., vol. 16, p. 353 (1980).

3. H. Kroemer, IEEE Proc., vol. 70, p. 13 (1982).

4. M. Konagai, K. Katsukawa, K. Tahakashi, J. Appl. Phys., vol. 48, p. 4389 (1977).

5. P. M. Asbeck, D. L. Miller, R. Asatourien, C. G. Kirkpatric, Electron. Dev. Lett., vol. 3, p. 403 (1982).

6. C. T. Kirk, IEEE Trans. Electron. Dev., vol. 9, p. 164 (1962).

7. C. D. Motchenbacher, F. C. Fitchen, "Low noise electronic design", John Wiley & Sons, New York (1973).

8. J. Katz, N. Bar-Chaim, P. C. Chen, S. Margalit, I. Ury, D. Wilt, A. Yariv, Appl. Phys. Lett., vol. 37, p. 211 (1980).

9. I. Ury, K. Y. Lau, N. Bar-Chaim, A. Yariv, Appl. Phys. Lett., vol. 41, p. 126 (1982).

10. M. Yust, N. Bar-Chaim, S. H. Izadpanah, S. Margalit, I. Ury, D. Wilt, A. Yariv, Appl. Phys. Lett., vol. 35, p. 795 (1979).

11. N. Bar-Chaim, Ch. Harder, J. Katz, S. Margalit, A. Yariv, I. Ury, Appl. Phys. Lett., vol. 40, p. 556 (1982).